Universidad Nacional de San Juan
Facultad de Ingeniería
Instituto de Energía Eléctrica

ESQUEMA DE PROTECCIÓN ULTRA-RÁPIDO MEDIANTE MORFOLOGÍA MATEMÁTICA CONSIDERANDO EL EFECTO DE GENERACIÓN BASADA EN INVERSORES CONECTADA AL SISTEMA DE TRANSMISIÓN

Tesis doctoral de:

Juan Carlos QUISPE HUARCAYA

Temas de Energía Eléctrica

94



Ministerio de Educación
Universidad Nacional de San Juan



Facultad de Ingeniería

ESQUEMA DE PROTECCIÓN ULTRA-RÁPIDO MEDIANTE MORFOLOGÍA MATEMÁTICA CONSIDERANDO EL EFECTO DE GENERACIÓN BASADA EN INVERSORES CONECTADA AL SISTEMA DE TRANSMISIÓN

Tesis doctoral de

JUAN CARLOS QUISPE HUARCAYA

aprobada por la
Facultad de Ingeniería de la
Universidad Nacional de San Juan
para acceder al grado académico de

DOCTOR EN INGENIERÍA ELÉCTRICA

Dirección de tesis:	Dr. Ing. Eduardo Orduña
Co-dirección de tesis:	Dr. Ing. John Morales
Jurado de tesis:	Dr. Ing. Francisco Gonzalez- Longatt
Jurado de tesis:	Dr. Ing. Arturo Suman Bretas

Fecha de defensa oral: 22 de marzo de 2024

Esquema de Protección Ultra-Rápido Mediante Morfología Matemática Considerando el Efecto de Generación Basada en Inversores Conectada al Sistema De Transmisión

---

Tesis de Doctorado de:

Juan Carlos Quispe Huarcaya

Primera edición – San Juan – agosto 2024.
Impreso en Argentina – Printed in Argentina
San Juan, Universidad Nacional de San Juan (UNSJ)



ISBN 978-631-00-4934-2

Queda hecho el depósito que marca la Ley 11.723

Prohibida la reproducción parcial o total, el almacenamiento, el alquiler, la transmisión o la transformación de este libro, en cualquier forma o por cualquier medio, sea electrónico o mecánico, mediante fotocopias, digitalización u otros métodos, sin el permiso previo y escrito del editor.

Este libro se imprimió en EFU (Editorial Fundación Universitaria) - UNSJ

Todos los derechos reservados
© 2024 Juan Carlos Quispe Huarcaya, UNSJ

Instituto de Energía Eléctrica – Universidad Nacional de San Juan - CONICET
Av. Libertador Gral. San Martín 1109 Oeste (J5400ARL), San Juan, ARGENTINA
Tel.: +54 264 4226444 - Fax: +54 264 4210299

Prefacio

El presente trabajo como tesis de doctorado se realizó en el Instituto de Energía Eléctrica (IEE) de la Facultad de Ingeniería de la Universidad Nacional de San Juan, Argentina bajo el financiamiento del Consejo Nacional de Investigaciones Científicas y Técnicas (CONICET) y del Servicio Alemán de Intercambio Académico (DAAD).

Quiero agradecer a mi familia por el apoyo incondicional que siempre me han brindado. A mis padres Carlos y Reyna y mis hermanos Cesar, Kevin y Karol quienes siempre me apoyan en la realización de mis metas y sueños.

Además, agradecer a los directores Dr. Eduardo Orduña y Dr. John Morales, por brindarme la posibilidad de realizar el trabajo bajo su dirección. Un especial agradecimiento a todo el personal del Instituto de Energía Eléctrica por su disponibilidad y buena voluntad a responder cualquier duda o consulta que me surgió durante la realización de este trabajo.

Juan Carlos Quispe Huarcaya

Abstract

Ultra-Fast Protection Scheme using Mathematical Morphology considering the Effect of Inverter-Based Resource Connected to the Transmission System

Juan Carlos Quispe H.

This research develops a new distance protection algorithm for transmission lines using fault-generated high-frequency transient signals by means of new digital filtering technique based on the mathematical morphology theory and spectral energy. Also, this method determines the behaviour of signals in the time-frequency domain through multi-resolution analysis with a 5 ms time window, making it ultra-fast compared to traditional protection schemes and avoiding the effect of inverter-based resources. The development of this thesis has provided the following contributions: A detailed review of the fault response characteristics of inverter-based resources and their influence on the main protection functions of transmission lines (distance, differential, overcurrent, directional). A detailed analysis of the behaviour of high-frequency transient signals caused by short-circuit travelling wave signals in transmission lines. Finally, a new methodology for distance protection using high-frequency transient signals based on a morphological filter and comparison techniques based on frequency and spectral energy thresholds is presented.

Resumen

Esquema de Protección Ultra-rápido mediante Morfología Matemática considerando el Efecto de Generación Basada en Inversores Conectada al Sistema de Transmisión

Juan Carlos Quispe H.

Este trabajo desarrolla un nuevo algoritmo de protección a distancia para líneas de transmisión utilizando señales transitorias de alta frecuencia generadas por fallas mediante una nueva técnica de filtrado digital basada en la teoría de morfología matemática y energía espectral. Además, este método determina el comportamiento de las señales en el dominio tiempo-frecuencia mediante un análisis multirresolución con una ventana de tiempo de 5 ms, lo que hace de este muy rápido y evite el efecto de las fuentes de energía renovables en comparación con los sistemas de protección tradicionales. Por lo tanto, el desarrollo de esta tesis proporciona las siguientes contribuciones: Un estudio detallado de las características de respuesta ante cortocircuitos de los generadores basado en inversores y su influencia en las principales funciones de protección de las líneas de transmisión (distancia, diferencial, sobrecorriente, direccional). Un estudio detallado del comportamiento de las señales transitorias de alta frecuencia causadas por las señales de onda viajera de cortocircuito en las líneas de transmisión. Por último, se presenta una metodología novedosa para la protección de distancia utilizando señales transitorias de alta frecuencia mediante el desarrollo de un nuevo filtro morfológico digital y tecnicas de comparación basado en umbrales de frecuencia y energía espectral.

Contents

1 Introduction **1**
- 1.1 General objective . . . 2
- 1.2 Specific objectives . . . 3
- 1.3 Challenges . . . 3
- 1.4 Thesis structure . . . 3

2 State-of-the-Art **5**
- 2.1 Introduction . . . 5
- 2.2 Short circuit response of IBR . . . 8
- 2.3 Review of the state-of-the-art . . . 14
  - 2.3.1 Protection scheme challenges with IBR integration . . . 15
  - 2.3.2 New protection schemes with IBR integration . . . 19
- 2.4 Analysis of the literature review . . . 22
- 2.5 Conclusions . . . 27

3 Transient signal analysis **29**
- 3.1 Introduction . . . 29
- 3.2 Fault-generated high-frequency transient signals in transmission lines . . . 30
  - 3.2.1 Reflection and refraction of traveling waves . . . 31
  - 3.2.2 Attenuation of high-frequency transient . . . 35
- 3.3 High frequency transient signals caused by the inverter . . . 36
  - 3.3.1 Inverter response due to a short circuit . . . 39
- 3.4 Conclusions . . . 41

4 Theorical models **43**
4.1 Introduction . . . 43
4.2 Digital filter . . . 45
4.2.1 Digital Morphologic Filter (DMF) . . . 45
4.2.2 Structuring element (SE) . . . 46
4.2.3 Multiresolution analysis (MRA) with mathematical morphology . . . 47
4.3 Processing algorithm . . . 50
4.3.1 Spectral energy index (SEI) . . . 50
4.3.2 Time-frequency domain signal calculation . . . 52
4.4 Conclusions . . . 54

5 Development of protection algorithm **57**
5.1 Introduction . . . 57
5.2 Fault zone identification . . . 59
5.3 Logical protection scheme . . . 64
5.4 Simulation analysis . . . 65
5.4.1 Case study: Generic model of a power system using only synchronous generators . . . 65
5.4.2 Case study: Current-source type generator . . . 85
5.4.3 Case study: Transmission line that connects a type 3 Wind Generator (DFIG) . . . 89
5.4.4 Case study: IEEH TU-Dresden laboratory model . . . 94
5.5 Comparison with wavelet transform . . . 97
5.5.1 MRA using DWT . . . 104
5.5.2 DWT vs DMF . . . 106
5.6 Conclusions . . . 107

6 Conclusions and future works **111**

7 Resumen versión español **115**
7.1 Resumen . . . 115
7.2 Introducción . . . 116
7.2.1 Objetivo general . . . 117
7.2.2 Objetivos específicos . . . 117
7.3 Estado del arte . . . 118
7.4 Análisis de las señales transitorias . . . 119
7.5 Modelos teóricos . . . 120

7.6 Desarrollo del algoritmo de protección 121
7.7 Conclusiones 122

Appendix **125**

A Appendix A: Main protection schemes in TLs **125**
A.1 Distance protection (function 21) 125
A.2 Differential protection (function 87) 127
A.3 Directional element protection (function 32) 129
A.3.1 Directional elements for phase fault protection . . . 129
A.3.2 Directional elements for ground fault protection . . . 130
A.4 Negative-sequence protection 132
A.4.1 Negative-sequence overcurrent element (function 50Q/51Q) 132
A.4.2 Directional negative-sequence overcurrent element (function 67Q) 132
A.5 Faulted-phase identification 133
A.5.1 FIDS Logic 134
A.6 Directional overcurrent protection (67) 135

Appendix **136**

B Appendix B: Transmission line model **137**
B.1 TL with distributed parameter model 137
B.2 Transient wave propagation characteristics 139
B.3 Reflections and refractions at the TL Terminals 140

Appendix **141**

C Appendix C: Signal processing methods **141**
C.1 Theory of Mathematical Morphology 141
C.1.1 Definitions for binary operations 141
C.1.2 Binary dilation and erosion 142
C.1.3 Set representations of functions 142
C.2 Morphological filters 143
C.2.1 Opening and Closing 144
C.2.2 Morphological Gradient Algorithm 144
C.3 Discrete Wavelet Transform (DWT) 146

Appendix **149**

D Appendix D: Equipment characteristics of test models **149**
D.1 Generic model of a power system 149
D.2 Current-source type generator 150
D.3 Type 3 wind generator 151
D.4 IEEH TU-Dresden laboratory 152

Bibliografía **159**

List of Figures

2.1 Characteristic of the structure of IBRs 7
2.2 Short-circuit behavior of current using a generic IBR model during a two-phase fault(AB) 10
2.3 Short-circuit behavior of voltage using a generic IBR model during a two-phase fault(AB) 10
2.4 Low voltage ride-through characteristics [25] 12
2.5 Positive sequence reactive current injection $\triangle Iq$ vs $\triangle U$ . . 13
2.6 IBR Negative Sequence Reactive Current Injection [25] . . . 13
2.7 Effect of IBR characteristics on the main protection functions 24
2.8 Response time scale for the IBR operation and relays operation 26

3.1 Decomposition of a transient signal 30
3.2 TW reflection and refraction - Lattice diagram. 32
3.3 Period of the signal for different reflection coefficient sign. . 33
3.4 Transient fault frequency ($Freq_{fault}$) vs fault distance (d) . 35
3.5 Attenuation of high-frequency transient 36
3.6 Time constant of the transient loops 37
3.7 LCL filter configuration 38
3.8 Configurations of the four fault current paths for a two-phase fault. 39
3.9 Circuit configurations for fault current pathways 40
3.10 Impedance magnitude behavior. 41

4.1 block diagram of the operation process of a relay 45

4.2 Structuring element shapes. 47
4.3 Relationship between the SE length and the time interval between samples 48
4.4 Relationship between SE length, frequency and fault distance 49
4.5 Multiresolution signal frequencies vs SE length 50
4.6 Relationship between SE length and Sampling frequency (1 MHz) 51
4.7 Relationship between SE length and Sampling frequency (500 kHz) 51
4.8 Relationship between SE length and Sampling frequency (100 kHz) 52
4.9 Flow chart of the digital morphological filter proposed method 54

5.1 Fault zone identification 59
5.2 Simulation of a two-phase short circuit (AB) for four fault location 60
5.3 Spectral energy index for four different fault location 61
5.4 Fault zone threshold 62
5.5 Spectral energy index threshold 63
5.6 Diagram of protection scheme logic 64
5.7 Generic model of a power system using only synchronous generators 66
5.8 Fault distance behavior 68
5.9 Comparison between simulated data and theoretical curve . 69
5.10 Time-frequency for Rf=0.01 Ohm. 70
5.11 Time-frequency for Rf=25 Ohm. 70
5.12 Time-frequency for Rf=50 Ohm. 71
5.13 Voltage behavior on the L bus for different fault start time 71
5.14 Time-frequency for fault start time: 25 ms 72
5.15 Time-frequency for fault start time: 29 ms 72
5.16 Time-frequency for fault start time: 33 ms 73
5.17 Time-frequency for fault start time: 37 ms 74
5.18 Without SNR 74
5.19 With SNR: 40 dB 75
5.20 With SNR: 30 dB 75
5.21 With SNR: 20 dB 76
5.22 Case Fs: 1 MHz 77
5.23 Case Fs: 500 kHz 78

5.24 Case Fs: 100 kHz 78
5.25 Case: SE shape sinusoidal 80
5.26 Case: SE shape triangle 80
5.27 Case: SE shape linear 81
5.28 Current transient signal due to a two-phase (AB) short circuit 81
5.29 Voltage transient signal due to a two-phase (AB) short circuit 82
5.30 Current and voltage behaviour due to a two-phase (AB) short circuit 82
5.31 Spectral energy for different fault locations 83
5.32 Spectral energy with threshold frequency 83
5.33 Definition of the frequency threshold and the SEI threshold 84
5.34 Spectral energy for many cases including the worst conditions 85
5.35 Electrical system with a current source at one end (Bus L) 86
5.36 Current behavior on the bus-L side 87
5.37 Voltage behavior on the bus-L side 88
5.38 MRA time-frequency 88
5.39 SEI vs time and frequency 89
5.40 Case study of type 3 Wind Generator (DFIG) 90
5.41 Two-phase fault at 80 km 91
5.42 Time-frequency multiresolution 92
5.43 Curve Frequency vs Time 92
5.44 Two-phase fault at 120 km 93
5.45 Time-frequency multiresolution 93
5.46 Curve Frequency vs Time 94
5.47 Overview diagram of the DNM 95
5.48 Frequency vs Fault location - laboratory 96
5.49 Fault at 40 km 98
5.50 Time-frequency multiresolution: Fault at 40 km 98
5.51 Fault at 60 km 99
5.52 Time-frequency multiresolution: Fault at 60 km 99
5.53 Fault at 90 km 100
5.54 Time-frequency multiresolution: Fault at 90 km 100
5.55 Fault at 100 km 101
5.56 Time-frequency multiresolution: Fault at 100 km 101
5.57 Fault at 120 km 102
5.58 Time-frequency multiresolution: Fault at 120 km 102
5.59 Fault at 140 km 103
5.60 Time-frequency multiresolution: Fault at 140 km 103

5.61 Decomposition tree using wavelet packet method. 104
5.62 Spectral energy of multiresolution signals, 2D. 105
5.63 Spectral energy of multiresolution signals, 3D. 106
5.64 Comparison of FMD and DWT methods 108

A.1 Fault in TL with two power supplies 126
A.2 Alpha plane characteristic 129
A.3 General electrical system for directional element operation 130
A.4 (a) Blue zone means forward condition, and (b) Orange zone means reverse condition 131
A.5 $X - R$ plane of the forward and reverse fault characterization 131
A.6 Apparent negative-sequence fault impedance seen by 67Q . 133
A.7 Fault identification logic 134

B.1 Differential element of a transmission line 137

C.1 Dilation of a one-dimensional signal 143
C.2 Erosion of a one-dimensional signal 144
C.3 Opening of a one-dimensional signal 145
C.4 Closing of a one-dimensional signal 145
C.5 Decomposition of signals by DWT. 147
C.6 Decomposition based on Wavelet packtes. 148

D.1 TL configuration (a)Line L-R (b) Line R-T 150
D.2 Power system model 152
D.3 Transmission line model 153
D.4 PI model of a line section 153
D.5 Mean values of self- and coupling impedances per component 154
D.6 Mean values of coupling capacitances and leakage resistances 154
D.7 Fault simulation control equipment 155
D.8 Short-circuit device 155
D.9 High-frequency signal extraction device 156
D.10 Substation control equipment 157

List of Tables

2.1 Influence of variables on the main functions and element protection . . . 15
2.2 Causes and effects on distance protection due to IBRs . . . 17
2.3 Causes and effects on differential protection due to IBRs . . . 18
2.4 Causes and effects on directional and negative-sequence overcurrent protection due to IBR . . . 19
2.5 Adaptive protection schemes and modification of traditional protection . . . 21
2.6 Protection schemes based on transient signals and artificial intelligence . . . 23

3.1 Relationship between time response and frequence . . . 37

5.1 Relationship between Fs and sample quantity . . . 76
5.2 Traveling wave frequency . . . 97
5.3 Traveling wave frequency . . . 104
5.4 Comparative table between two signal processing methods obtained for the analysis of this thesis . . . 107

A.1 Polarization configuration . . . 128
A.2 Polarization for zero- and negative-sequence . . . 132
A.3 FIDS logic . . . 135

C.1 Wavelet decomposition . . . 148

D.1 Grid parameters . . . 149

D.2 Step-up power transformer 151
D.3 Current-source characteristics 151
D.4 DFIG characteristics 151

CHAPTER 1

Introduction

Power system protection design and studies are carried out to determine the settings, schemes and logic of protection relays. Moreover, these devices continuously measure the main signals of an electrical network, such as voltage, current, frequency, etc.; therefore, based on the known behaviour of these signals under fault conditions, the relays should detect, identify and clear the fault through the principles of speed, selectivity, reliability, sensitivity, etc. In addition, the following fault conditions are usually taken into account when performing protection studies: fault type, location, resistance and angle of inception.

The inclusion of new generation technologies based on power electronics, such as converters, changes the common fault behaviour because they have different fault current contribution characteristics. In this sense, there are two types of generation technology:

- Generators based on synchronous machines: hydroelectric, thermal, nuclear, biomass, etc.
- Generators based on power electronic: photovoltaic, type 3 wind generator, type 4 wind generator, etc.

Renewable Energy Sources (RES) include a group of generators based on synchronous machines and generators based on power electronics; however, this last have an inverter in their structure, these technologies

are also known as Inverter-Based Resources (IBR). The terminology of IBR is used to denote generation sources such as solar, wind, and energy storage that are connected to the power network through inverters. It is recognized that other notations for such sources include converter interfaced generation (CIG), power electronic interfaced power sources (PEIPS), and inverter interfaced resources (IIR). Consequently, based on the topology, configurations and response time of the inverters, the main effects on transmission line protection are classified as follows [1; 2; 3]:

- Limited fault current amplitude.
- Controlled duration of fault current.
- Depends on FRT configuration (grid codes).
- Unstable internal impedance.
- Controlled current phase angle
- Low amount of negative sequence
- There is no zero sequence quantity

These effects manifest themselves in various problems in the operation of protection devices, such as zone reach, polarization, start-up, insufficient negative sequence quantities, etc [1]. There is therefore a clear need to develop new criteria for protection algorithms that are easy to implement and take into account all possible fault scenarios, including the behaviour of new generation sources or the avoidance of being affected.

In this context, the following question arises: How can protection schemes on transmission lines be improved to avoid being affected by the effect of IBRs?

1.1 General objective

To develop a new algorithm and protection scheme for transmission lines by analysing high-frequency transient signals with a short time window, making it an ultra-fast method that is not affected by the behaviour of the IBR control system.

1.2 Specific objectives

- Analyze the behavior of traditional algorithms due to the inclusion of IBR.
- Analyze the behavior of high-frequency transient voltage and current signals using a signal processing method based on mathematical morphology.
- Development of protection logic based on thresholds.
- Development of simulations for several events in a transmission system.
- Verify the new protection algorithm by comparing with other method.

1.3 Challenges

Protection challenges arise because the output current of an IBR device is very different from that of a conventional rotating synchronous source device under short-circuit conditions. These types of unexpected behaviours are typically not detected until the plant is in operation and a grid event occurs that warrants investigation into the plant's abnormal behaviour.

The reliability of traditional line protection schemes, which rely solely or largely on short-circuit current contributions from IBR devices, can be unreliable without additional measures.

The high penetration of high-capacity IBR devices into the transmission system now poses new challenges to these traditional protection schemes. In addition, distance and directional overcurrent protection schemes are widely used in transmission line protection relaying and are therefore the most challenging. This is discussed in detail in the following chapters.

1.4 Thesis structure

1. Introduction: It includes a brief description of the problem, general objective, specific objectives, and challenges in general.

2. State-of-the-art: The research problem is identified and detailed through an analysis of the literary review.

3. Transient signal analysis: The basic characteristics of transient signals and the component used in this thesis are described.

4. Theorical models: The mathematical technique for extracting or filtering the transient signal for use in protection is detailed.

5. Development of protection algorithm: The proposed protection logic is described and verified through many simulations for different test cases.

6. Conclusions and future works: The conclusions, contributions, and future work that are the result of this thesis are described.

7. Resumen versión español: The thesis summary is presented in Spanish.

8. Appendix

9. Bibliography

CHAPTER 2

State-of-the-Art

Currently, the transmission line protection is facing challenges due to the high penetration of Inverter-Based Resources (IBR); therefore, an in-depth study of this issue is required, which considers the analysis of the main causes and new methodological criteria solutions. This chapter presents a comprehensive literature review on the evaluation of electrical protection performance and the effects of IBR. The bibliographical data of many representative publications on the subject are obtained to show the current lines of research and their proposed solutions. In addition, this work identifies the main protection functions affected and describes the new protection systems that take IBR into account. Finally, an analysis and discussion of the selected bibliography is presented.

2.1 Introduction

In recent years, Electrical Power Systems (EPSs) have experienced a continuous evolution of new facilities, many of which are RESs. This is largely driven by international commitments to reduce CO_2 emissions, social demands to address climate change, government incentives for clean energy, and fast cost reduction of new technologies. Wind farms (WF) and photovoltaic plants (PVP), which are growing faster, have a major impact on EPS behaviour. A previous report [4] suggests that their presence in

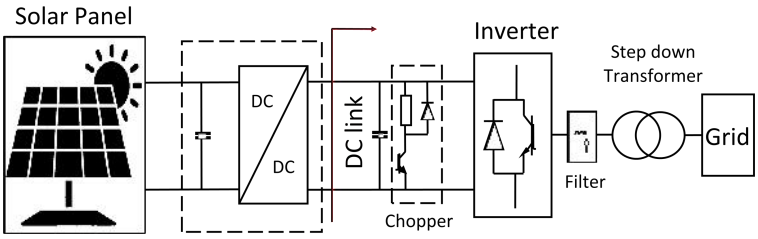
EPS will continue to increase.

From a dynamic point of view, RES can be divided into two groups. The first group includes generation sources based on rotating machines connected directly to the grid, while the second group includes generation sources connected to the grid through power electronic (PE) equipment operating on the principles of fast converter switching and associated control systems. Many authors refer to the second group as a generator connected to the grid through an inverter as an interface, or simply as inverter-based resources (IBRs), as shown in Fig. 2.1. This configuration is designed to take advantage of the efficient use of energy [5], and new ways of generating energy have been developed and implemented on a large scale, such as a renewable power plant presented in [6].

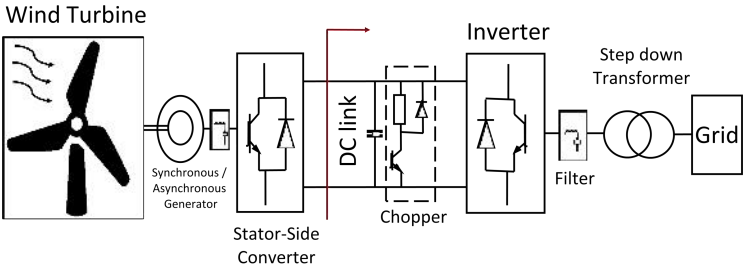
An important aspect of the IBR is the ability to control the rate of current rise and limit the short circuit current (SCC) without the intervention of external circuits. With regard to WFs, each type of technology has a different SCC behaviour [7]. Therefore, SCC performance is an important issue as the use of IBRs in EPS continues to grow [8]. As a result, traditional schemes in transmission line protections (distance, differential and directional overcurrent protection), which are composed of protection elements as the logic inputs of the main scheme, may experience challenges. Each protection element is based on algorithms with input phasor signals such as voltage and current in both cases using the positive, negative and zero sequences, so the IBR may significantly affect some input quantities of the protection algorithms and therefore affect certain schemes such as the negative sequence directional element, the fault type identification element, the phase directional element, impedance measurement, among others [1; 2; 3]. Traditional relays may not have sufficient performance because protection schemes and logic consider a system made up of synchronous generators.

On the other hand, voltage and current signals have limited transient magnitudes accompanied by high harmonic distortion, as studied in [9; 10]. Low inertia systems, complex IBR models, interactions between synchronous machine controllers and inverter controllers are studied in [11]. Consequently, a high penetration of IBRs implies changes in the paradigms for coordination of control and protection systems, as indicated in [12].

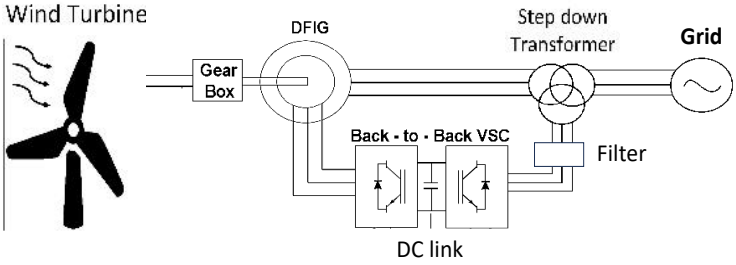
New generation source technologies can affect the operation of traditional protection schemes, which has made it an interesting topic in



(a) Photovoltaic generator



(b) Type 4 wind turbine generator



(c) Type 3 wind turbine generator

Figure 2.1: Characteristic of the structure of IBRs

recent years. Accordingly, this chapter analyses, through an exhaustive bibliographic review, the most representative challenges in transmission

line (TL) protection systems affected by IBRs. Finally, a summary is given of the main solutions proposed to minimise or mitigate these effects.

2.2 Short circuit response of IBR

As part of the IBR structure, an important component is the DC link (Fig. 2.1) because it decouples the fault dynamics in the grid from events associated with variations in wind speed and solar intensity. In other words, the response time to a fault is very fast compared to the variable response of the generation sources. The inverter is the main device that influences the dynamic behaviour of IBRs during a short circuit, as its actuation time is mainly focused on the response time of the power system controller [13]. Also, the main inverter control system uses voltage and current signals measured at the point of common coupling (PCC), and then its control process uses phasor signals obtained by Fast Fourier Transform (FFT) of the measured signals, which typically requires a 1 cycle time window [14]. However, a mutual agreement on the response time requirements between IBR owners and operators needs to be based on clear technical bases [15].

In the presence of short circuits, energy conversion by traditional generation sources or synchronous generators (SG) is based on electromagnetic processes and energy storage involves magnetic fields; therefore, variations in the stored magnetic energy cannot occur instantaneously during a short circuit, as a certain transient period must elapse before stabilising under new conditions. The SCC is given by the equation (2.1).

$$\begin{aligned} i_{SG} = \sqrt{2}E_q[(\frac{1}{x''_d} - \frac{1}{x'_d})e^{-\frac{t}{T''_d}} + \frac{1}{x_d}]cos(\omega t + \varphi_\phi) \\ -\sqrt{2}\frac{E_q}{x''_d}cos(\varphi_\phi)e^{-\frac{t}{T_a}}, t \geq t_0 \end{aligned} \tag{2.1}$$

where:

x''_d: Subtransient reactance on the d-axis
x'_d: Transient reactance on the d-axis
T''_d: Subtransient time constant

T'_d: transient time constant
E_q: Voltage
x_d: Synchronous reactance on the d-axis
T_a: Armature time constants
t_0: Start time

On the other hand, signals directly affected by IBRs are divided into three periods. In the first stage there is a current peak, the value of which depends on the parameters of the LCL filter and the capacitor in the intermediate circuit; it can also reach values greater than 2 per unit (p.u.) of the rated current. The second stage involves regulation,during which the inverter's control system works to regulate the DC link voltage to deliver the grid code (GC) regulated current according to a Fault Ride-Through (FRT) characteristic and to limit the SCC. Finally, during the third stage, the inverter output current reaches and maintains an approximately constant value (Fig. 2.2 and Fig. 2.3), this behavior is referential. Consequently, the IBR's behavior is different and may be represented as a function of fault conditions, their structures, and their control system setting parameters, as shown in equation (2.2).

$$i_{IBR} = f(FC, ST, CSS), t \geq t_0 \tag{2.2}$$

where:
f: Function
FC: Fault Conditions (fault resistance, inception angle, location)
ST: Structure
CSS: Control System Setting
t_0: Start time

The characteristics of a Type 4 wind turbine generator or Full Scale Converter (FSC) differ from those of a Type 3 wind turbine generator or Doubly Fed Induction Generator (DFIG), while the characteristics of these generators also differ from those of a Type 1 and Type 2 wind turbine generator. A clear example of the SCC behaviour of different types of wind turbine generators are described in [16; 17].

In order to protect the power electronics, the inverters have a saturation block that limits the currents. This block is generally set to values between 1.1-1.3 p.u.[18], but can be up to 1.5 p.u. in special cases. On the other hand, it is known that the impedance angles of synchronous generators are stable and close to 90°, whereas the internal impedance angles of

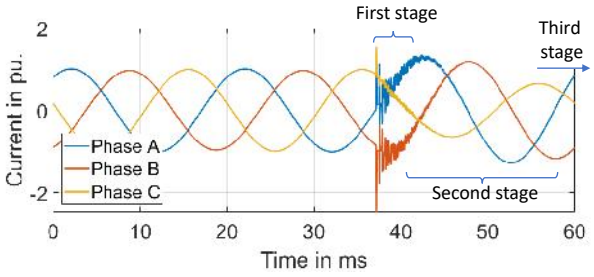


Figure 2.2: Short-circuit behavior of current using a generic IBR model during a two-phase fault(AB)

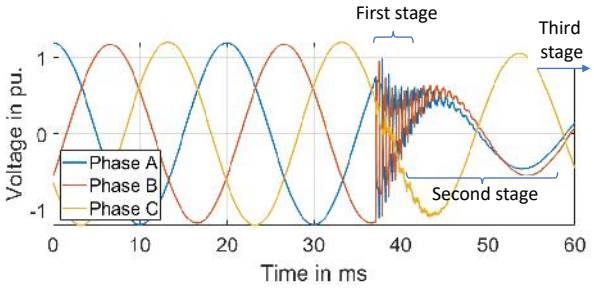


Figure 2.3: Short-circuit behavior of voltage using a generic IBR model during a two-phase fault(AB)

IBRs can oscillate, which can even be capacitive, resistive or inductive, depending on the operating mode. The inverter's control system causes these characteristics as it tries to keep the phase shift balanced even in the presence of faults, also the behaviour of IBRs is highly dependent on the control system strategies during FRT, which are defined by modern grid

codes [19].

The FRT requires inverters to remain connected to the grid and provide dynamic support during a fault or short circuit without tripping. In addition, utilities set the FRT requirements for each interconnection, and IBRs are expected to behave in a certain way during disturbances, as specified in the IEEE-1547 standard [20]. The characteristics of FRT are highly dependent on the electrical system's behavior, while [21; 22; 23; 24] summarise the requirements and GC configurations adopted in many countries from Europe, Asia, and America.

Different operating modes can be considered in relation to international standards and trends in modern network codes:

- IBR Low Voltage Ride-Through.
- IBR Positive Sequence Reactive Current Injection.
- IBR Negative Sequence Reactive Current Injection.
- IBR Frequency Ride Through

According to Low Voltage Ride-Through (LVRT), the source is to remain connected when the voltage depression from an external fault is within the low voltage ride-through requirement of the applicable grid code e.g. the Fig. 2.4 shows the characteristics of the German grid code [25].

In case of voltage depression, the IBR is required to supply positive sequence reactive current, irrespective of fault type. This increased reactive current is required to minimize the voltage depression during faults and assist in preventing loads such as induction motors from stalling and further depressing the voltage.

The required reactive current (I_q) behavior may change according to the system requirements. For example, the Fig. 2.5 shows the variation of the reactive current with respect to the voltage variation. The control system is activated outside the indicated dead band, i.e. when the voltage variation reduces or exceeds 10% of the nominal voltage. The slope k may vary in the range of $2 \leq k \leq 6$, the current limits ($\triangle Iqmax$, $\triangle Iqmin$) may be ± 1.0 or ± 1.1 p.u. and the dead bandwidth ($U_{deadband}$) can be valued in the range $2.5 - 10\%$. These characteristics cause a different behavior in the reactive fault current.

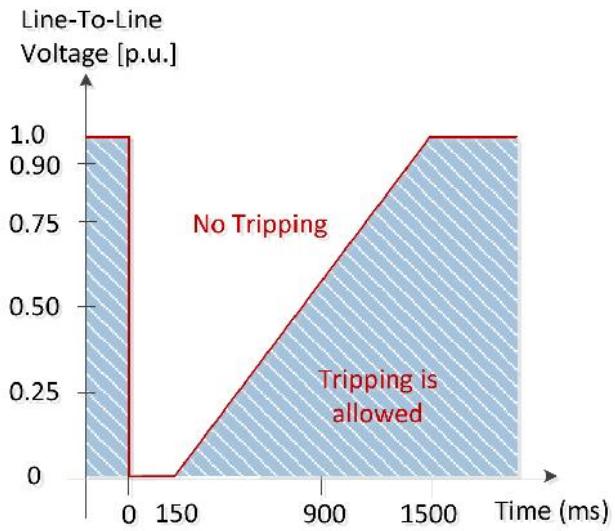


Figure 2.4: Low voltage ride-through characteristics [25]

According to a structure of IBRs, the inverters do not supply zero-sequence current (I_0) because of no ground return connection [26; 27].

Traditionally, IBR manufacturers suppressed negative sequence current (I_2) in their current control system designs as it was not required by grid codes [28]. Absence of adequate negative sequence current during unbalanced faults, as a consequence, is threatening protection reliability i.e. its ability to adequately protect the line during unbalanced faults [25]. The German grid code exploited this effect through a feature as shown in the Fig. 2.6. The k is the line slope of the negative sequence reactive current injection requirement. An IBR with adjustable line slope i.e. gain (k) from 2 to 6 may emulate apparent j1/k pu. negative sequence reactance largely similar to a synchronous generator which typically has negative sequence reactance in range from j0.12 pu to j0.4 pu [25].

Even when required, injection of a negative sequence current during unbalanced faults from IBRs would be limited by the inverter ratings and the required positive sequence reactive injection [2; 8; 29; 30; 31; 32]. Therefore, the final amount of injected negative sequence reactive current

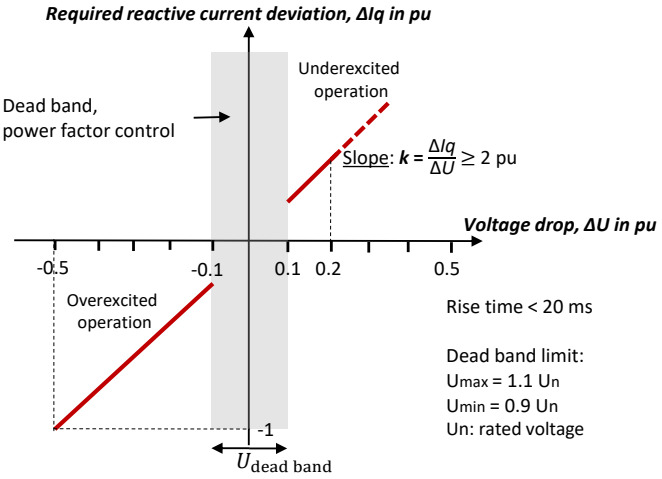


Figure 2.5: Positive sequence reactive current injection $\triangle Iq$ vs $\triangle U$

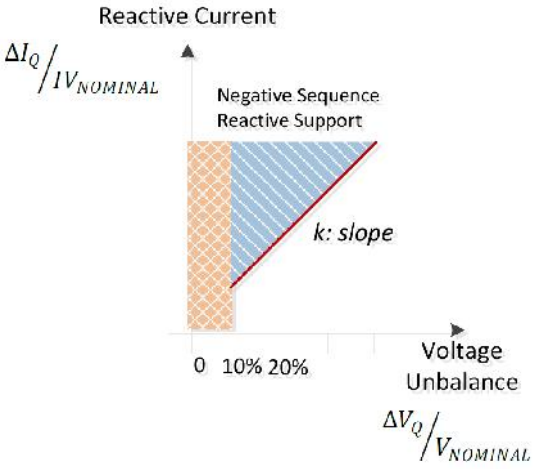


Figure 2.6: IBR Negative Sequence Reactive Current Injection [25]

depends also on the current limiter of the invertir because the vector sum of load current (if present), positive sequence reactive current and negative sequence reactive current cannot exceed the current limit of an IBR.

On the other hand, the operating characteristics of traditional relays are summarised in Appendix A. It has been verified that all the functions and protection elements are based on different schemes and that some of them have certain variations due to the logic of each manufacturer.

In this sense, the results of IBR's impact on traditional relays from various authors' research are presented below.

2.3 Review of the state-of-the-art

This review focuses on the challenges of TL protection schemes considering the influence of IBRs. The cited works are based on previous experiences and theoretical developments, while many new protection methods have been developed to suppress or minimize the effect of IBRs.

Based on current protection scheme criteria, some of them present certain variations due to operating logic of each manufacturer. In general, phasors and polarization are two important and useful tools in the traditional power system protection, these concepts are essential in understanding power system performance during both steady-state and fault operation. Phasors are composed by magnitude and its angle; while polarization is the comparison between two phasor quantities.

The table 2.1 also gives a reference percentage of influence of the phasor quantities and comparisons between them for each protection function. It is observed that distance protection and the directional element require the most signals for their protection scheme. This indicates that distance protection will be greatly affected by influence of IBRs while differential protection will be largely unaffected.

where:

1. Distance protection, only impedance calculation and fault detector.
2. Differential protection.
3. Directional element protection.
4. Fault-type identification logic, phase selection logic (FIDS).
5. Negative-sequence protection.
6. Overcurrent protection.

Table 2.1: Influence of variables on the main functions and element protection

	I_1	V_1	Z_1	I_2	V_2	I_0	V_0	I_1, V_1	I_2, V_2	I_0, V_0	I_2, I_0	I_{ABC}, V_{ABC}	I_L, L_R	%
1.	✓	✓	✓			✓	✓	✓		✓		✓	✓	69.2%
2.	✓												✓	15.3%
3.	✓	✓		✓	✓	✓	✓		✓	✓		✓		69.2%
4.	✓			✓		✓					✓	✓		38.4%
5.				✓	✓				✓		✓			30.7%
6.	✓			✓		✓								23.0%

2.3.1 Protection scheme challenges with IBR integration

Challenges on distance protection

This section describes the main problems of distance relays in TL connecting to IBRs. The previous study in [33] describes the impedance behavior of IBRs with FRT under two different grid codes, the European (EU) one and the North American (NA) one. It is shown that the reactive current required by the EU translates into impedances seen near the reactive axis. In contrast, the power factor required by the NA translates into impedances along the resistance axis [33]. As a result, in both cases, the impedances seen from faults are far from the actual fault impedances. It is therefore concluded that the variations in impedance seen depend on the control strategies implemented in the IBRs. This is further stated in [34], where it is reported that the impedance measured on the IBR side has a different characteristic, causing the conventional distance protection to malfunction, as the inverter control system limits the SCC and controls the angle shift. However, in [35], it emphasizes problems in the response time of the control system (rise time) when the IBRs supply reactive power. It shows that a slow response time causes a malfunction in distance relay, since zone 2 might be mistaken for zone 1 during a fault. In [36], distance protection behavior is detailed in a distribution system with high penetration of IBRs, a dynamic analysis is conducted in a three-dimensional system (R, X, t). Different behavior from synchronous generators is observed due to the fault current limit. In [1], it shows that the phase distance element of zones 1 and 2 may overreach and drop out, respectively, because of an oscillating apparent impedance caused by currents injected by the IBRs. This is reinforced in [37], that

the impedances seen by distance relays outside an IBR present problem of overreaching zones, caused by the inverter control system.

Reference [38] presents a polarization problem in an impedance relay type mho affected by the variable impedance of type 3 wind turbine generator or DFIG. This is caused by transient and steady-state components in the SCC injection before reaching a stable value. Furthermore, reference [39] describes some effects of type 3 wind turbine generator on distance protection. As protection relays are not acquainted with the behavior of the generator, it leads to large variations between the phases of the fault current and voltage. Consequently, this causes a chaotic trajectory for the impedance values.

In the same line of research, reference [40] describes the presence of back-to-back converters as a predominant problem source and their effects on distance protection. It indicates that power electronic converters not contributing to fault current are the main problem. Meanwhile, in [42], the impact of high voltage direct current voltage source converters (VSC-HVDC) on distance relay coordination is described, which presents an overestimation effect on impedance measurements due to the control system, and is similar to the behavior of IBRs. In [43], it shows that effects on distance protection due to the control scheme of the VSC-HVDC connected offshore wind farm during an AC fault is caused by the amplitude and phase of currents controlled by the wind farm. In [44], impacts of a modular multi-level converter (MMC-HVDC) on distance protection is described, which is due to changes in the operation mode of the converter control reduced the range of zone 2 of the distance relay, resulting in malfunction. Finally, reference [41] shows the effects of a VSC on distance protection due to the control strategies of the converter, so a synchronous compensator is considered in the installation. A summary is shown in Table. 2.2.

Challenges on differential protection

In [52], problems in the differential protection of TLs are described, and it indicates that the differential relay on side of IBRs presents some challenges in line protection sensitivity, such as a starting logic and phase detection. This is due to a low influence of current penetration and the inverter control strategy, which presents different behaviors in each phase of the three-phase current system as they depend on the voltage drop level of each

Table 2.2: Causes and effects on distance protection due to IBRs

Function	Reference	Technology	Cause	Effect
21	[33]	IBR	Control system parameters, current limit setting.	The relay impedance can be far away from the actual fault impedance.
21	[35]	IBR	Low SC-current, reactive current rise time.	The initial fault impedance by distance relay moves closer to zone 1 setting, even for zone 2 faults.
21	[39]	DFIG	The frequencies of the signals can be well apart.	Oscillating impedance.
21	[34]	IBR	Phase angles are controlled by the inverter control system.	The impedance has a great amplitude and phase offset.
21	[40]	Back-to-back	Power electronic converters do not tend to contribute to the fault current.	The impedance determined by the relay is quite high and it can see outside of the protection zones.
21	[41]	VSC	Design of control system, lower SC-current level.	The measured impedance locus has transients. The impedance moves in and out from the effective zone during the fault.
21	[1]	IBR	Low-magnitude currents that may behave incoherently with the voltages.	In the phase distance element the zone 1 may overreach, the zone 2 may drop out and there is apparent oscillating impedance.
21	[37]	IBR	Inverter control system.	Effect on impedance, zone 1 overreach.
21	[42]	VSC-HVDC	Reactive power control of VSC-HVDC.	Relay tends to overestimate the fault distance.
21	[43; 44]	DFIG, IBR, VSC-HVDC	Different fault ride through controls, control current's amplitude and phase.	Malfunction of the distance relay, the higher line distance relay zone 2 is narrowed.
21	[45]	IBR	Inverter reactive power current.	Overreach or underreach of impedance measurement.
21	[46; 47; 48]	DFIG	Depends on the operating mode.	Affects the trip boundaries of the distance relay.
50	[36]	IBR	Inverters are nonlinear electronic devices.	Insufficient SC-current, delay in time operation.
32	[38]	DFIG	The SC-current mainly consists of a transient component.	Effect on positive sequence voltage polarized impedance relay.
32	[1]	IBR	Current limited by the inverter.	The phase directional element may misbehave when a three-phase fault disconnects the IBR.
32	[1]	IBR	Negative-sequence current limited.	The negative-sequence directional element may misbehave.
32	[49]	DFIG	Low voltage ride requirements.	The relationship between the current and voltage phase angle in negative sequence is not readily known.
32	[29]	IBR, DFIG	Improper magnitude and phase angle of negative-sequence current.	The negative-sequence current is not the leading voltage as it is in a conventional source.
32	[50]	DFIG	Low-voltage ride requirements.	Improper magnitude and phase angle of the negative-sequence current.
FID	[51]	DFIG	Slip and crowbar resistance.	Approximately unequal positive and negative currents will critically affect the phase selectors.

phase. Reference [53] shows an important factor that affects differential protection, where the angular difference of the fault phasor current at the line terminals may be greater than 90° under a phase-to-phase fault but not enough. It concludes that the problem lies in the angular difference between the currents, as a phase-to-phase fault generates an angular difference of almost 180° on the network side, while remaining at almost 120° on the IBR side. This is due to control strategies during the FRT period, as seen in Table. 2.3.

Table 2.3: Causes and effects on differential protection due to IBRs

Function	Reference	Technology	Cause	Effect
Threshold current start	[52]	DFIG, IBR	Current limit protection by inverter control.	Starting current does not operate.
Phase selection logic	[52]	DFIG, IBR	Inverter control strategy, low-voltage ride-through.	The inverter acts to increase the phase current phase.
Phase selection logic	[53]	IBR	Control strategies during FRT.	The angular difference of the faulted phase will be larger than 90°.

Challenges in negative sequence overcurrent starting and polarized directional with negative sequence voltage

In [54] a real event was analyzed, the authors observed problems in the directionality of an overcurrent relay due to a distortion in the fault signals and the change in the angular differences between voltages and currents did not correspond to the common behavior. The problem was identified because the quantities used were in negative sequence.

Other previous studies [2; 29] describe the main factors of IBRs in negative-sequence protection. For the 50Q/51Q elements, the main problem affects the pick-up, as the negative-sequence current may be smaller than the activation threshold. For the 67Q element, as in the previous case, there are starting problems. It also shows directional problems as the angular relationship of the negative-sequence voltage and current.

In [50], problems in TL protection are described and, in particular, the use of negative-sequence quantities to detect unbalanced faults. Furthermore, grid codes consider the behavior of negative-sequence quantities in unbalanced faults [30]. The negative-sequence control capability of the DFIG is limited, whereas the FSC is able to suppress the negative-sequence current completely. Finally, effects of IBRs on their own

protections are considered, though it further involves systemic protections while experiences in Germany are shown [55].

Table 2.4: Causes and effects on directional and negative-sequence overcurrent protection due to IBR

Function	Reference	Technology	Cause	Effect
Directional Element	[54]	IBR	Strategies inverter control.	Distortion signals, abnormal angle between V and I.
Directional Element	[3]	IBR (FSC)	Control the phase angle.	Malfunction of phase comparison.
Negative-sequence protection	[29; 31]	IBR	Limited current, inverter control.	Activation threshold. Different angles between V_2 and I_2.
Negative-sequence protection	[50]	IBR	Insufficient amount of negative sequence.	The overcurrent function will not be activated.
Negative-sequence protection	[30]	DFIG, FSC	Specification of the amount of negative sequence in the grid codes.	The increased amount of the negative-sequence influences the amount of the positive-sequence.
Negative-sequence protection	[32]	DFIG, FSC	Insufficient amount of negative sequence.	Fault response interferes with directionality.

2.3.2 New protection schemes with IBR integration

Adaptive protection schemes and modification of traditional protection

In [56], a combination of the conventional distance protection, voltage drop, a new directional element, and a communication-assisted method are used. In [39], a modification of a permissive overreaching transfer trip (POTT) of the tele-protection scheme is proposed; the remote relay (grid side) uses an overreach zone based on impedance, while the IBR side relay detects the fault direction according to the properties of the current waveform. However, in [34], an improved scheme based on time delay and the zero-sequence impedance and overcurrent signal for starting is proposed, whereas [40] proposes the mandatory use of differential protection on TL in the presence of IBRs. In [42], a new method is proposed to reset the distance protection parameters that present overreach or underreach by calculating an apparent impedance based on impedance matrix modification. An adaptive coefficient of variation is proposed in [57] to calculate the zone 2 configuration according to the fault type and the equivalent sequence impedances of wind turbine generators.

Furthermore, due to the large fluctuations of the wind turbine generators connected to the grid, reference [58] proposes an adaptive method for distance protection using information on bus voltage, current, and the number of generating units connected at that time. In [50], the use of zero-sequence current generated by high voltage side of the IBR step-up transformer is proposed, in this case, it is necessary to have a grounded star connection on the grid side. Additionally, in [44], an adaptive distance relay based on the measurement information on HVDC side common connection points is developed.

Regarding differential protection, reference [52] develops new adaptive protection schemes taking signals from auxiliary undervoltage components for starting the differential protection logic and components with zero-sequence for phase selection. An aspect to consider in this criterion is the verification of faults in remote lines as they also produce undervoltage. Another study in [54] proposes an adaptation of a directional detection algorithm through line angle modification and positive-sequence modification in order to increase the magnitude of negative-sequence quantities, whereas [61] presents a voltage-based phase selector scheme as the adjustment using current-based phase selectors present problems under the influence of IBRs. In [62], a scheme based on reactive power flow is developed, while [60] proposes an adaptive scheme for phase selection. This method is based on the weighting of different parameters, such as current magnitude, delta current, voltage magnitude and delta voltage, impedances, and symmetric components. The above described methods are summarized in Table. 2.5.

Protection schemes based on transient signals and artificial intelligence

In [63], a differential protection method is developed using transient current signals, which uses the Pearson correlation method of transient signals from line ends. Therefore, this correlation focuses on the similarity of the waveforms and the polarity, and is not influenced by amplitude. The method found weaknesses for long lines (>200 km) due to the capacitive effect. Reference [64] develops a protection scheme using frequency components, also a frequency spectrum of internal and external fault currents are extracted, and the calculation of an attenuation factor distinguishes the protection zones, thereby determining a threshold for

Table 2.5: Adaptive protection schemes and modification of traditional protection

Reference	Function	Proposed	Advantages	Disadvantages
[56]	Distance	Combination of voltage drop and a new directional element and is communication assisted.	Fast operation and reliability.	Communication wire is required, more costly.
[39]	Distance	Modification in the POTT teleprotection scheme.	Easy implementation, fast operation and reliability.	Requires a channel of communication, more costly.
[34]	Distance	Use time delay and zero-sequence.	Avoid using negative-sequence.	Drag zero-sequence problems.
[40]	Distance	Use differential protection.	Fast operation.	More costly, no back-up protection.
[42]	Distance	Resets distance parameters based on Zbus.	This method may be safe.	No adaptive in nature.
[57]	Distance	Adaptive coefficient and equivalent sequence impedance.	Adaptive in nature.	Logic circuit is more complicated due to complex calculation.
[58]	Distance	Adaptive scheme using voltage and current information.	Adaptive in nature.	Complex calculation.
[50]	Distance	Use zero-sequence from the transformer.	Avoid using negative-sequence.	Drag zero-sequence problems.
[44]	Distance	Adaptive scheme based on the measurement information on common connection points.	Adaptive in nature.	Implementation of the logic circuit is more difficult.
[52]	Distance	A new transmission line pilot protection scheme based on the accurate distributed line model.	Easy implementation and fast operation.	Communication wire is required, more costly.
[59]	Distance, differential	Use of a modified differential protection scheme.	Fast operation.	More costly, no back-up protection.
[52]	Differential, phase selection	Use auxiliary undervoltage components. Use zero sequence.	Avoid using negative-sequence.	Drag zero-sequence problems.
[54]	Directional element	Line angle modification in positive sequence.	Adaptive in nature and it may be safe.	Complex calculation.
[60]	Phase selection	Use the weighting of different parameters ($V, I, \triangle V, \triangle I, Z, etc.$)	Easy implementation and adaptive in nature.	Complete study is required.
[61]	Directional element, phase selector	Based on voltage (Undervoltage)	Easy implementation.	It is not entirely safe because, it only relies on tension.
[62]	Directional element	Based on reactive power flow.	Easy implementation.	It is not entirely safe because it only relies on reactive power, no adaptive in nature.

those zones. This study concludes that the signals generated by converters present higher noise. However, the proposed work requires many spectral

analyses with very high-frequency signals so high-speed signal processing is needed.

In [65], the importance of signal processing methods for information extraction is highlighted. Many methods are presented considering the use of transitory signals, based on Wavelet Transform (WT) of traveling waves [66; 67; 68; 69; 70], Principal Components Analyse (PCA) [71; 72], park transform of traveling waves [68], Teager Energy Operator (TEO) [73], empirical decomposition in the Joint Mode (JM) [74] of the traveling wave, and Mathematical Morphology (MM) [75; 76; 77]. All these methods are used to transient signal extraction and require short time windows, therefore, they are less affected by the inverter control system, as these methods require the acquisition of signals at high-frequencies.

A method using Artificial Neural Networks (ANN) is proposed in [48], they design an adaptive unit based on the calculation of the weighting factor of the impedance seen in real time, with the aim of adjusting the trip characteristic of the distance relay. This work considers the effect of intermittent operation of wind generators and therefore proposes that the settings of different zones of a distance relay must be constantly adjusted.

In [78], a scheme to detect and classify faults within a DFIG using an adaptive neural-fuzzy inference system method is developed, while methods using machine learning for systems with high penetration of distributed generation governed by investors have also been developed. Reference [79] proposes a method of distance protection with Support Vector Machine (SVM). Furthermore, reference [80] proposes a methodology to determine the directionality of currents in distribution feeders caused by distributed generation, based on Decision Tree (DT) and SVM. The above described methods are shown in the Table. 2.6.

2.4 Analysis of the literature review

Based on the literature review, it can be concluded that most works consider that the main challenges arise when the IBR controls the main variables used by the relays.

The low SCC magnitude causes overcurrent-dependent algorithms to be inactive, such as overcurrent start and the limited current can affect the measurement of the fault impedance and thus the impedance calculation.

Inverters may force the fault current contribution to be fully balanced

Table 2.6: Protection schemes based on transient signals and artificial intelligence

Reference	Function	Proposed	Advantages	Disadvantages
[63]	Differential protection	Uses the Pearson correlation method.	This method is dependable.	Complex calculation.
[64]	Differential protection	Uses signals in different frequency spectral.	This method is dependable and secure. Avoids phasor signals.	Complex calculation and requires a good method to filter the signal.
[65]	All functions	Uses signal processing (WT, PCA, TEO, JM, MM, etc.).	This method is dependable and secure.	Often present complex calculation and requires finding the appropriate mother function.
[48]	Distance protection	ANN.	This method is dependable and secure. Fast and adaptive in nature.	Require a lot of information for training.
[78]	Detect and classify faults	Neuro-fuzzy.	This method is dependable and secure. Good performance to identify faults.	Complex calculation and it requires a lot of information for training.
[79]	Distance protection	SVM.	This method is dependable and secure.	Only applies under certain conditions.
[80]	Directional element	DT-SVM.	This method is dependable and secure. Good performance to identify directionality.	Complex calculation.

regardless of the type of fault. When the angle of phasor signals is controlled by IBRs, the shift angle of voltage and current in all sequence quantities for each phase (abc) may exhibit non-traditional behavior; also the electrical system behaves inductive, while the inverter control may behave as inductive, capacitive or resistive. This may lead to errors in impedance measurements, comparison of positive- and negative-sequence shift angles, comparison of shift angles for each phase, comparison of the phasor current signals of the TL ends, and the relationship between polarized quantity and operational quantity.

Traditionally, negative sequence quantities can be used as the main protection to avoid relying on zero sequence quantities. In this case, directional supervision for distance elements can be used to increase safety, thereby the lack of negative sequence current from IBRs can cause the directional supervision not to trip and, in turn, disable the distance elements.

Fig. 2.7 shows a summary of all the main protection functions of TLs, each IBR characteristic affects a different algorithm, so a colored square is

included to indicate the correlation.

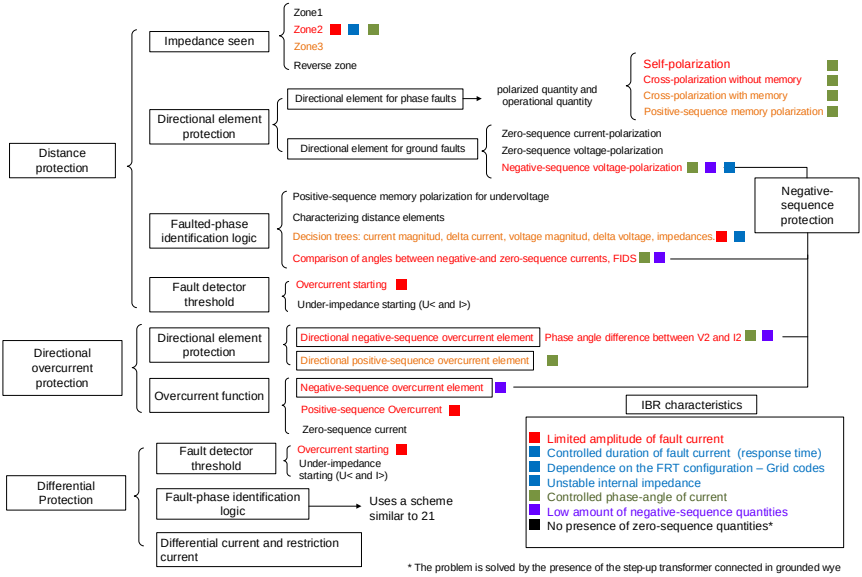


Figure 2.7: Effect of IBR characteristics on the main protection functions

In most of the cases cited, there is a greater emphasis and analysis on distance protection because this function and its elements are most affected by the inclusion of IBRs. The strategies most widely implemented in traditional protection schemes emphasize adaptive algorithms and the modification of traditional protection, these schemes perform impedance calculations taking into account the variable impedance of IBRs and are also supported by the use of other quantities or schemes not affected by IBRs, e.g:

- Voltage drop/ undervoltage
- Zero-sequence quantities
- Direct transfer trip scheme

- Modification teleprotection
- Differential protection
- Adaptation impedance
- Reactive power flow
- Fast voltage and current drop

Direct transfer trip scheme, modification teleprotection and differential protection require communication-assisted and high investment costs; voltage drop, reactive power flow, fast voltage and current drop schemes require back-up elements. The zero-sequence quantity is affected by coupling effects and the adaptation impedance depends on the source impedance, which is unstable.

In terms of response times, Fig. 2.8 shows a reference of the operating time scale of the relays compared to the fault response time scale of the IBRs. The overlap between the two behaviors can be observed, so any change in the IBRs can create new challenges for the relays. As a result, it can be observed that protection functions based on the phasor domain can present new challenges, and the currently proposed solution of modifying traditional schemes could reach a point where the schemes become very complex to implement, expensive to acquire, or even reduce the sensitivity of the equipment.

On the other hand, transient signal protection schemes are based on the time domain and use electromagnetic transient signals. In this case, the new methods use high-frequency signals with short time windows, most literary references associate these protection schemes as ultra-fast, since they process the signal and send the trip in shorter times than the traditional relay [81; 82]. The signal processing for the digital filter can be developed using the different methods described above, which emphasize the immunity to the effect of IBR control; however, the literary review shows us that they still have weaknesses, such as high sensitivity to harmonics and noise, high computational requirement, hard to select the mother function, and depends on periodic signals. In addition, artificial intelligence algorithms can use time domain and phasor domain information, these algorithms focus on training these parameters or machine learning, which means they require high information processing.

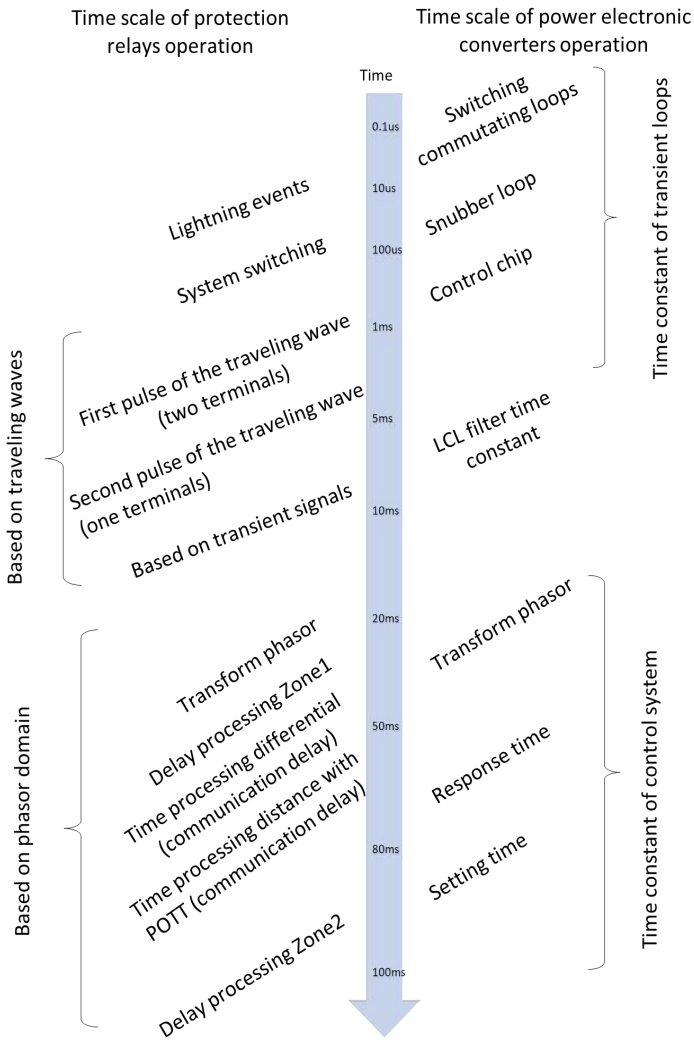


Figure 2.8: Response time scale for the IBR operation and relays operation

Consequently, the analysis of the impact of IBRs on EPS is considered a great challenge that requires research into the criteria for their operation for a systematic transformation of the current electrical grid to allow high penetration of sustainable energy.

2.5 Conclusions

This chapter described the challenges introduced by IBRs in these protection schemes and some possible solutions proposed by several authors. In that sense, it was observed that the operation behavior, governed by the settings of its inverter power control system, and the structure of these IBRs cause such challenges affecting mainly the functions used by a distance and directional relay. In addition, the influence factors are related to the same operating time scale, since the response times of inverters power controller are the same as the operating times of relays. Therefore, high penetration of IBRs into transmission systems requires an in-depth study of the development of new and existing protection schemes, as the modification or adaptation is inevitable in the future.

On the other hand, ultra-fast protection schemes have time scales shorter than the response time of the power control system and are theoretically unaffected, such is the case of protections based on traveling waves. However, these methods need complementary functions and, in many cases, may depend on the source behavior. Therefore, for systems with high penetration of IBRs, pertinent studies are required to confirm the reliability of these schemes.

CHAPTER 3

Transient signal analysis

This chapter presents the theoretical concepts of the origin and characteristics of transient signals caused by short circuits in transmission lines, this analysis focuses on the calculation of the traveling wave frequency and the main operating characteristics of IBRs in the high-frequency range.

3.1 Introduction

Short circuits can be analyzed from two perspectives: the phasor domain and the time domain. The phasor domain is determined by a previous transformation of instantaneous sinusoidal signals, this method uses a sampling time window of one cycle and the fault analysis starts afterwards. In the time domain, instantaneous sinusoidal signals are used, so the sampling time window can be less than one cycle, which means that fault analysis can be initiated within a few milliseconds. This approach offers a wide variety of methods, which were described in the state of the art and many of them are complex, making it a challenge in terms of information processing.

The use of the time domain signal involves the analysis of transient signals at different frequency ranges, which in many cases are caused by short circuits. Moreover, it has the ability to only need information of the first milliseconds (< 10 ms), which makes it very interesting for fast fault

clearance [83; 84; 85]. On the other hand, if the signal is observed at the fundamental frequency, the transient signals were born as a *noise* concept caused by electrical faults because traveling waves (TWs) and resonances affect the voltage and current waveforms when a short circuit occurs on a TL [86; 87; 88]. It was then analyzed as a transient spectrum of a series of harmonics caused by TW, where the presence of high frequency components in the signal is identified [89; 90; 91; 92].

This chapter focuses on the features of the transient signal behavior caused mainly by the reflection of short circuit traveling waves generated in the transmission lines and the operating characteristics of IBRs in this time scale.

3.2 Fault-generated high-frequency transient signals in transmission lines

Signal analysis with an electromagnetic transient (EMT) approach covers different frequency ranges, which involves dealing with a wide spectrum of frequencies. In this sense, it is convenient to characterize the signal components such as the information signal, the base signal and the noise, as shown in Fig. 3.1.

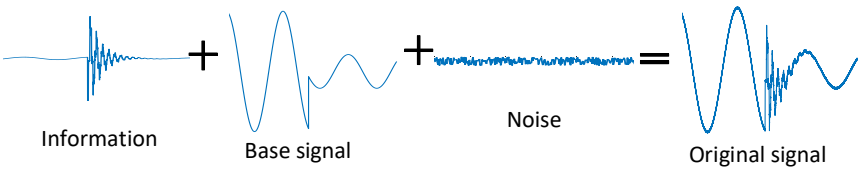


Figure 3.1: Decomposition of a transient signal

The features of these signals can be categorized according to their oscillating frequency. The base signal is broad trending and the frequency range is low, normally at the rated frequency of the electrical system 50 or 60 Hz. The noise signal, which is desired to eliminate or mitigate as much as possible, generally occurs at a very high-frequency. The information signal, which is of interest to process, is generally in a medium- or high-frequency range. Although there is no exact difference between the noise

frequency and the information signal frequency, the transient signal caused by the traveling waves can be extracted as the information signal.

When a short circuit occurs on a TL, traveling waves (TWs) and resonances occur that affect the voltage and current waveforms. These signals have a high-frequency spectrum and are associated with a transient signal frequency, which in turn is related to the fault distance [93]. Therefore, the fault-generated high-frequency transient signals involve the analysis of TW features.

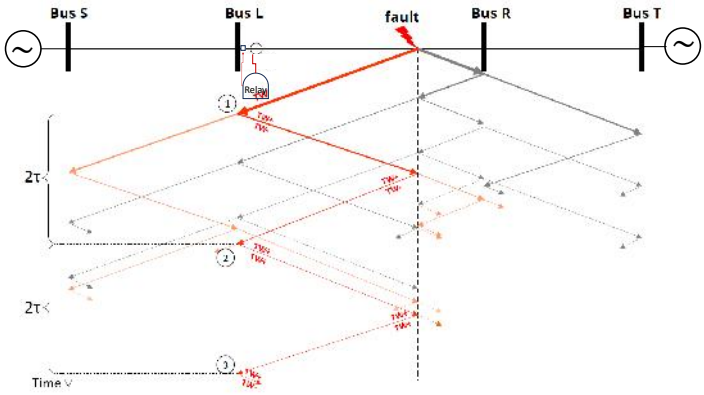
3.2.1 Reflection and refraction of traveling waves

The reflection and refraction phenomena of TWs cause distortions in the electrical signals [86]. These phenomena can be considered periodic, since the period depends on the times of impact of the TW and the reflection on the fault. This can be represented by a lattice diagram as shown in Fig. 3.2. In addition, for a detailed study of the behavior of traveling wave crests, it is important that a TL be modeled with distributed parameters; however, it is possible to extract traveling wave frequency characteristics even from TL models with multiple PI element sections in series (see Appendix B).

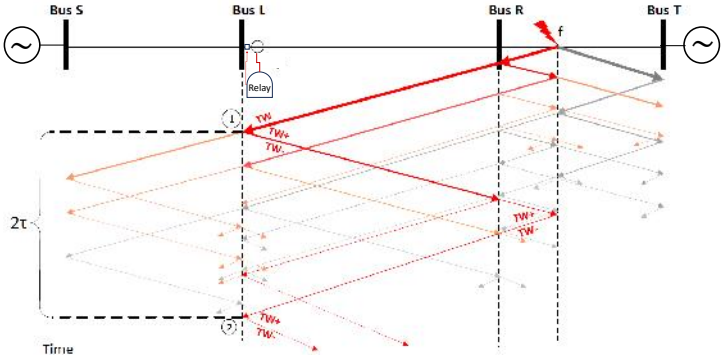
Due to the change in propagation medium, when a TW generated by a short circuit in a TL impacts its terminals, it causes a reflected and refracted wave, i.e. the TW enters a new medium with different characteristic impedance of the adjacent line. This effect is repeated as the wave finds new boundaries, but the phenomenon is attenuated because the wave loses intensity with each impact.

The magnitude and distribution of TWs arrivals are affected by fault location, reflection coefficient and system topology. Therefore, a relay located on the bus L of the L-R transmission line (see Fig. 3.2) detects the second impact of the reflected wave on the fault after several previous arrivals. The impact caused by reflection on the fault takes 2τ time as shown in points 1 and 2 of the red color in the Fig. 3.2(a) for an internal fault and the Fig. 3.2(b) shows for external fault (line R-T). This phenomenon leads to distortion of the base signal and is associated with a period, which implies the presence of the frequency of the traveling wave.

In order to calculate the period of this signal the reflection coefficient (Γ_{TW}) plays an important role. In a test system as shown in Fig. 3.3(a), there are two possibilities, when the TW impacts the Bus L. The reflected



(a) Internal fault.



(b) External fault.

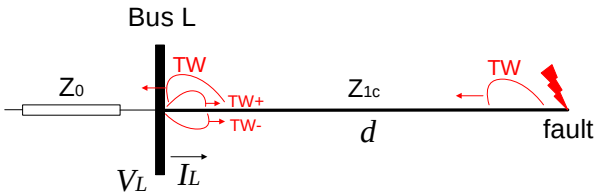
Figure 3.2: TW reflection and refraction - Lattice diagram.

wave may be positive sign or negative sign. This is determined by the relationship between the characteristic impedances of the two media as

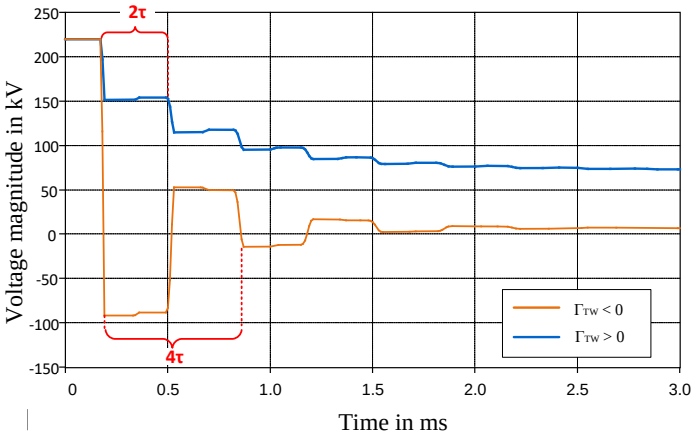
shown in the equation (3.1).

$$\Gamma_{TW} = \frac{Z_{1c} - Z_0}{Z_{1c} + Z_0} \tag{3.1}$$

where, Z_{1c} is the characteristic impedance of the main line and Z_0 is the characteristic impedance of the adjacent line.



(a) Fault in the main TL.



(b) TW features at bus L.

Figure 3.3: Period of the signal for different reflection coefficient sign.

If Z_0 is greater than Z_{1c}, the TW back to the fault with negative sign;

otherwise, if Z_0 is smaller, the TW back to the fault with a positive sign. In the first case, the impact of the TW on the fault must be repeated twice to return to the initial case, this means that to repeat the cycle 4 τ seconds must elapse. While in the second case, the impact of the wave on the fault must be repeated once to return to the initial case, the cycle is completed in 2 τ seconds. This fact can be clearly identified in the Fig. 3.3(b). As a result, the traveling wave frequency is the inverse of their period as shown in equation (3.2) and (3.3).

$$Freq_{fault} = \frac{1}{4\tau} \quad [Hz], \quad Z_0 : large \tag{3.2}$$

$$Freq_{fault} = \frac{1}{2\tau} \quad [Hz], \quad Z_0 : small \tag{3.3}$$

where, τ is the wave travel time from fault to bus L and it is determined by the equation (3.4).

$$\tau = \frac{d}{v} \quad [seg] \tag{3.4}$$

where:
d: is the fault distance in [km].
v: is the TW speed in [km/seg].
The TW's speed (v) and the line's characteristic impedance are determined by the inductance (L) and capacitance (C) of the TLs as shown in equations (3.5) and (3.6).

$$v = \frac{1}{\sqrt{LC}} \quad [\frac{km}{s}] \tag{3.5}$$

$$Z_{1c} = \sqrt{\frac{L}{C}} \quad [Ohm] \tag{3.6}$$

As an example, the theoretical curve can be determined with the following values of a transmission line: $L = 0.8467\ mH/km$ and $C = 0.014\ uF/km$, representative values for 220kV transmission line, then $v = 290450\ km/s$ and $Z_{1c} = 245.92\ Ohm$. The frequency values associated with the fault distance are determined for both period cases as shown in Fig.3.4.

Consequently, the predominant frequency of the signals indicates the fault location, so it is important to visualize the decomposition of the signals for different frequency bands.

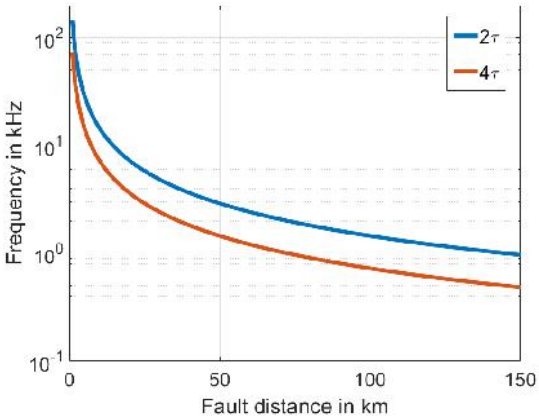


Figure 3.4: Transient fault frequency ($Freq_{fault}$) vs fault distance (d)

3.2.2 Attenuation of high-frequency transient

The attenuation effect of the signals is caused by the change in behavior of the frequency-dependent elements [94; 95]. In the case of high-frequencies, while inductive impedances present very large values, capacitive impedances present very small values. This effect causes the propagation of signals to be conducted through capacitive impedances between a busbar and ground. The high-frequency current transients generated by electrical faults are attenuated as they propagate along the transmission system.

Equipments with capacitive impedance such as reactive compensation (ECR), capacitor bank, parasitic capacitance of the busbar with ground (Cs) and even the presence of AC filters to restrict harmonics are the elements that influence this effect (Fig. 3.5). In this sense, shunt capacitance becomes a predominant factor in network impedance as high-frequency components are lost to ground. As a consequence, the transient signal of internal faults contains more significant high-frequency components compared with external faults.

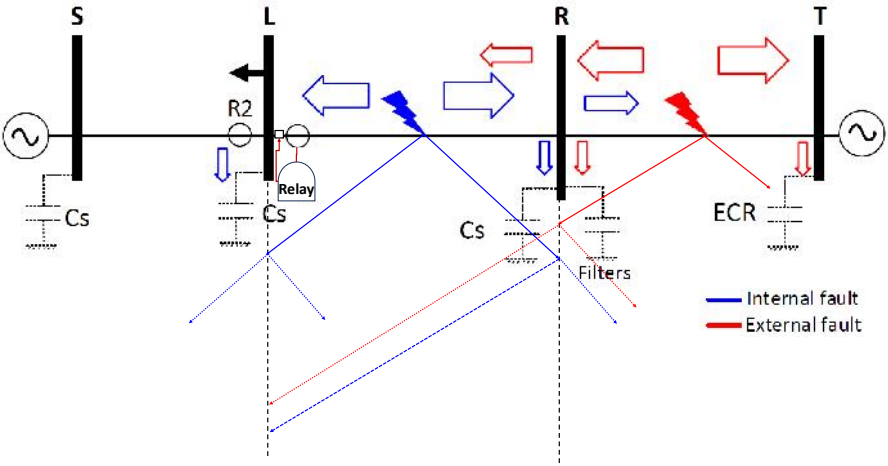


Figure 3.5: Attenuation of high-frequency transient

3.3 High frequency transient signals caused by the inverter

Inverter power electronics have different components in their design that make it not easy to accurately describe their behavior. Moreover, since the power electronic converter always operates in Pulse Width Modulation (PWM) mode, there are several nonlinearities and uncertainties that are difficult to describe through mathematical models [96]. In view of this, it is necessary to describe the general characteristics of processes or components that could affect the behavior of high-frequency signals during electrical faults in the grid. In that sense, in [96] indicate that the fast movement of current carriers inside semiconductors produces transients that are completed in $ns - \mu s$ time intervals.

The EMT in converters covers a wide range of time scales due to different components in the power electronics design as shown in Fig. 3.6. This is due to the fast EMT in the switching process, the system is strongly influenced by the transient behavior of the power switch.

In addition, the response times of the transient processes is related

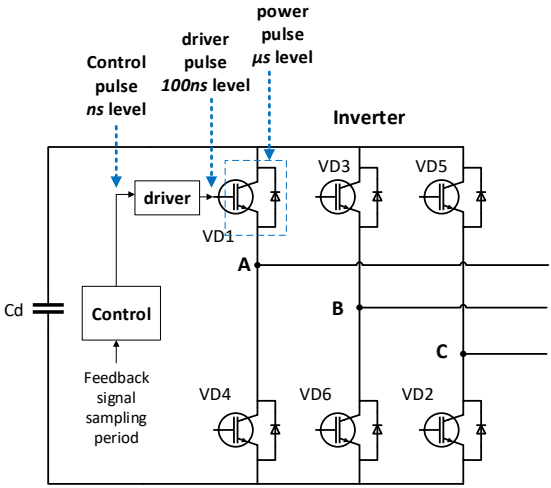


Figure 3.6: Time constant of the transient loops

to the time constant for the different control loops. Therefore, if these intervals become the domain of frequency, we get the relation shown in Table 3.1.

Table 3.1: Relationship between time response and frequence

	Response time	Frequency
Switching loop	$\sim$ 100 ns	$\sim$ 10000 kHz
Switching loop with bus-bar parasitics	$\sim$ 200 ns	$\sim$ 5000 kHz
Switching loop with the snubber circuit	$\sim$ 2.5 us	$\sim$ 400 kHz
DSP (digital signal processors) control loop	$\sim$ 156.3 us	$\sim$ 6.4 kHz

The switching on of converters causes the emission of harmonics caused by PWM in the frequency range of 2-150 kHz, also known as supra-harmonics [97; 98; 99]. However, with the implementation of LCL filters

and the step-up transformer at the power plant output, it is possible to minimize or mitigate this effect in transmission systems, but there are limited noise contributions to the high-frequency signal; therefore, this consideration is essential.

The Fig. 3.7 shows the representation of an LCL filter installed with an inverter.

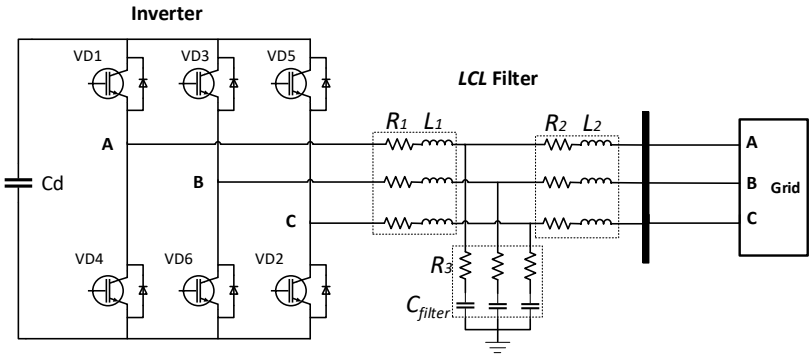


Figure 3.7: LCL filter configuration

where inductive (L_1) restricts the inverter's output current harmonics, while capacitive (C_{filter}) is used to provide the path for high-frequency current components and inductive (L_2) is used for attenuation. The LCL filter design considers that the resonant frequency (f_r) should be in the range of $10f_0 \leq f_r \leq f_{sw}/2$, where f_0 is the fundamental frequency of the network (50 or 60 Hz) and f_{sw} is the switching frequency (Aprox. 10 kHz). In addition, this filter is tuned to the inverter characteristics. Conventional LCL filters are designed to consider harmonics only up to 2.5 kHz, which is the harmonic range considered in existing harmonic regulations [100]. Also, the selected frequency is preferably below 3 kHz, since the bandwidth of the current loop is usually smaller than this, so that the effect of control strategies can basically be ignored [101].

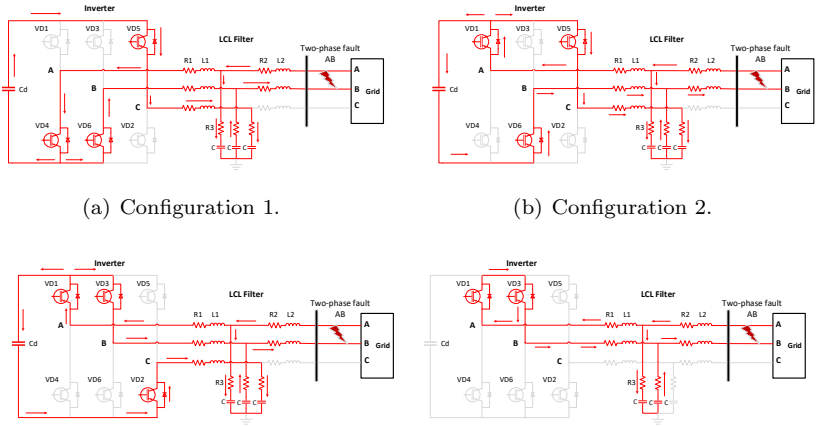
Therefore, it is essential to use the LCL equipment because its main purpose is to filter high-frequency components in the network and the filters have a damping circuit in order to meet the requirements of the

THD of the network [102].

3.3.1 Inverter response due to a short circuit

This section analyzes the high-frequency transient response of the drive. The high frequency impedance characteristics of the IBR are mainly dominated by the LCL filter, the Cd capacitor, and the switching key. The filter consists of R_1, L_1, R_2, L_2, R_3, and C. The switching keys create paths for the current [103].

The fault current flows by the inverter and through all three phases (see Fig. 3.8). Based on the fault current paths, the equivalent impedance of the IBR can be calculated for different frequency ranges. The different topologies are presented for the case of a two-phase short circuit, the circuit is dismembered into four topologies as shown in Fig. 3.8. A ground fault is not analyzed because the inverter does not have a ground return.



(a) Configuration 1.

(b) Configuration 2.

(c) Configuration 3.

(d) Configuration 4.

Figure 3.8: Configurations of the four fault current paths for a two-phase fault.

The four impedance configurations represent the possible structures of each loop for all the different inverter switching conditions. For the

purposes of this thesis, it is noted that under fault conditions, the IBR has a high-frequency impedance value defined only by the LCL parameter and is not affected by the settings of the power control system [69; 104]. The four SCC paths can be represented by the following configurations based on electrical circuits (see Fig. 3.9).

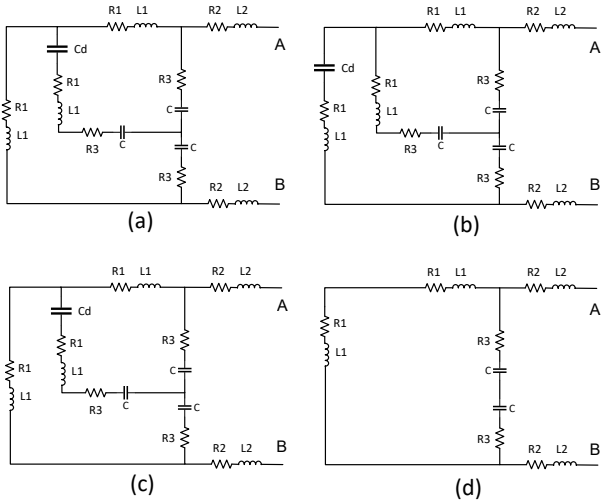
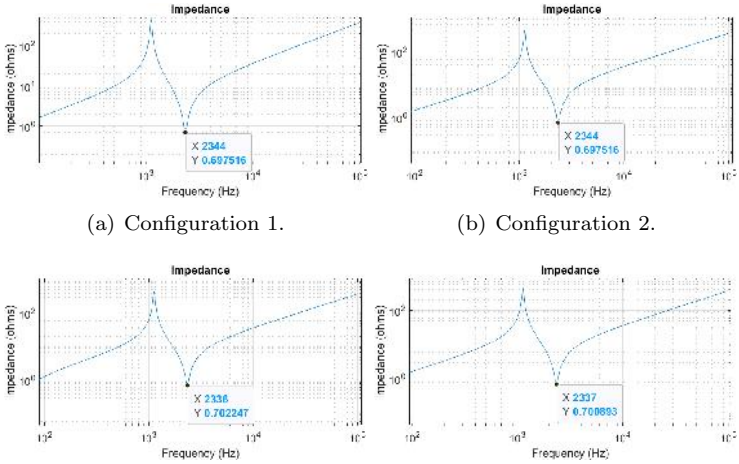


Figure 3.9: Circuit configurations for fault current pathways

The impedance magnitude behaviour of each configuration is determined for different high-frequency values as shown in Fig. 3.10 (the parameter were used from the Table. D.3). In all cases, the impedance's features are similar to magnitude variation ranges between 1100 Hz to 2350 Hz due to its design. Consequently, the impedance value is dominated by inductance at relatively low frequencies and by capacitance at relatively high frequencies.

The impedance of the step-up transformer is added to the characteristic of this impedance, so that the effect on the transmission network is reduced; in addition, the effect of the LCL filter causes a peak in the current signal with no associated frequency, which does not affect the transient behavior caused by traveling waves.



(a) Configuration 1. (b) Configuration 2.

(c) Configuration 3. (d) Configuration 4.

Figure 3.10: Impedance magnitude behavior.

3.4 Conclusions

The analysis of transient signals caused by short circuits involves the analysis of the traveling wave behavior on transmission lines. It has been shown that the effect of traveling waves produces a periodic distortion in voltage and current signals at high frequencies. Moreover, this transient generated by the short circuit implies a multiresolution matrix. In addition, the phenomenon of attenuation in transmission lines due to the increased capacitive effect of the system components causes the magnitude of the transient signals to change greatly between internal and external faults.

On the other hand, the behavior of the converters in the high frequency range is described in order to verify the effects on the transmission system. From a high-frequency point of view, the fundamental frequency voltage source and the harmonics generated by the IBR can be ignored. Finally, for a high frequency model the control system is not considered because the response time occurs after tens or hundreds of milliseconds, so it is long

term compared to the initial fault transient. Due to this fact, the high frequency model of an IBR will not change if it has different power control system settings and only the LCL filter model and the Cd capacitor are considered.

CHAPTER 4

Theorical models

This chapter describes the mathematical models used to develop a new digital filter for transmission line protection. This filter is based on mathematical morphology theory and the processing algorithm is based on a spectral energy index. In addition, the multiresolution signal in the time-frequency domain is determined.

4.1 Introduction

Microprocessor-based relays have allowed the rapid evolution of new signal processing techniques and the development of new protection algorithms, thereby improving performance and allowing the development of new methods to meet greater challenges, while incorporating economy and simplicity in their algorithm principles [105]. The development of protection schemes is closely related to the technological progress of signal processing, computer and communication technologies; therefore, their algorithms and/or protection schemes have evolved throughout history. In this regard, the trend of methods are associated with signal processing and are classified as: fault component protection, adaptive, traveling wave, transient, parameter recognition, artificial intelligence, among others. The fast progress of microprocessor technology and signal processing capabilities over time has made it possible to consider new processing

techniques that were impractical until a few years ago. This has included a growing interest in the use of transient signals and traveling waves generated by faults.

Techniques that filter the base signal and noise to obtain the information signal represent it in the time-frequency domain as described in [106], meanwhile in [93; 107] highlights that the behavior of the frequency spectrum of a fault provides information about its location and [108; 109] present protection analysis based on this theory. This shows the great relevance of the transient components analysis; however, these methodologies require an adequate digital signal filter.

In the electrical network, events such as electrical faults, especially short circuits, are unavoidable; therefore, protection equipment or Intelligent Electronic Device (IED) has the responsibility to detect, identify and remove the fault as quickly as possible; however, fault analysis of electrical networks has always been a challenging subject from different perspectives, since it involves aspects as detection strategies, information management and decision criteria. All these analysis methods require useful signal information, which in many cases mix with components that must be filtered, for this reason, the protection devices have a digital filtering stage of the signals prior to the protection algorithms and logics as shown in Fig. 4.1; these processes are constantly evaluated and improved by means of new methodological criteria. There are research works that address the use of protection techniques through the use of traveling wave signals originated by the short circuits, since they have verified that they contain enough information for their analysis. However, due to the broad spectrum of the high-frequency components, signal processing based on multiresolution techniques is necessary.

Multiresolution analysis (MRA) refers to breaking up a signal into components, it allows extracting signals features over a wide range of frequency spectra; therefore, the high-frequency signals generated by electrical faults (short-circuits) in transmission lines can be characterized. The extraction of fault information in different spectral frequency bands is achieved through MRA or multiscale approximation where the most employed technique is developed using the discrete wavelet transform (DWT) which was introduced in this context in 1988/89 by Stephane Mallat [110; 111]. However, although DWT has proven to be a good analysis method, it still presents certain weaknesses that have not allowed its implementation in real applications. Therefore, the development of a

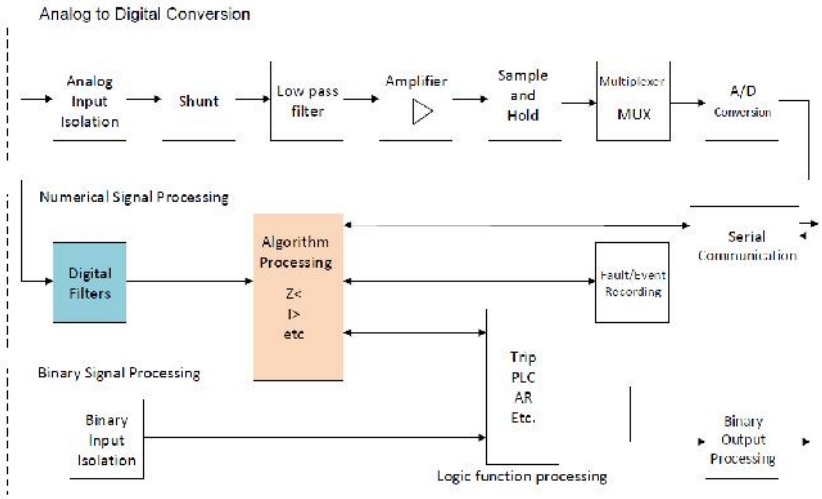


Figure 4.1: block diagram of the operation process of a relay

digital filter based on mathematical morphology (MM) is proposed in this chapter.

4.2 Digital filter

The description of the basic concepts of the mathematical morphology theory is described in Appendix C. Based on the MM theory, the concept of morphological digital filter for multiresolution analysis is proposed.

4.2.1 Digital Morphologic Filter (DMF)

With the aim of filtering noise from a signal, two morphological operators were developed in [112; 113], which gave good results and are therefore crucial for their use in this thesis. These are digital morphologic filter open-close and digital morphologic filter close-open using the same structuring element (SE) as shown in the equations (4.1) and (4.2).

$$DMF_{OC}f(x) = (f \circ g \bullet g)(x) \tag{4.1}$$

$$DMF_{CO}f(x) = (f \bullet g \circ g)(x) \tag{4.2}$$

where:
$f(x)$: Analysis function or input signal.
DMF_{OC}: Digital morphological filter closing and opening.
DMF_{CO}: Digital morphological filter opening and closing.
$g(x)$: Structuring element.

Due to the reduction of the opening operation, the output of the opening-closing filter becomes smaller, and due to the expansion of the closing operation, the output of the closing-opening filter becomes larger [112; 113]. Therefore, a new filter is built from the average value of the previous two filters shown in (4.1) and (4.2) as presented in (4.3).

$$DMF_g f(x) = \frac{DMF_{OC}f(x) + DMF_{CO}f(x)}{2} \tag{4.3}$$

where: DMF_g is the digital morphological filter with g as the structuring element.

4.2.2 Structuring element (SE)

The SE can take different shapes and lengths, this depends on the signal features to be analyzed. Some research proposes the use of a linear shape; however, it is possible to use geometrical shapes such as a triangle or sine, since transient signals do not have definite shapes. In this sense, the sine, triangle and linear function are shown in equations (4.4), (4.5) and (4.6), respectively.

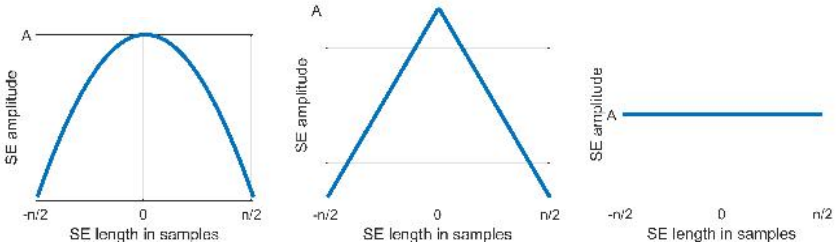
$$g(n) = A.sin(\frac{\pi}{2}(1 + \frac{Le}{n})), \quad Le = [-n/2 : n/2] \tag{4.4}$$

$$g(n) = A(\frac{2.Le}{n} + 1), \quad Le = [-n/2 : 0] \quad g(n) = A(\frac{-2.Le}{n} + 1), \quad Le = [0 : n/2] \tag{4.5}$$

$$g(n) = A, \quad Le = [-n/2 : n/2] \tag{4.6}$$

where:
A: is a constant that means the amplitude ($A > 0$).
n: is the level, wich represents the SE length ($n > 0$).

Le: is the SE length.
The Fig. 4.2 shows the different shapes of SE.



(a) Sinusoidal (b) Triangular (c) Linear

Figure 4.2: Structuring element shapes.

4.2.3 Multiresolution analysis (MRA) with mathematical morphology

Multiresolution analysis aims to obtain information for different frequency spectrums, this can be achieved by modifying the scale or length of the SE. The process begins by filtering the signal to a defined SE length (see equation 4.7).

$$f_1(x) = FMD_{g1}f(x), \quad H_1(x) = f(x) - f_1(x) \tag{4.7}$$

where f_1 is the filtered signal, g_1 is the SE at level "1" and H_1 represents the first multiresolution signal. This analysis is repeated for g_2 with a new SE length (see equation 4.8).

$$f_2(x) = DMF_{g2}f_1(x), \quad H_2(x) = f_1(x) - f_2(x) \tag{4.8}$$

It is developed in a similar way for the following levels, therefore, it can be generalized as shown in the equations (4.9) and (4.10):

$$f_n(x) = DMF_{gn}f_{n-1}(x), \quad H_n(x) = f_{n-1}(x) - f_n(x) \tag{4.9}$$

$$f = f_n + f_{n-1} - f_n + ... + f_1 - f_2 + f - f_1 \tag{4.10}$$

where n is the resolution level

Regarding the length of the SE, it indicates the level of resolution (see Fig. 4.3) because the SE length variation is associated with a transient signal frequency ($Freq$), see equation 4.11. It also depends on the sampling frequency of the signal (Fs), see equation 4.12.

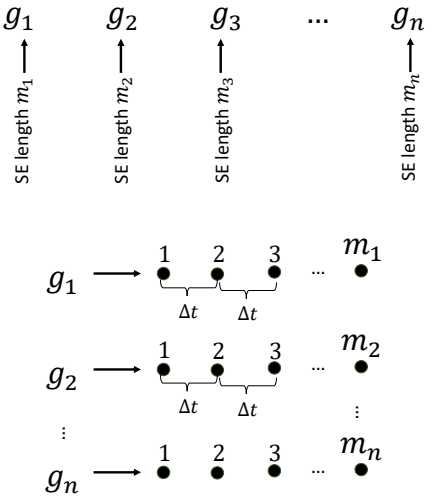


Figure 4.3: Relationship between the SE length and the time interval between samples

where m is the number of samples of each level n

$$Freq = 1/(m_n \Delta t) \tag{4.11}$$

$$\Delta t = 1/Fs \tag{4.12}$$

This definition is the basis for the construction of the multiresolution matrix (MRM). On the other hand, it is known that the relationship between SE length, frequency and fault distance is represented by the sequence shown in Fig. 4.4.

The SE length is measured in samples whereby its length depends on the sampling frequency. For a frequency of 1 MHz, 0.5 MHz and 100 kHz

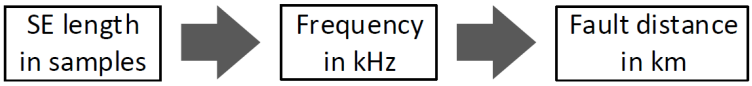


Figure 4.4: Relationship between SE length, frequency and fault distance

the following behavior is presented in Fig. 4.5. It shows the relationship of the multiresolution signal frequencies (kHz) with the SE lengths (samples). According to the Shannon Nyquist theorem [114], the sampling frequency must be greater than double the highest frequency component of interest in the measured signal, then the maximum frequency component will be 500 kHz, 250 kHz and 50 kHz for each case respectively. This does not affect the development of the method since the short circuits are in the frequency range below these values. It is important to note that in all cases, frequencies above 250 Hz are considered. A characteristic of the morphological filter is the use of high resolution for different frequency bands as opposed to the wavelet transform.

The values represented by 2000, 1000 and 200 are the number of maximum samples of the SE length for each case respectively. However, for the purposes of this study, only 120 levels of resolution are considered. In addition, in order to avoid the use of high levels of multiresolution, which could require high computational costs, a differentiator in the extraction of SE samples is performed. The length of the SE is set as a function of the sampling frequency of the signal, for a frequency of 1 MHz, lengths spaced at 10 samples (*step*) are considered as shown in Fig. 4.6.

In the case of a sampling frequency of 500 kHz, the SE lengths are spaced in 5 samples (*step*) as shown in Fig. 4.7. It should be noted that the signal size is N=2500 samples.

Finally, in case of a sampling frequency of 100 kHz, the SE lengths are spaced in 1 sample (*step*) as shown in the Fig. 4.8. It should be noted that the signal size is N=500 samples.

However, for values below 100 kHz of the sampling frequency, the maximum SE length will decrease, which means that lower resolution levels (< 120) should be used.

The number of resolution levels is user-defined, which implies that for high resolution values, precision is increased and speed is decreased; while

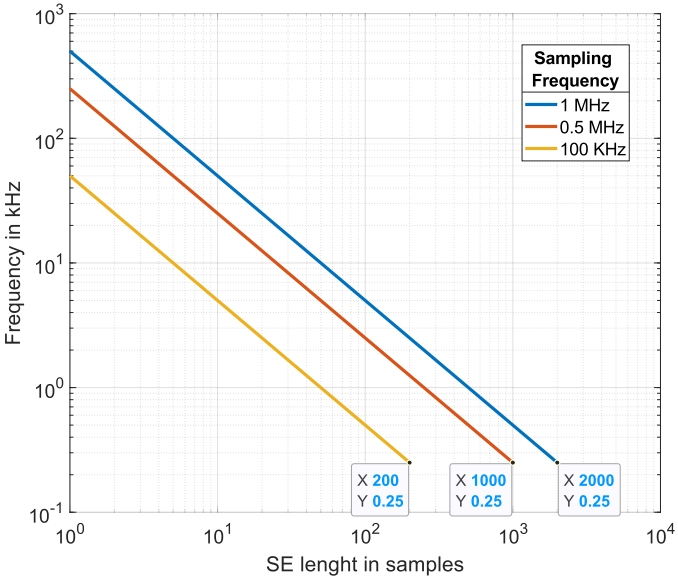


Figure 4.5: Multiresolution signal frequencies vs SE length

for lower resolution levels, speed is increased and precision is decreased.

4.3 Processing algorithm

4.3.1 Spectral energy index (SEI)

The spectral energy index is determined as the sum of the squares of the instantaneous voltage or current signal values as shown in equation (4.13).

$$SEI_i = \sum_{k=1}^{N} H_i^2 k \triangle t \tag{4.13}$$

where SEI_i is the spectral energy for a level i, H_i is the multiresolution signal (voltage or current) for level i, k is the index, N is the number

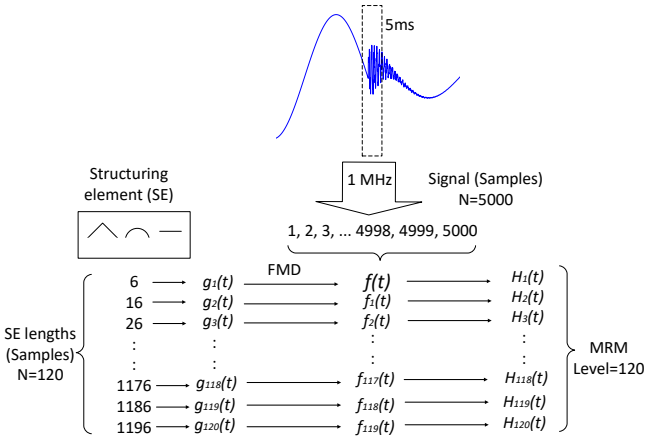


Figure 4.6: Relationship between SE length and Sampling frequency (1 MHz)

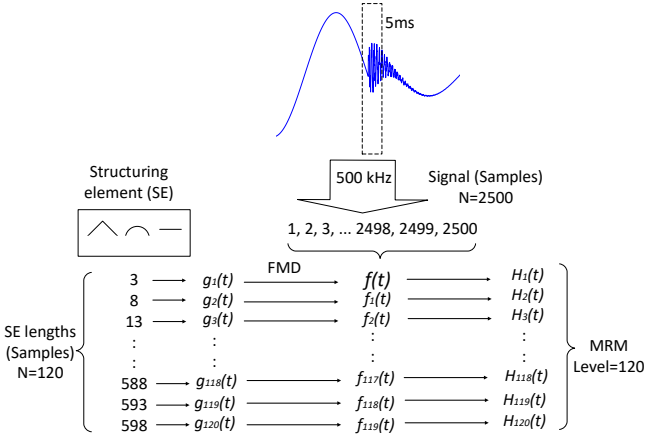


Figure 4.7: Relationship between SE length and Sampling frequency (500 kHz)

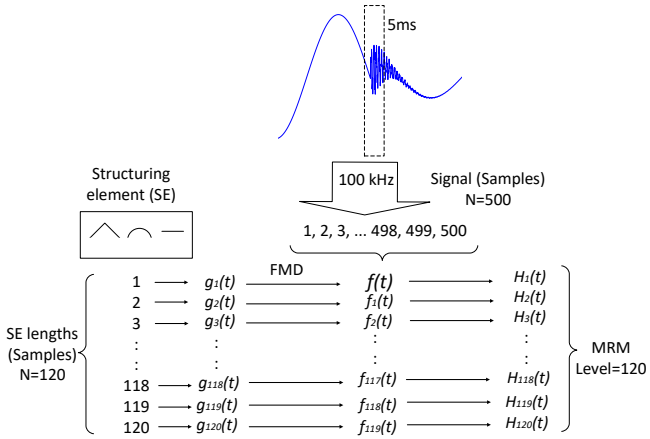


Figure 4.8: Relationship between SE length and Sampling frequency (100 kHz)

of samples for a time window and $\triangle t$ is the time interval of the signal which depends on the sampling frequency. The SEI calculation helps to determine the fault location, thus internal and external faults can be identified. In addition, the voltage and current signals used are in pu, so the SEI is also measured in pu.

4.3.2 Time-frequency domain signal calculation

The spectral frequency value indicates the reference of fault location, therefore, a method for transmission line protection based on frequency calculation is proposed.

The sequence for calculating the signal in the time-frequency domain is as follows:

- The process starts with the monitoring of voltage and current signals on a transmission line.
- The three-phase signals are read from the system through an IED. These signals are extracted at a certain sampling frequency through of analog/digital equipment (A/D conversion). However,

this method can be adapted to devices with different sampling frequency.

- An analysis time window of 5 ms is proposed, this time window can increase or decrease. These values are less than the time used by traditional relays.

- The three-phase signals (abc) are transformed to modal signals ($\alpha\beta 0$) by means of the Clarkes transformation [115; 116].Where the subscript 0 means for the ground mode quantities, being α and β related to the aerial mode signals as shown in equations (4.14) and (4.15).

$$f_{\alpha\beta 0}(t) = 2/3 \begin{bmatrix} 1 & -1/2 & -1/2 \\ 0 & \sqrt{3}/2 & -\sqrt{3}/2 \\ 1/2 & 1/2 & 1/2 \end{bmatrix} \begin{bmatrix} f_a(t) \\ f_b(t) \\ f_c(t) \end{bmatrix} \tag{4.14}$$

$$f_{abc}(t) = \begin{bmatrix} 1 & 0 & 1 \\ -1/2 & \sqrt{3}/2 & 1 \\ -1/2 & -\sqrt{3}/2 & 1 \end{bmatrix} \begin{bmatrix} f_\alpha(t) \\ f_\beta(t) \\ f_0(t) \end{bmatrix} \tag{4.15}$$

- In the digital filter block the maximum resolution level and the geometrical shape of the SE are set (see equations 4.4, 4.5 and 4.6). The process starts with the level "$n = 1$" where the SE length is determined. Afterwards, the signal is transformed by means of the DMF (see equation 4.3), then "H_n" is determined (see equation 4.7). Finally, the spectral energy of the latter signal is calculated (see equation 4.13), this information is stored in an MRM.

- It is verified that the n level of analysis is less than the maximum set level M.

- If it is satisfied that $n < M$ the process is repeated for the next level.

- Finally, the multiresolution signal is extracted in the time-frequency domain. The flow chart is shown in Fig. 4.9.

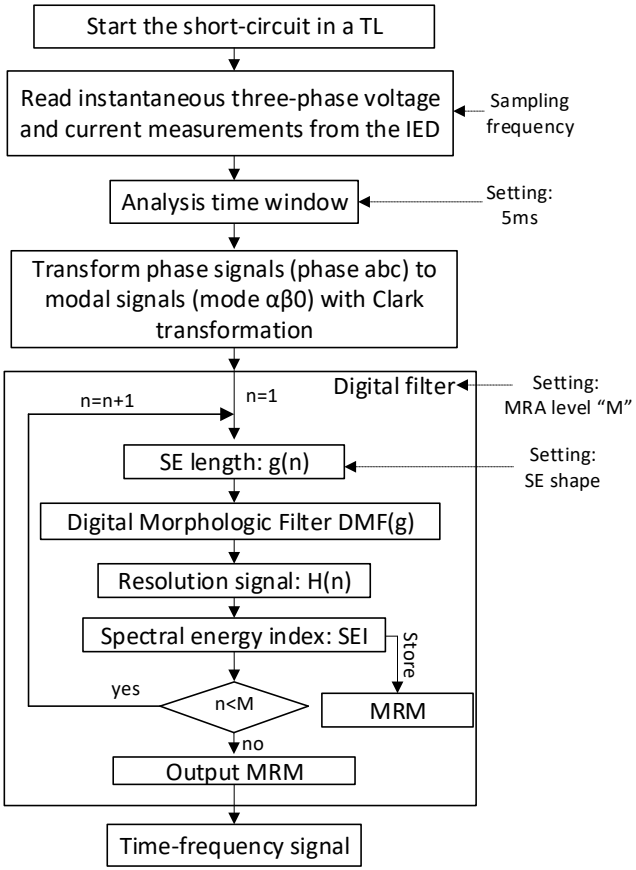


Figure 4.9: Flow chart of the digital morphological filter proposed method

4.4 Conclusions

This chapter develops the theoretical models of this work. It is based on the development of a digital filter for protection devices using a morphological filter. The characteristics of the structuring element, the process of

obtaining the multiresolution signals and the relationship between the SE length with the frequency of each resolution signal are verified. In addition, it is presented for different sampling frequencies and the differentiation process to avoid high computational cost. On the other hand, the algorithm processing based on the spectral energy index and the time-frequency domain signal are developed in order to identify the protection zones through frequency values.

CHAPTER 5

Development of protection algorithm

This chapter describes a method for identifying the fault zone based on frequency thresholds and maximum spectral energy index, and includes a diagram of the protection logic sequence. In order to verify the adequate performance of the protection scheme, many short circuit simulations are developed for different electrical systems.

5.1 Introduction

Short circuits in electrical networks has always been a challenging topic from different perspectives as it involves aspects such as detection strategies, information management and decision criteria [117]. All these analysis methods require useful signal information, which in many cases are superimposed by components that must be filtered. Therefore, protection devices perform a digital filtering process prior to execution by means of algorithms and logics; these methods are constantly evaluated and improved through new methodological proposals. In that sense, many research works approach the use of traveling wave signals originated by faults, since it has been verified to have enough information for the analysis.

The extraction of fault information in different spectral frequency bands has been developed using the wavelet transform [110]. The use of

wavelet transform was an alternative to process high-frequency transient signals as shown in [118; 119; 120; 121; 122; 123; 124] who analyzed signal behavior for different frequency spectrums. Many of these methods require only the TW arrival time information from the line terminals and use this transform to extract the peaks caused by the TW in the voltage or current signals. The difference between the arrival times of the two line terminals is then used to determine the location of the fault. However, this method requires a communication channel and suffers from the risk that the fault occurs at the moment of voltage zero crossing and the TW cannot be clearly identified [125]. On the other hand, methods based on multiresolution decomposition perform in a limited range of frequencies. This implies that the very high-frequency components are not observed and there is a risk of losing information, also the wavelet transform break down a signal into frequency bands, which does not allow obtaining high resolution. The techniques using mathematical morphology (MM) theory have become part of the study of transient signals, as indicated in [82; 126; 127; 128]. This technique develops a filter that suppresses noise mixed with the transient TW and resolves TW peaks, and it has been shown to be more efficient than the wavelet transform in filtering noise, but the transient behavior of high-frequency components for MRA was not studied in depth. The MM theory presents qualities to continue improving its methodological criteria and adapting to the applications required in power systems as mentioned in [129]. In this sense, the motivation arises to develop the MRA with high resolution and the lowest computational cost because it only uses basic mathematical operations and compares maximum and minimum points. In addition, it is emphasized that the morphological method is suitable for analyzing signals with nonlinear characteristics and has the ability to extract frequency components from point values.

The MRA obtained allows the traveling wave frequency to be determined and used as input for the distance protection logic. This protection scheme makes it possible to identify the fault zones and to coordinate them with the relays of the subsequent lines by setting a suitable time delay.

The signals are filtered using the DMF with different values of SE length due to the relationship between SE length, frequency and fault distance (SE length $\rightarrow$ Frequency $\rightarrow$ Fault distance) as described in chapter 4. Finally, this method works with a time window of 5 ms, which is

sufficient to cover the transient behavior.

5.2 Fault zone identification

In distance protection schemes, it is important to identify the zone corresponding to the short circuit. The zone 1 is set to cover the largest percentage of the protected TL, this implies that the time setting is set instantaneously. Zone 2 is set to cover the entire protected line and a percentage of the adjacent line, this implies that the time setting has a delay for coordination with the main relay of the adjacent line. To verify the setting of zone 1, it is based on the internal fault zone, i.e. inside the protection line. Zone 2 refers to the internal and external fault zone both viewed forward (see Fig. 5.1).

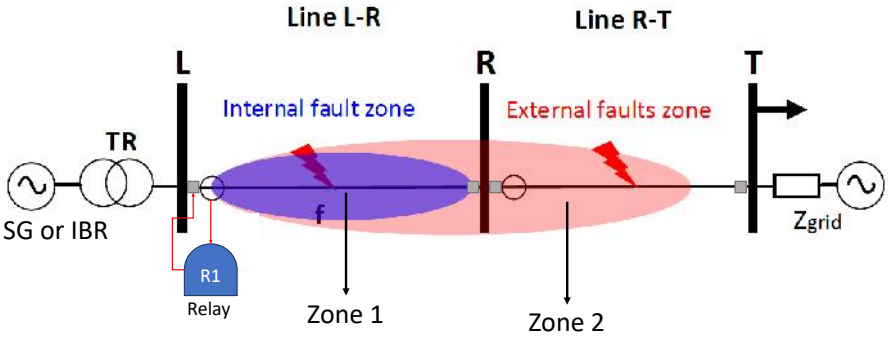


Figure 5.1: Fault zone identification

The boundary of both zones is used as a reference to define the protection threshold. Traditionally, protection equipment is based on the use of impedance. The experience has shown that there are always been errors of various types in the process of measurement, calculation or setting, which leads engineers to be more conservative in the definition of the threshold. Therefore, it is proposed to decrease the zone 1 slightly by

a percentage; in traditional relays, 20% is considered. For that reason a zone 1 is set to 80% of the total line impedance, to cover the rest it is set up to 120% of the line impedance.

In this sense, in order to define the protection threshold, various simulations were carried out with the characteristics of a generic system (see Appendix D.1). The Fig. 5.2 shows the behavior of the voltage signals for different fault locations, then the spectral energy index is determined as a function of frequency/distance as presented in the flow chart in chapter 4 (see Fig. 4.9).

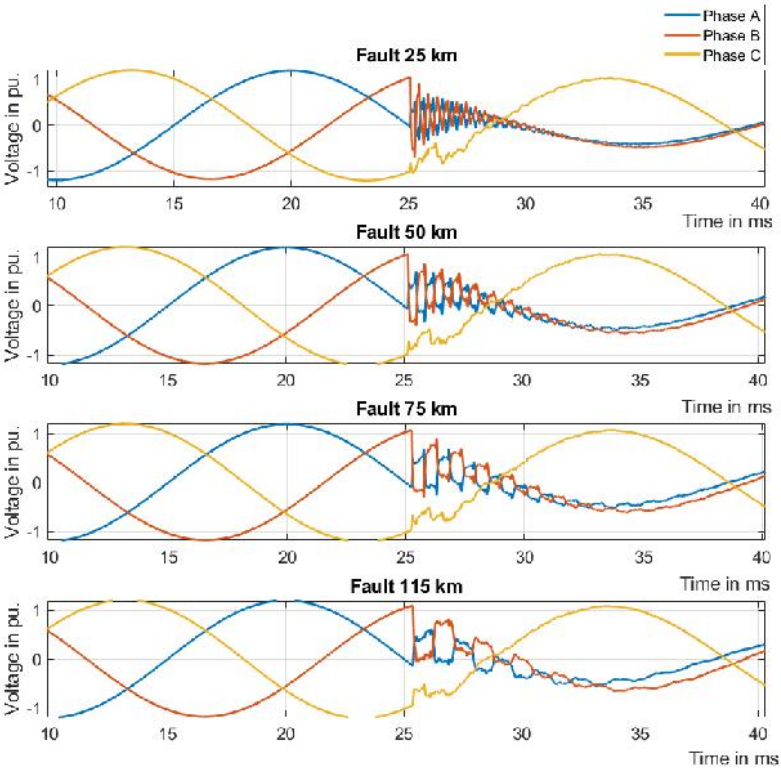


Figure 5.2: Simulation of a two-phase short circuit (AB) for four fault location

After performing the digital filter, the spectral energy index in each case is determined and the SEI characteristics in pu as a function of SE length/Frequency/Distance are shown in Fig. 5.3.

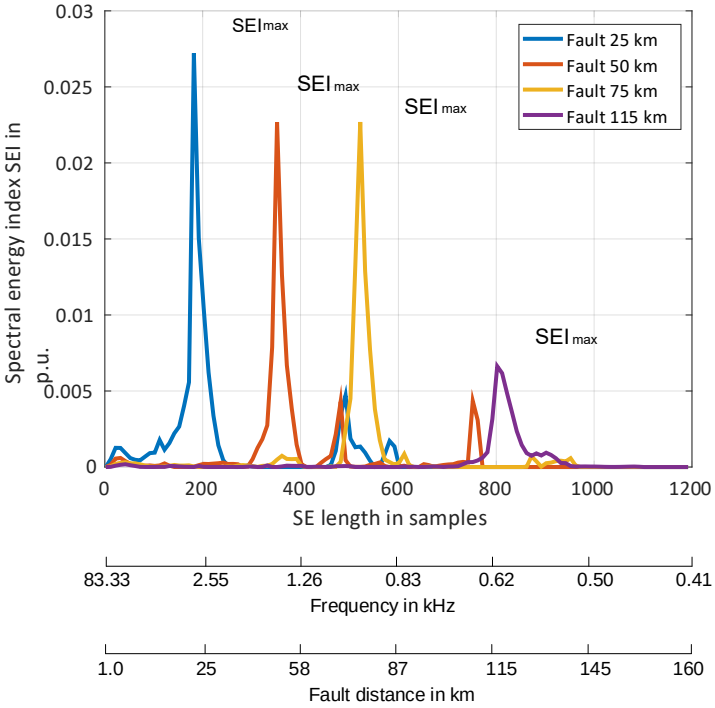


Figure 5.3: Spectral energy index for four different fault location

The relevant feature that highlights is the magnitude of SEI, as it decreases for far faults. The relationship between fault distance and signal frequency allows defining a frequency threshold that classifies internal and external faults. This can be calculated by a fault at the remote terminal on the line, i.e. a fault at terminal "R", therefore, a protection threshold can be defined at the boundary of the main line with the adjacent line, as

shown in Fig. 5.4.

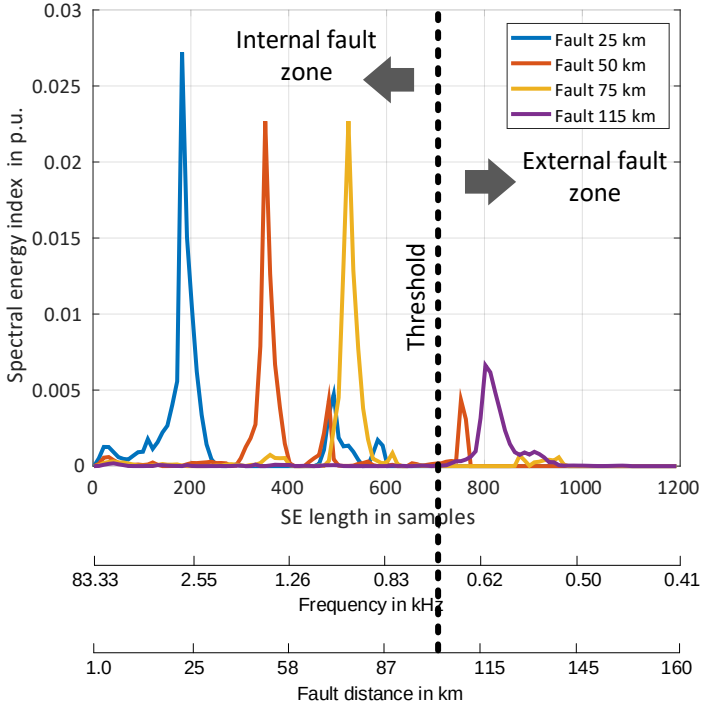


Figure 5.4: Fault zone threshold

Internal faults are defined as zone 1 and external faults as zone 2. However, as with traditional equipment, the zone 1 setting can be adjusted conservatively with an error between 5 to 10 %. Consequently, the frequency threshold is 90% of the frequency of the failed signal at the remote end.

When a fault is farther away and the fault conditions are unfavorable, the signals show more prominent noise due to the introduction of high frequency harmonics from many devices connected to the system and the

TW signals caused by reflections on elements of the electrical system, i.e. more reflections are produced when the fault is farther away. This causes more noise, which can greatly affect the characteristics of the high frequency signals. Consequently, in order to avoid this effect, apart from having a good digital filter, it is important to consider a SEI threshold that differentiates fault signals and noise as shown in the Fig. 5.5 (this image includes simulations of more distant faults).

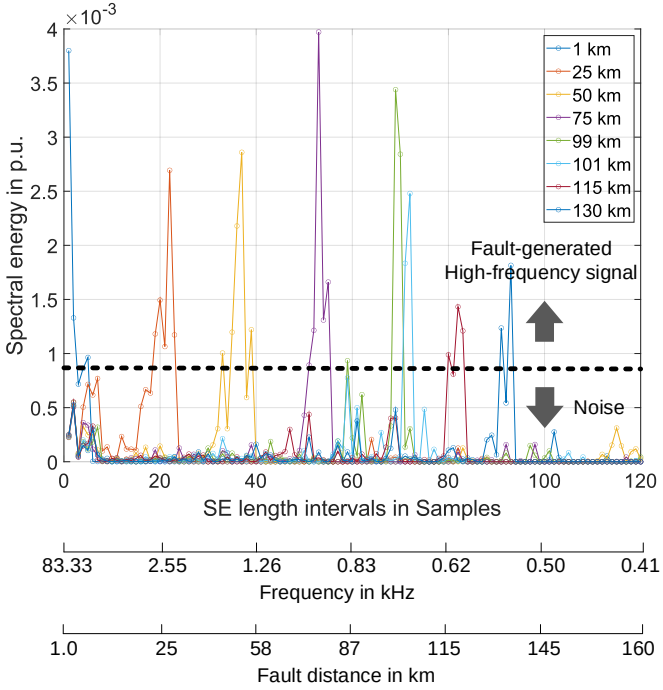


Figure 5.5: Spectral energy index threshold

The SEI threshold can be defined based on previous studies that identify extreme disturbances (worst-case conditions) along the main and adjacent transmission lines. The values of the SEI are verified and a threshold is defined at the limit where signals with lower values represent

noise. On the other hand, it is possible to define an SEI threshold for internal faults (Zone 1) and a threshold for external faults (Zone 2).

5.3 Logical protection scheme

From the previously calculated time-frequency signals described in the chapter 4, the maximum values are determined and compared with two thresholds. The frequency threshold and the spectral energy index threshold as shown in the Fig. 5.6. For this, it is necessary to set some parameters such as threshold spectral energy and threshold signal frequency.

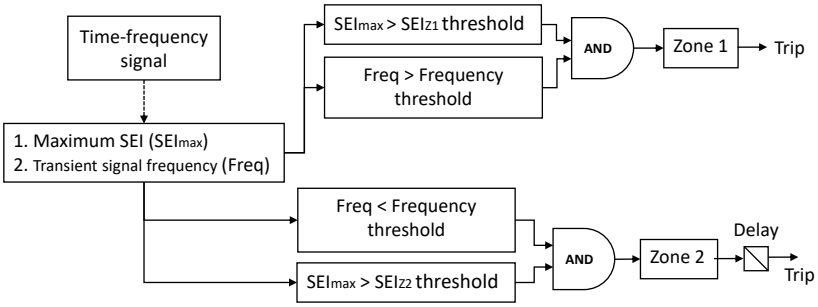


Figure 5.6: Diagram of protection scheme logic

where:

Time-frecuency signal: This is achieved through the process flow chart in Fig. 4.9

Maximum SEI (SEImax): This results from the peak values shown in Fig. 5.3

Transient signal frecuency (Freq): This is determined by the projection of the maximum SEI values onto the abscissa axis (see Fig. 5.3); and the relationship between SE length and frequency (see Equation. 4.11)

Frecuency threshold: This represents the boundary or limit of frequencies between internal and external faults, and is obtained by

simulating a short circuit on the remote bus, the frequency of the transient signal is determined from its theoretical curve (see Fig. 3.4). It is also a setting parameter.

SEIz1 threshold: This is determined by a previous evaluation with various internal faults (see Fig. 5.5). It is also a setting parameter.

SEIz2 threshold: This is determined by a previous evaluation with various external faults (see Fig. 5.5). It is also a setting parameter.

These parameters are determined in the following simulation analyses for more details.

5.4 Simulation analysis

5.4.1 Case study: Generic model of a power system using only synchronous generators

A 220 kV power system is developed in the ATP-Draw software for EMT simulations (Fig. 5.7). The lengths of the TLs are 100 km (L-R line) and 80 km (R-T line).

The power system model includes the tower configuration structure as shown in the Fig. D.1. In addition, these TLs were modeled using the frequency-dependent JMarti method. The IED, as a measurement device, is placed on the L bus facing the R bus (L-R). The characteristics of the network parameters are shown in the table. D.1 (See Appendix D.1).

According to the DMF parameters, 120 levels of multiresolution are used for this analysis, related to 120 lengths of SE (6-1200 with a step of 10 samples), this with the objective of having a good precision of the remote faults.

Factors affecting short circuit behavior:

- Fault resistance: values of 0.01Ω, 25Ω and 50Ω are considered.
- Fault inception angle or fault start time: it verified for 4 instants, considering values close to the maximum and minimum points, and instants close to the zero crossing.
- Fault location: 5 internal faults (1, 25, 50, 75 and 99 km) line L-R, 3 external faults (1, 15 and 30 km measured from R to T). For the last cases, the 100 km of the L-R line are added, resulting in distances of 101, 115 and 130 km from bus L.

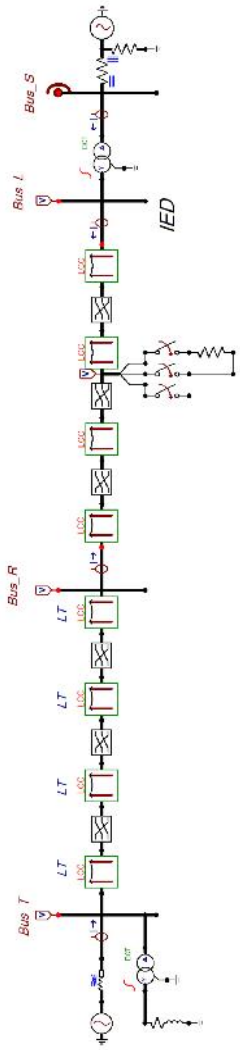


Figure 5.7: Generic model of a power system using only synchronous generators

- Noise: In order to verify the robustness against noise, white Gaussian noise with signal-to-noise ratio (SNR) about 20, 30 and 40 dB with very high frequency.

- Sampling frequency: 1MHz, 500 kHz and 100 kHz are considered.

- SE shape: Three different geometric shapes are considered (sine, triangle, and linear waveforms).

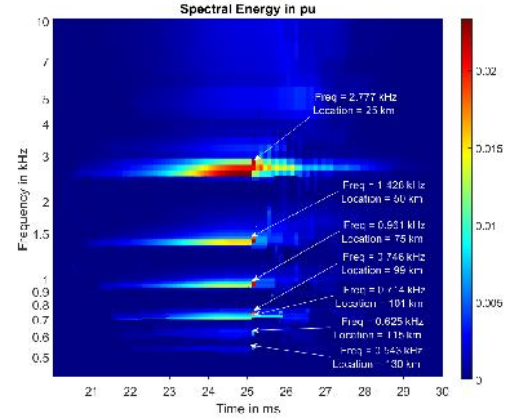
Fault distance analysis

The frequency of the transient signal depends on the location of the fault, as discussed in the theoretical section; therefore, it is essential to know the dominant frequency in the multiresolution analysis. For this analysis, faults with distances of 1, 25, 50, 75, 99, 101, 115, 130 km have been considered, and Fig.5.8a shows the characteristics of the cases in the time-frequency domain, where the predominant frequency spectrum for each case can be clearly identified. Another highlight is the magnitude of the SEI amplitude, which decreases as the fault moves away, as shown in Fig.5.8b.

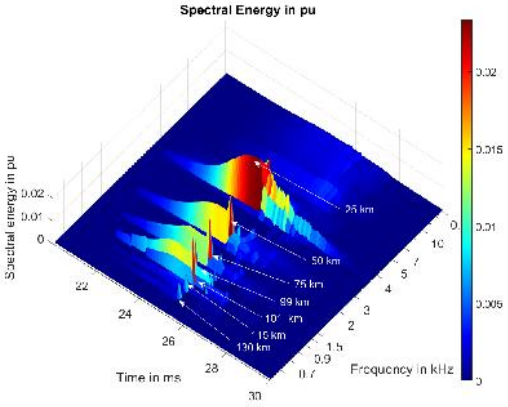
The values obtained are compared with the theoretical curve. Unlike the first case, the error percentages of the other cases are very low as it gives us a good accuracy of the fault location as shown in Fig. 5.9. With this method, the multiresolution signals can be set uniformly along the entire line and the step can be reduced for higher accuracy. However, this requires a higher computational cost, which could be used for an offline fault locator, while it is not necessary to identify fault zones for protection. On the other hand, the resolution can be reduced in the first kilometers of the line and increased at the end of the lines, this can be used in real time, allowing its use as a protection device that detects internal and external faults or a distance protection based on zones.

Influence of fault resistance (Rf)

The performance of the method is verified for a fault 50 km from the IED and with different fault resistances such as: 0.01Ω, 25Ω and 50Ω. The Fig. 5.10 shows the first case, where 0.0153 pu of the maximum SEI value is obtained.



(a) View 2D



(b) View 3D

Figure 5.8: Fault distance behavior

In the second case, the maximum value of SEI is 0.0138 pu, as shown in Fig. 5.11. This value is slightly smaller compared to the first case.

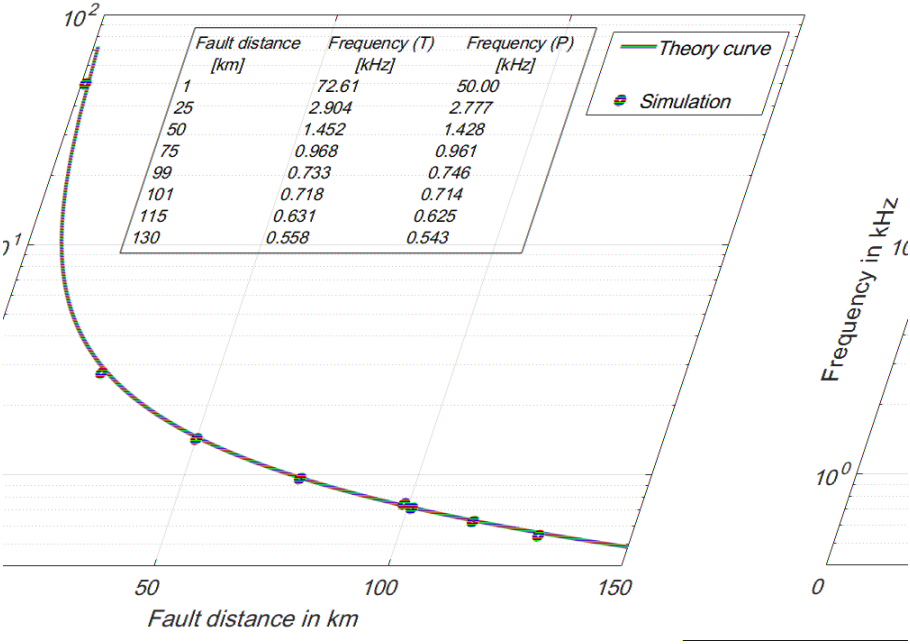
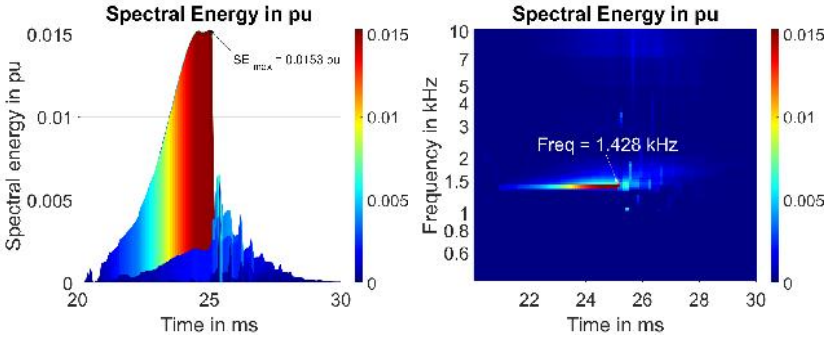


Figure 5.9: Comparison between simulated data and theoretical curve

In the latter case, the maximum value of the SEI is 0.0119 pu, as shown in Fig. 5.12. Although it can be seen that the SEI decreases for high resistance values, the characteristics of the time-frequency signals can be clearly identified, since in all cases the frequency of the fault signal is identified at 1.428 kHz, which represents a fault distance of 50 km on the theoretical curve.

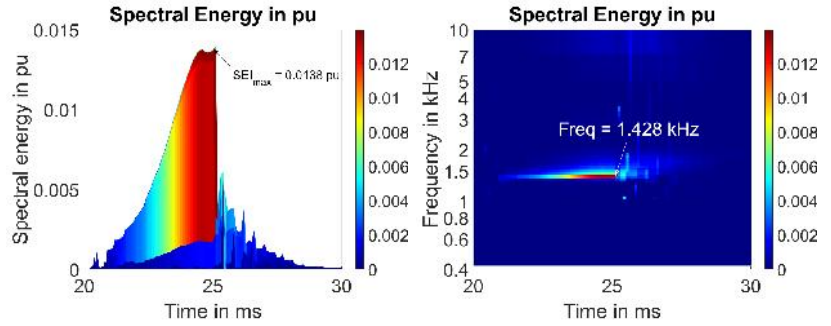
Influence of the inception angle or fault start time

The analysis of the TWs in the TL caused by short circuits involves the analysis of the TWs crest magnitude. Therefore, it is essential to consider the instant of the fault, since the faults very close to the zero-crossing of the voltage signal do not generate outstanding TWs. In this sense, the



(a) SEI vs Time (b) MRA Time-frequency

Figure 5.10: Time-frequency for Rf=0.01 Ohm.

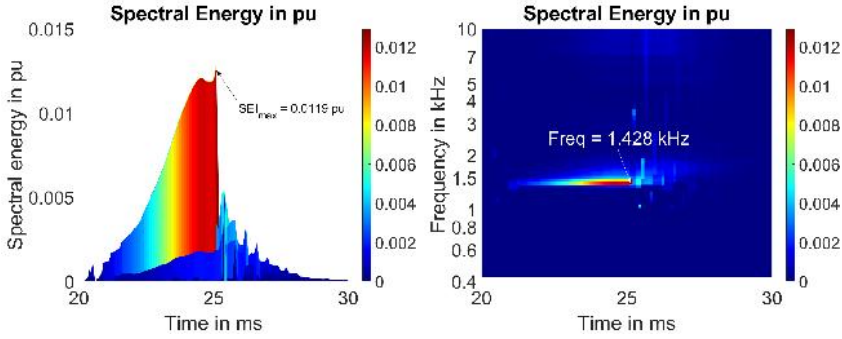


(a) SEI vs Time (b) MRA Time-frequency

Figure 5.11: Time-frequency for Rf=25 Ohm.

faults have been verified for different inception angles such as the negative half-cycles, positive half-cycles and near zero crossings as shown in Fig. 5.13 where fault start time are considered at 25 ms, 29 ms, 33 ms and 37 ms time.

In the first case, the high frequency component is prominent in the



(a) SEI vs Time (b) MRA Time-frequency

Figure 5.12: Time-frequency for Rf=50 Ohm.

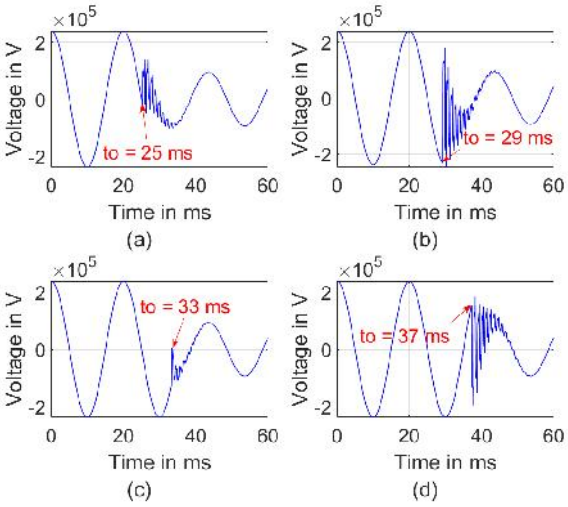
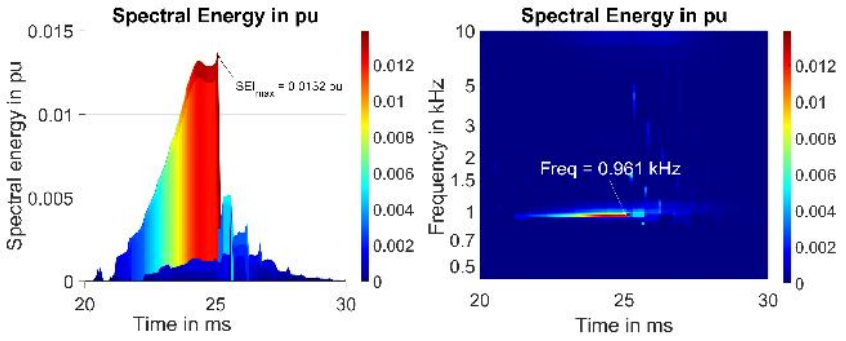


Figure 5.13: Voltage behavior on the L bus for different fault start time

MRA, and it is easy to identify the frequency because the maximum

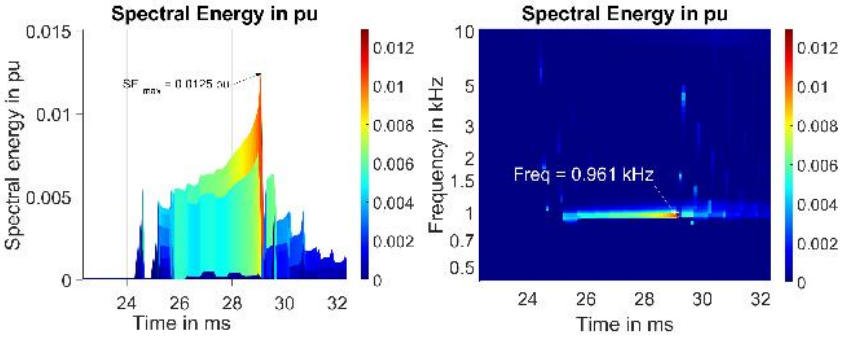
magnitude of the SEI clearly indicates that frequency. The figure 5.14 shows that the maximum magnitude of the SEI is 0.0132 pu.



(a) SEI vs Time (b) MRA Time-frequency

Figure 5.14: Time-frequency for fault start time: 25 ms

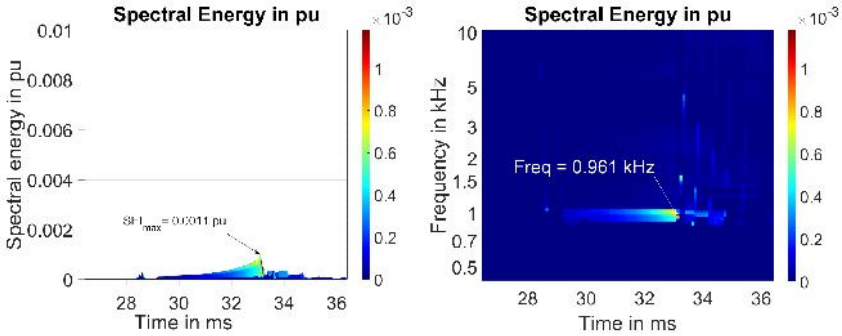
In the second case, high frequency signals are also highlighted and the maximum magnitude of SEI is 0.0125 pu. (Fig.5.15).



(a) SEI vs Time (b) MRA Time-frequency

Figure 5.15: Time-frequency for fault start time: 29 ms

The third case presents low levels in high frequency signals compared to the other cases, where the maximum SEI reaches 0.0011 pu as shown in Fig. 5.16a. However, in the time-frequency plot, it is possible to identify the frequency of the signal without distortion for all cases (Fig. 5.16b).



(a) SEI vs Time (b) MRA Time-frequency

Figure 5.16: Time-frequency for fault start time: 33 ms

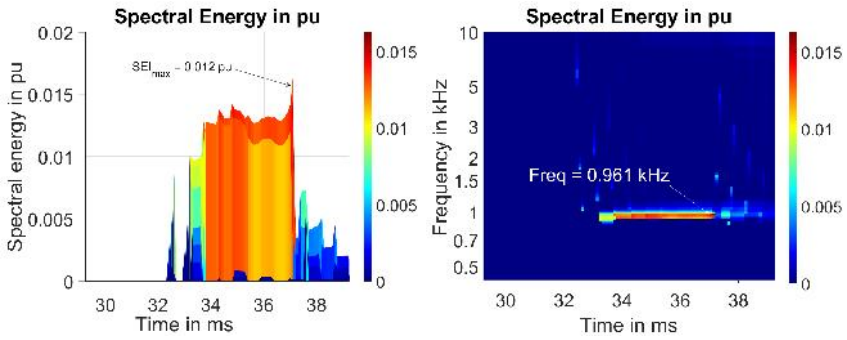
Finally, the fourth case also shows high levels of high frequency transient signals, where the maximum magnitude of SEI is 0.0120 pu. (Fig. 5.17).

The frequency of the signal component with the highest SEI for all the cases is 0.961 kHz and it corresponds to a fault 75 km distant. On the other hand, the magnitude of the SEI for the third case is smaller, which can be confused with distortions or noise due to very distant faults.

Influence of high-frequency noise

The noise comes from various sources in the electrical system, so this analysis takes into account the inclusion of white noise in the signals with SNR values of: 20, 30 and 40 dB with a very high noise frequency. To analyze the behavior of the signals at very high frequencies, the SEI is plotted as a function of frequency and the noise component is included in the signal.

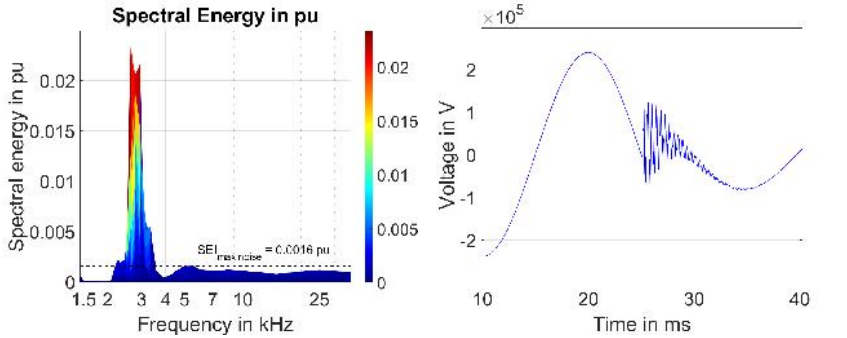
The maximum spectral energy of the signal without noise is 0.0016 pu



(a) SEI vs Time (b) MRA Time-frequency

Figure 5.17: Time-frequency for fault start time: 37 ms

as shown in Fig. 5.18. This value represents 8%, in terms of the maximum signal frequency, but this does not present a problem for the method.

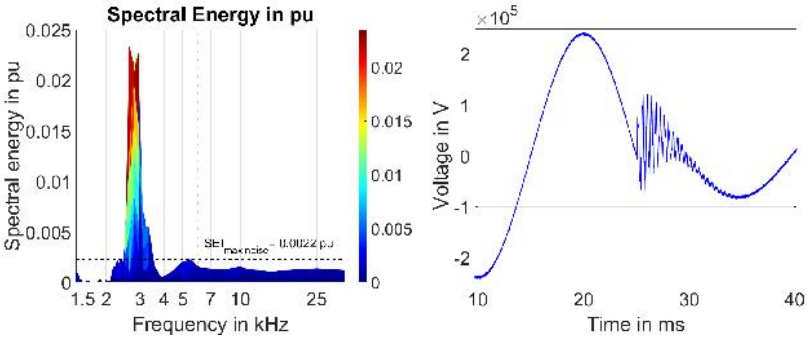


(a) SEI vs Frequency (b) Voltage signal

Figure 5.18: Without SNR

The signal with 40dB of noise has a maximum SEI of 0.0022 pu. This represents 8.8% of the maximum SEI of the signal which means that it

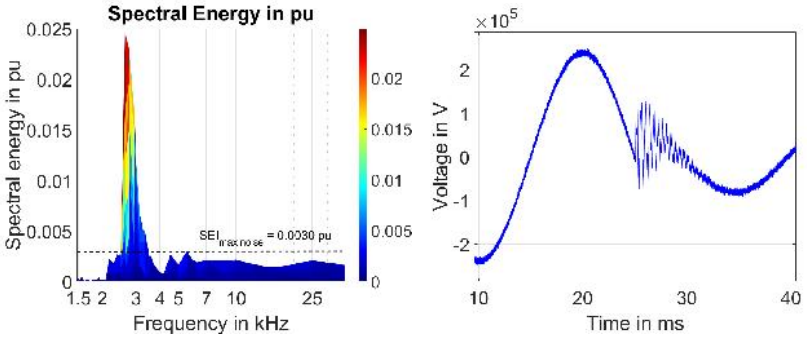
does not affect the method as shown in the Fig. 5.19.



(a) SEI vs Frequency (b) Voltage signal

Figure 5.19: With SNR: 40 dB

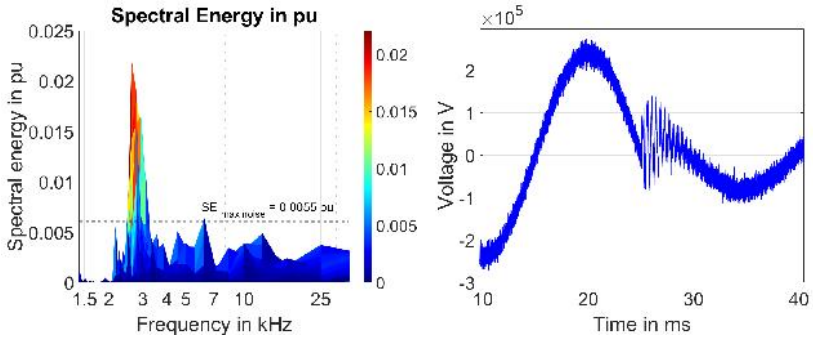
The signal with 30dB of noise has a maximum SEI of 0.0030 pu. This represents 12% of the maximum SEI of the signal as shown in the Fig. 5.20. Therefore, it is possible to clearly distinguish the analysis signal from the noise.



(a) SEI vs Frequency (b) Voltage signal

Figure 5.20: With SNR: 30 dB

The signal with 20dB of noise has a maximum SEI of 0.0055 pu. This represents 22% of the maximum SEI of the signal as shown in the Fig. 5.21. In this case, it is still possible to identify the signals, but it can be risky for distant faults with high fault resistance and inception angles close to the zero crossing.



(a) SEI vs Frequency (b) Voltage signal

Figure 5.21: With SNR: 20 dB

Influence of sampling frequency

As mentioned in the section of the theoretical model (see equations 4.11 and 4.12), the SE length is measured in samples, so it depends on the sampling frequency (Fs). A time window of 5 ms is considered in the analysis, then the relationship between sampling frequency and number of samples is shown in the table. 5.1 for three cases.

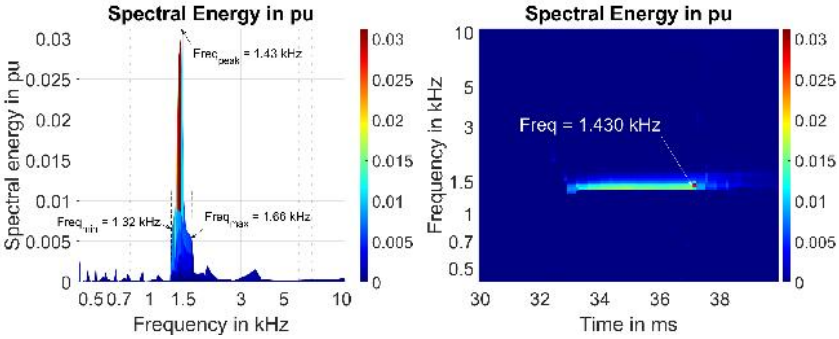
Table 5.1: Relationship between Fs and sample quantity

Sampling frequency	Sample quantity
1 MHz	5000
500 kHz	2500
100 kHz	500

Although the analyses developed above were performed with a sampling

frequency of 1 MHz. Only 120 multiresolution levels were considered, and these 120 levels were selected in a distributed manner to avoid high computational effort. When analyzing signals with a sampling frequency of 500 KHz, SE length values from 5 to 600 are considered in steps of 5 samples. Finally, when analyzing signals with a sampling frequency of 100 KHz, SE length values from 1 to 120 are considered in steps of 1 sample.

The Fig. 5.22 shows the results for a fault located at 50 km with a sampling frequency of 1 MHz. The peak frequency value is 1.430 kHz and the frequency ranges are [1.32-1.66] kHz.



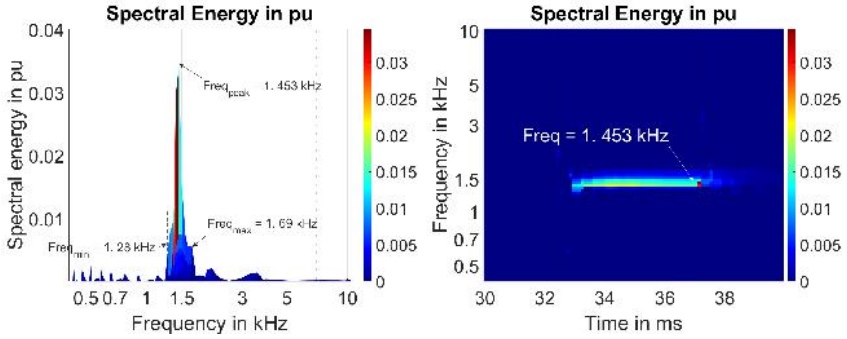
(a) SEI vs Frequency (b) MRA Time-frequency

Figure 5.22: Case Fs: 1 MHz

The Fig. 5.23 shows the results for a fault located at 50 km with a sampling frequency of 500 kHz. The peak frequency value is 1.453 kHz and the frequency ranges are [1.28-1.69] kHz.

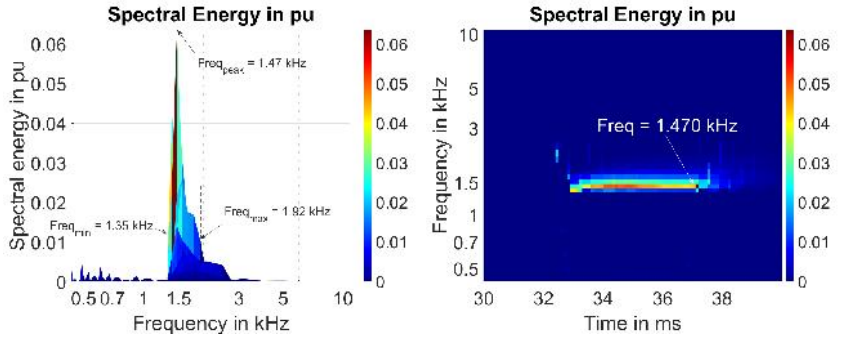
The Fig.5.24 shows the results for a fault located at 50 km with 100 kHz sampling frequency. The peak frequency value is 1.470 kHz and frequency ranges are [1.35-1.92] kHz.

Although the peaks are very close, the frequency ranges tend to increase as the sampling frequency decreases, with ranges of 0.34 kHz, 0.41 kHz, and 0.57 kHz, respectively. However, the expected signal frequency is 1.452 kHz. If even lower sampling rates are used, the multiresolution level will be less than 120, which may affect the accuracy of the fault location.



(a) SEI vs Frequency (b) MRA Time-frequency

Figure 5.23: Case Fs: 500 kHz



(a) SEI vs Frequency (b) MRA Time-frequency

Figure 5.24: Case Fs: 100 kHz

Influence of the type fault

According to the proposal of the International Electrotechnical Commission (IEC) and CIGRE, the frequency ranges of events in electrical networks are characterized as: ferroresonance (0.1 Hz - 1 kHz), fault clearing

(50 Hz - 3 kHz), line switching (50 Hz - 20 kHz) and lightning surges (10 kHz - 3 MHz) [130]. For this study, traveling waves caused by short-circuits are analyzed; however, there are other phenomena that cause traveling waves, such as lightning. This can be differentiated by the distortion and periodicity generated by the effect of the TW on the voltage and current signals due to short-circuits.

The simulations developed are two-phase short circuits (AB), since for the purposes of this study only the characteristics of aerial modal components are analyzed. This can be replicated in the ground modal component and thus identify the type of fault (three-phase, two-phase, two-phase to ground or single-phase to ground) [131]. For this, the modal loops must be analyzed, which is not part of the subject of this work.

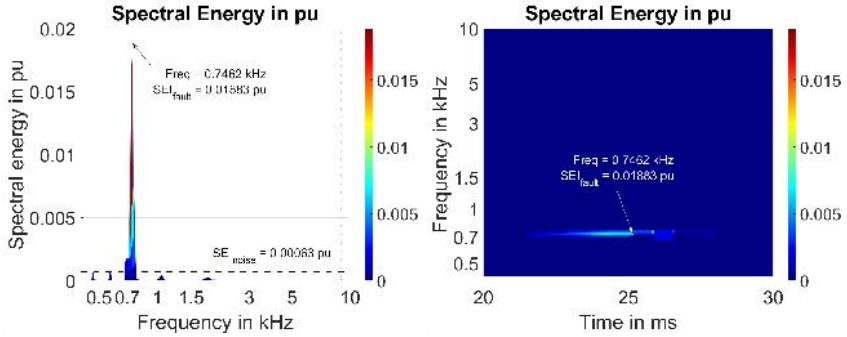
Influence of the SE shape

The shape of the SE is an important issue, since this function correlates with the main function. Based on the theoretical principles of the MM, the use of SE shapes similar to the main signal is proposed; however, the transient behavior caused by traveling waves presents a distorted characteristic where the impact of a TW causes a steep drop or rise in the signal and this changes each time more TW arrive. Since the main signal is treated as a one-dimensional function, the three geometric shapes described above are considered. These events were developed for a fault located at 99 km.

In Fig. 5.25, Fig. 5.26 and Fig. 5.27. It can be seen that the variation of the transient signal frequency is not so different, because in all three cases it is possible to identify the frequency value; however, the case of the linear function presents slightly more noise.

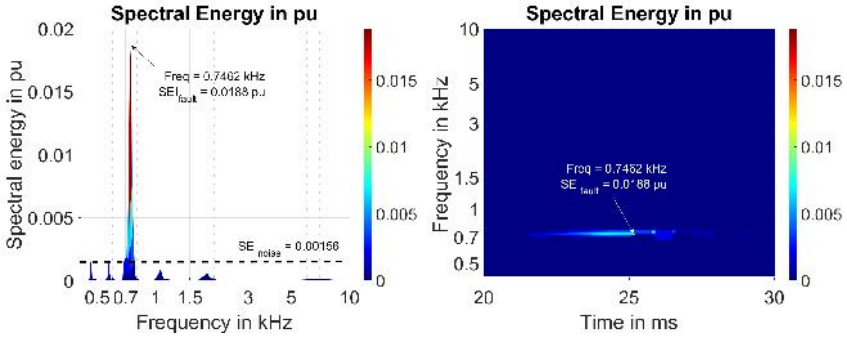
Voltage and current signal behavior

The cases that result in low voltage signal variance due to: low inception angle, high fault resistance or in the case of low bandwidth CVT, the high frequency components in the secondary voltage are further attenuated due to the associated transient response [132].Under such conditions, the magnitude of the TW voltage may be lower than the monitoring threshold, thus compromising the reliability of the protection scheme. In this sense, the current transient signal is also evaluated. On the other



(a) SEI vs Frequency (b) MRA Time-frequency

Figure 5.25: Case: SE shape sinusoidal

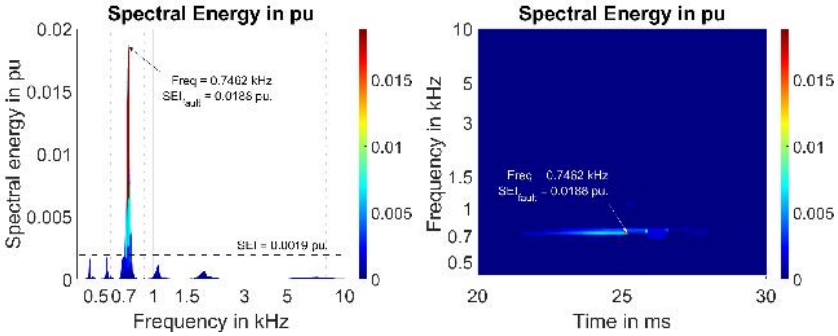


(a) SEI vs Frequency (b) MRA Time-frequency

Figure 5.26: Case: SE shape triangle

hand, an alternative solution for the traveling wave scheme is developed in [133], using a pre-fault voltage sample acquired at a much lower sampling frequency, which is sampled along with the current traveling wave.

Fig. 5.28 shows the transient behavior of the current signal, while Fig. 5.29 shows the transient behavior of the voltage on the same bus L.



(a) SEI vs Frequency (b) MRA Time-frequency

Figure 5.27: Case: SE shape linear

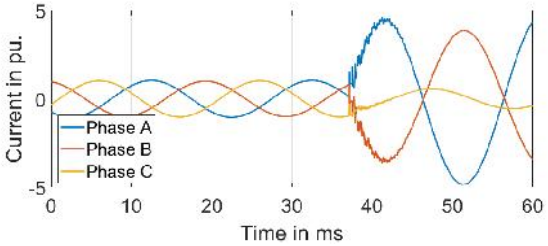


Figure 5.28: Current transient signal due to a two-phase (AB) short circuit

The transient phenomenon caused by the traveling waves affects both signals; however, the effect on the voltage signal is more noticeable with respect to the current signal, which can be verified by the magnitude of the SEI shown in Fig. 5.30.

Protection scheme verification

The multiresolution spectrum is developed in all cases taking into account the fault conditions such as: fault location, resistance, and inception angle. There are 96 cases in total, ordered as a function of distance as shown in

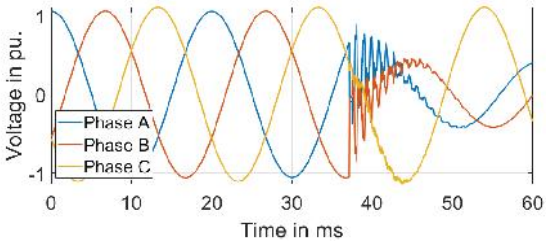
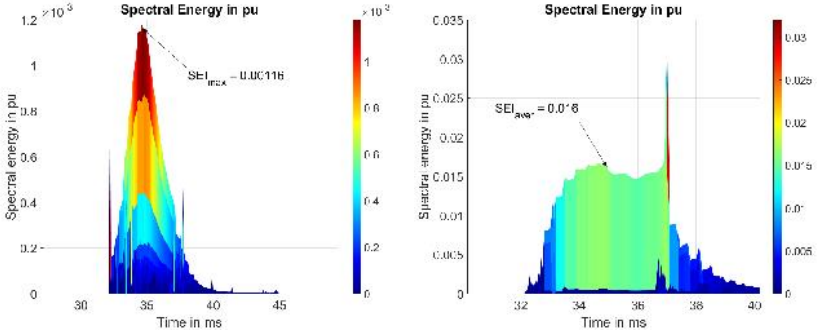


Figure 5.29: Voltage transient signal due to a two-phase (AB) short circuit



(a) SEI vs time - Current

(b) SEI vs time - Voltage

Figure 5.30: Current and voltage behaviour due to a two-phase (AB) short circuit

Fig. 5.31. The first 60 cases are internal faults and the last 36 cases are external faults. It also shows the relationship between the analyzed cases as a function of the multiresolution signal, which depends on the frequency (83.3 - 0.41 kHz).

A frequency threshold is verified, which differentiates internal from external faults as shown in the Fig. 5.32. An important feature is the slight change in the slope of the fault distance behavior. This effect is due to the change in the line's characteristic impedance due to WTs changing the propagation medium.

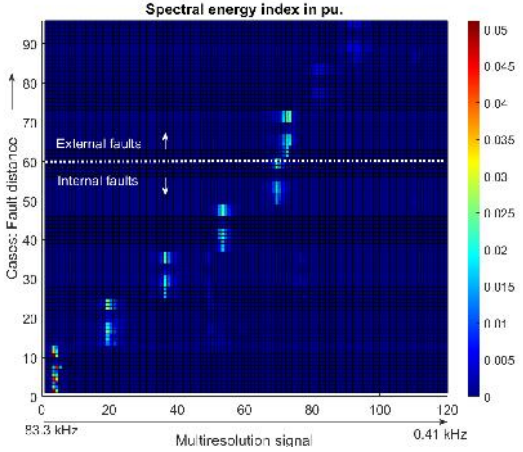


Figure 5.31: Spectral energy for different fault locations

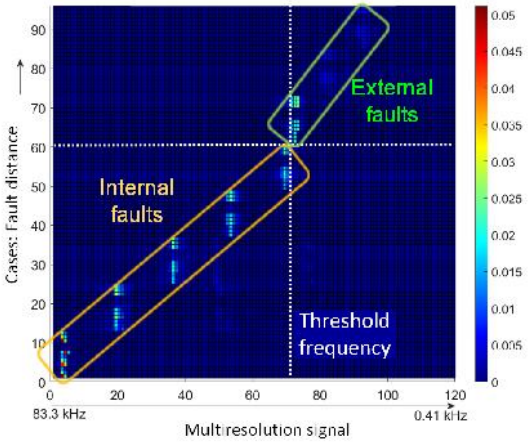


Figure 5.32: Spectral energy with threshold frequency

To get a better view of the threshold frequency, the maximum values

of the spectral energy are determined to distinguish between internal and external faults as shown in the Fig. 5.33. The threshold frequency setting is 0.71 kHz, where it is correctly verified in all cases (100% effectiveness). The simulation of faults at 99% of the main LT and at 1% of the remote LT gives us the reference to determine this frequency threshold. Although it presents 100% effectiveness in the cases analyzed, for greater safety this threshold can be modified up to a certain percentage of the TL (90 or 95%) and the rest of this line together with a large percentage of the adjacent TL (50%) will be adjusted with a delay.

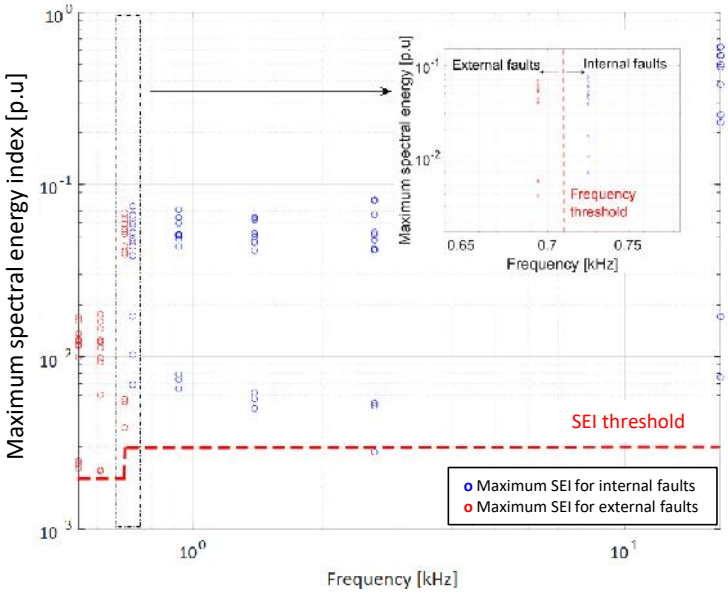


Figure 5.33: Definition of the frequency threshold and the SEI threshold

It is very important to verify the most extreme conditions during the development of these events. The worst conditions are shown for high values of fault impedance ($\sim$ 50 Ω) and inception angles close to zero crossing; however, the method was able to identify the frequency of the signal.

The magnitude of the SEI is used to activate the fault condition, i.e.

it allows us to differentiate between fault signals and possible noise in the signal or simply steady state conditions. In this case, the energy threshold (> SEI) is set to 0.002 for zone 1 and 0.001 for zone 2.

Fig. 5.34 shows that the magnitude of the spectral energy and even in the worst cases it is higher than the noise magnitude. However, for a fault much further away the SEI values will be similar to the noise which could cause confusion to the protective equipment. This can be avoided by setting different SEI thresholds for internal and external short circuits.

- Zone 1 faults: SEI_1 threshold = 0.002 pu.
- Zone 2 faults: SEI_2 threshold = 0.001 pu.

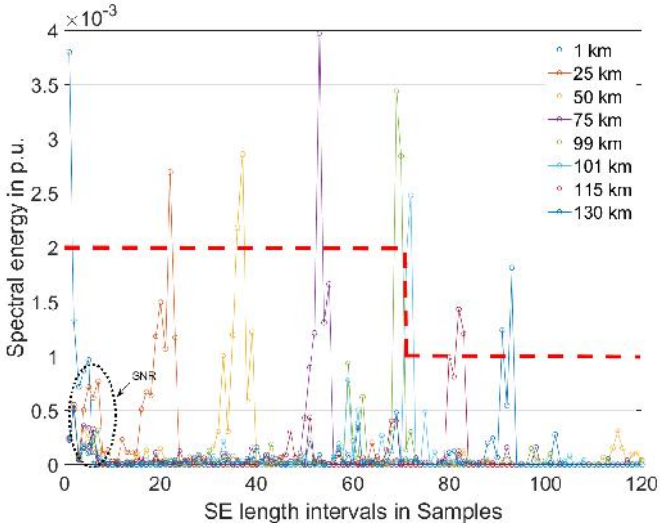


Figure 5.34: Spectral energy for many cases including the worst conditions

5.4.2 Case study: Current-source type generator

For this case, a power system with a current-source type generator at one end of the transmission line is considered as shown in the Fig. 5.35. The characteristics of the TLs is the same as in the previous case.

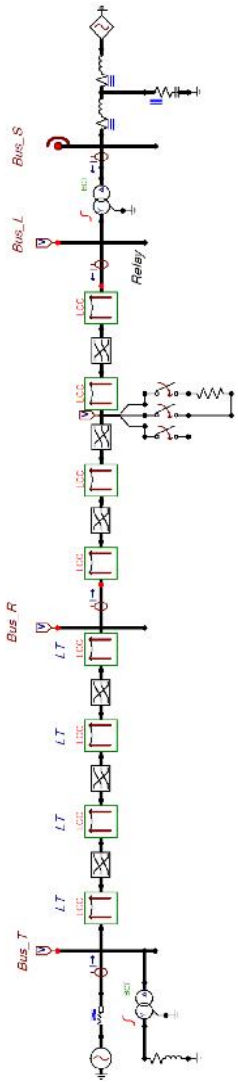


Figure 5.35: Electrical system with a current source at one end (Bus L)

The power transformer model is shown in the Table D.2. An equivalent source of a renewable power plant is modeled for transient analysis, this model is the current-source type without controls. Moreover, the parameters of the inverter, LCL filter are shown in the Table D.3 (See Appendix D.2).

The following fault and equipment characteristics are considered:

- Sampling frequency: 100 kHz
- Time window: 5 ms
- SE shape: Sine
- Type fault: two-phase short circuit (AB)
- Fault resistance: 50Ω
- Inception angle: 37 ms
- Fault location: 50 km

The characteristics of the three-phase current and voltage signals are shown in the Fig. 5.36 and Fig. 5.37 respectively. It is important to note that the magnitude of the fault current amplitude does not exceed 1.5 times the rated value; this behavior is typical of IBRs.

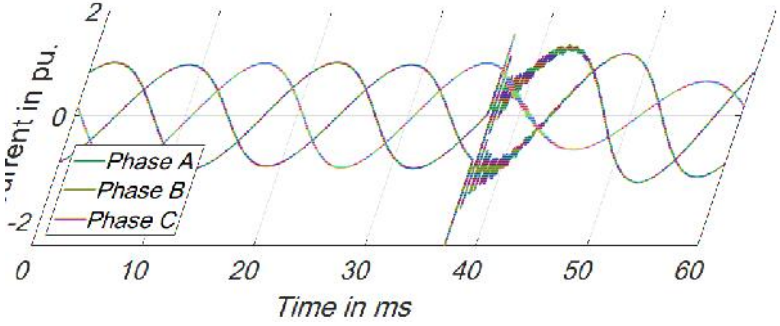


Figure 5.36: Current behavior on the bus-L side

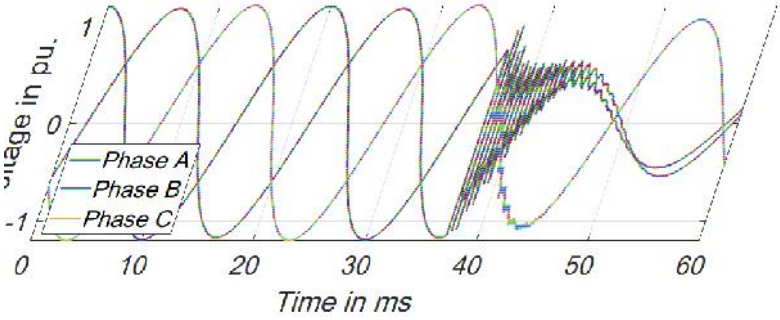


Figure 5.37: Voltage behavior on the bus-L side

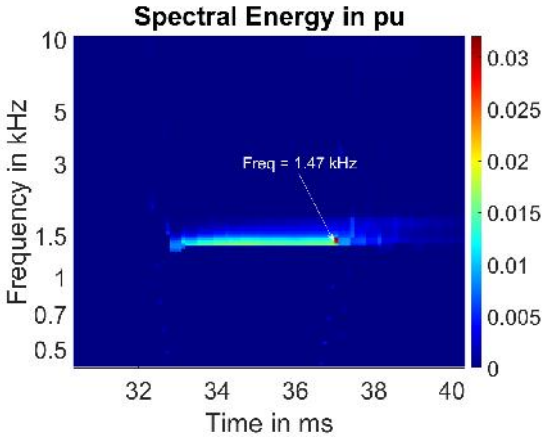
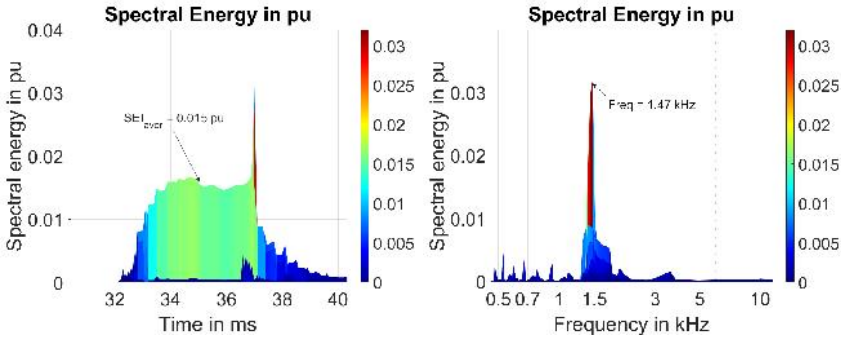


Figure 5.38: MRA time-frequency

Fig. 5.38 shows the short-circuit behavior in the time-frequency domain, the dominant frequency of the short-circuit signal is 1.47 kHz, and there are no effects of noise or high-frequency filter impedance.

The frequency value obtained can be confirmed in Fig. 5.39b (SEI vs. Frequency), the maximum SEI corresponds to a frequency of 1.47 kHz. According to the theoretical curve in Fig. 5.9, the frequency is 1.452 kHz, so the percentage error is 1.2%, which means that good performance is

achieved. In addition, the frequency is higher than 0.71 kHz, which means that this is a Zone 1 fault, and the spectral energy index is 0.015 pu and is higher than 0.002 pu, as shown in Fig. 5.39a, it has a high noise immunity.



(a) SEI vs time (b) SEI vs Frequency

Figure 5.39: SEI vs time and frequency

Regarding the *LCL* filter impedance for high frequencies, there is no major influence, since in the development of the simulations it was verified that the equivalent impedance is represented with a large value, because it takes into account the power transformer. This means that the signals are presented over a fixed period of 4τ; however, if there is a TL behind the relay instead of the transformer, it is necessary to check its characteristic impedance and then check the reflection coefficient in order to determine the period of the faulty signal.

5.4.3 Case study: Transmission line that connects a type 3 Wind Generator (DFIG)

In this case, an electrical power system with a type 3 wind generator at one end of the transmission line is considered as shown in the Fig. 5.40. The wind power source is modeled using the wind turbine model given in [134]. This example case presented by Piergiovanni La Seta in the EEUG Course in 2009. The characteristics of the TLs are the same as in the previous case (See Appendix D). In addition, the specifications of

the complementary equipment are included as shown in the table below (Table. D.4).

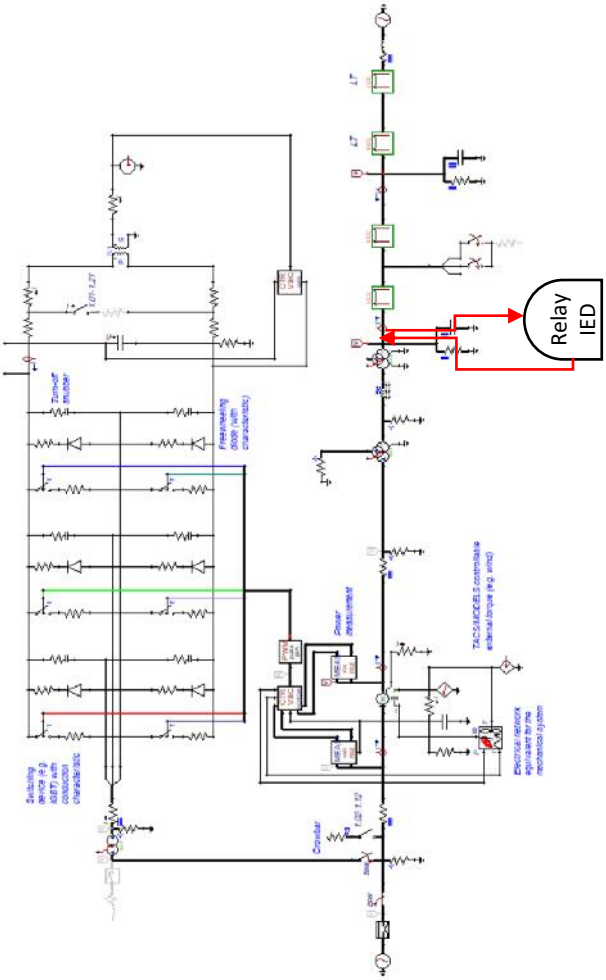


Figure 5.40: Case study of type 3 Wind Generator (DFIG)

The following fault characteristics and protection logic settings are considered:

- Sampling frequency: 100 kHz
- Time window: 5 ms
- SE shape: Sine
- Type fault: two-phase
- Fault resistance: 50Ω
- Inception angle: 37 ms
- Fault location: 80 km

Internal fault

A two-phase fault 80 km from the IED is simulated. The Fig. 5.41 shows the transient behavior before and after the fault.

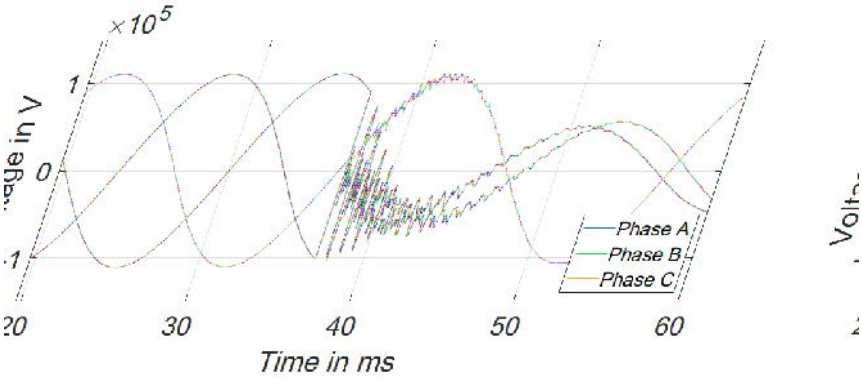
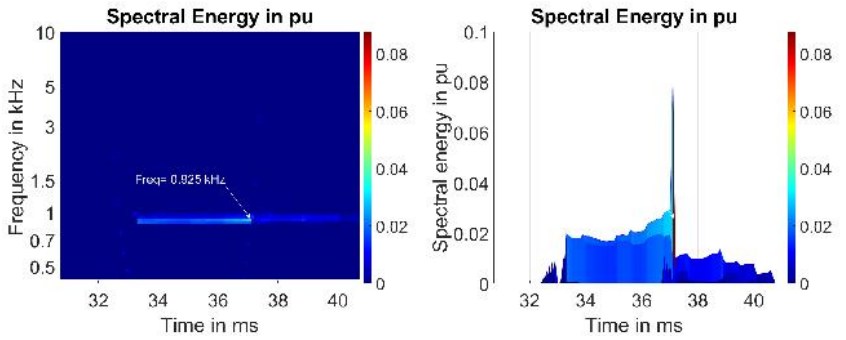


Figure 5.41: Two-phase fault at 80 km

The time-frequency multiresolution matrix is shown in Fig. 5.42a, while the behavior of the spectral energy as a function of time is shown in Fig. 5.42b. Note that the frequency of the transient signal is 0.925 kHz.



(a) Frequency vs time (b) SEI vs time

Figure 5.42: Time-frequency multiresolution

Based on the frequency vs. fault distance curve (Fig. 5.9) and the resulting frequency (0.925 kHz), the fault location can be determined. The result is 79 km as shown in Fig. 5.43, which implies an error of 0.6%.

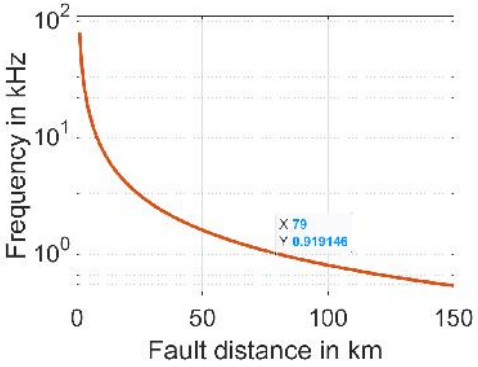


Figure 5.43: Curve Frequency vs Time

In addition, the frequency is greater than 0.71 kHz, which means it is a Zone 1 fault. The spectral energy index is greater than 0.002 pu, which means it is not affected by noise.

External fault

A two-phase fault is simulated 120 km from the IED. The Fig. 5.44 shows the transient behavior before and after the fault.

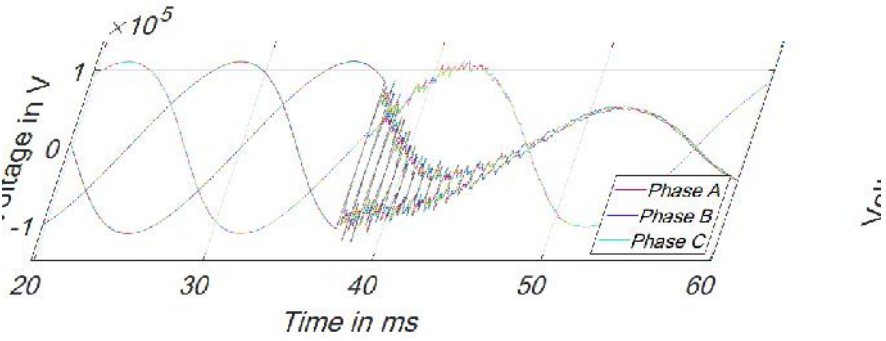
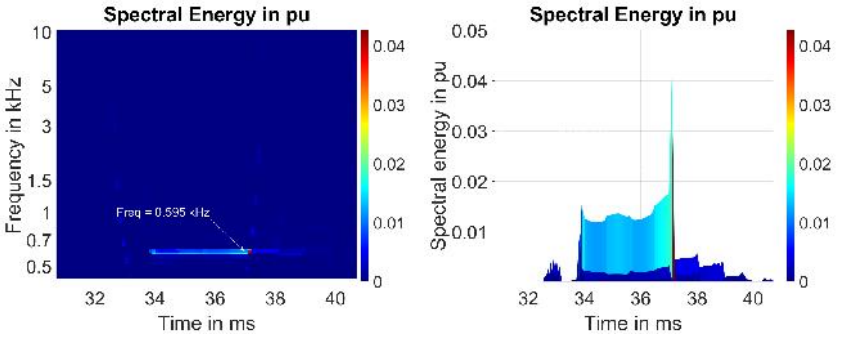


Figure 5.44: Two-phase fault at 120 km

The time-frequency multiresolution matrix is shown in Fig. 5.45a, while the behavior of the spectral energy as a function of time is shown in Fig. 5.45b. Observe that the transient signal frequency is 0.595 kHz.



(a) Frequency vs time

(b) SEI vs time

Figure 5.45: Time-frequency multiresolution

Based on the frequency vs. distance curve (Fig.5.9) and the obtained frequency (0.595 kHz), the fault location can be determined. The result is 121 km as shown in Fig.5.46, which implies an error of 0.8%.

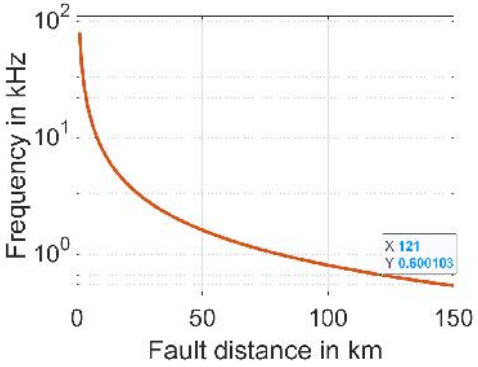


Figure 5.46: Curve Frequency vs Time

In addition, the frequency is less than 0.71 kHz, which means it is a Zone 2 fault. The spectral energy index is greater than 0.001 pu which means it is not affected by noise.

5.4.4 Case study: IEEH TU-Dresden laboratory model

The Institut für Elektrische Energieversorgung und Hochspannungstechnik (IEEH) of the Technical University Dresden (TU Dresde) has the Dynamic Network Model (DNM). It is a replica of a 220kV network section (Fig. 5.47).

A model voltage of 440V is used, which is easy to handle on a laboratory scale. It is divided into three stations, with which real network processes can be simulated. The power supply is provided by two synchronous generators and the possibility to feed power from the grid. Through disconnectors and circuit breakers, active and passive loads as well as the simulation of a 150 km long 220 kV double line can be interconnected in order to simulate operating and fault to investigate operating and fault processes [135]. The characteristics of the equipment are shown in

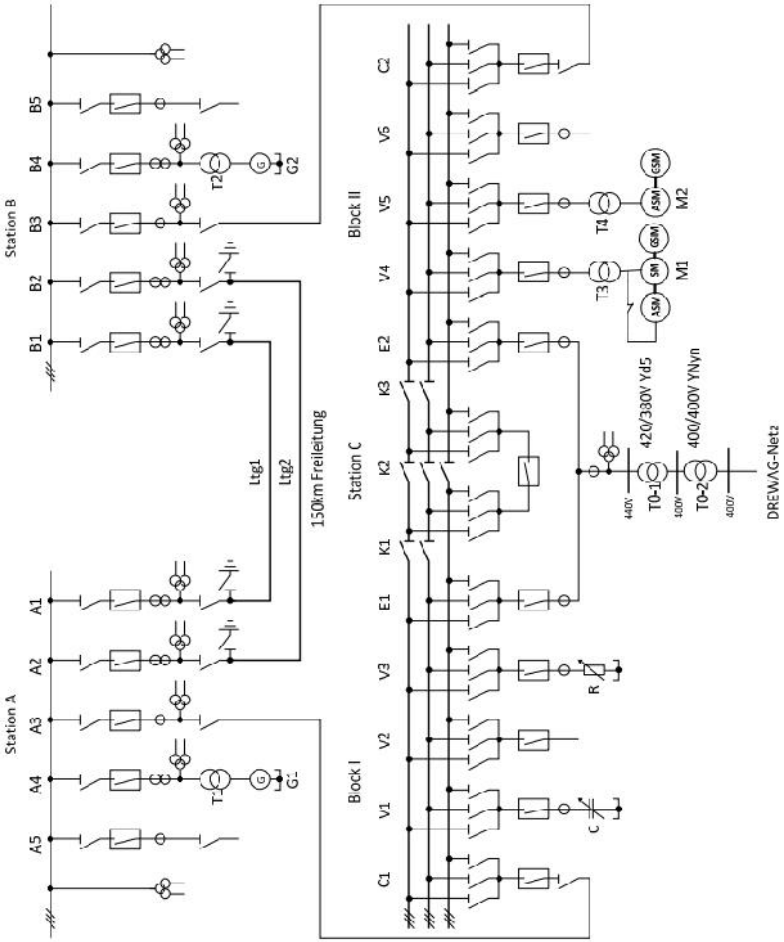


Figure 5.47: Overview diagram of the DNM

Appendix D.4.

- Transmission line (TL) length:150 km.

- Rated voltage: 220 kV.
- PI model of TL: 5 km.
- Amount PI sections: 30.
- Speed of TW: 282210 km/seg
- Sampling frequency: 1MHz.
- Parameters of TL: Ro=0.004 ohm/km, Lo=0.075e-3 H/km, Co=0.16741e-6 F/km, Go=0.

Based on the above parameters, the frequency response is determined as a function of the fault distance as shown in Fig. 5.48 (theoretical curve).

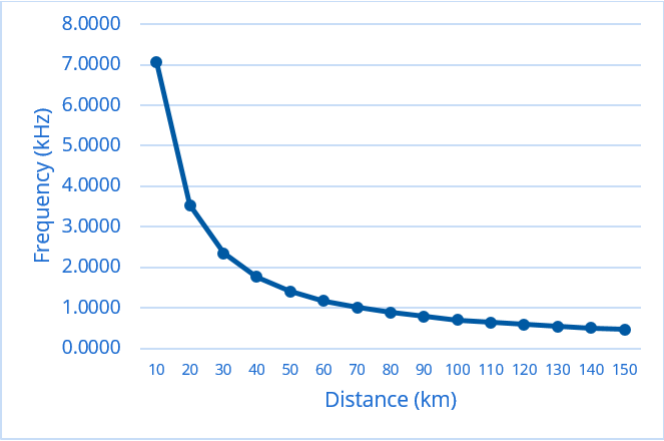


Figure 5.48: Frequency vs Fault location - laboratory

Then the Table. 5.2 shows the frequency for faults from 10 to 140 km.

To verify the performance of the algorithm, simulations are performed in different locations. Although the transmission line does not represent the distributed parameter model; however, the number of sections of the PI model it is useful to be able to identify in an approximate way the transient behavior caused by traveling waves [136]. Thus, it is possible to extract the information of their frequencies.

Table 5.2: Traveling wave frequency

Fault location (km)	$\tau(mseg)$	Frequency (kHz)
10	0.0354	7.0553
20	0.0709	3.5276
30	0.106	2.3518
40	0.142	1.7638
50	0.177	1.4111
60	0.213	1.1759
70	0.248	1.0079
80	0.283	0.8819
90	0.319	0.7839
100	0.354	0.7055
110	0.390	0.6414
120	0.425	0.5879
130	0.461	0.5427
140	0.496	0.5039

The simulated faults are for 40, 60, 90, 100, 120 and 140 km. The behavior of the transient signals are shown in Fig. 5.49, Fig. 5.51, Fig. 5.53, Fig. 5.55, Fig. 5.57 and Fig. 5.59, respectively. The frequency and spectral energy behavior is shown in Fig. 5.50, Fig. 5.52, Fig. 5.54, Fig. 5.56, Fig. 5.58 and Fig. 5.60, respectively.

The results of the simulations are shown in Table 5.3. The error rates increase for nearer faults because of the line model's loss of sections, which results in a low approximation of the transient behavior.

In addition, the faults farther away exhibit a good approximation, this is due to the good approximation of the line model, which causes better traveling wave behavior. In this sense, it can be seen that the algorithm presents good performance for real systems.

5.5 Comparison with wavelet transform

The discrete wavelet transform (DWT) theory is described in Appendix C. The objective of this section is to verify the multiresolution signal analysis methodology using the wavelet transform and then compare it with the method applied to the morphological filter.

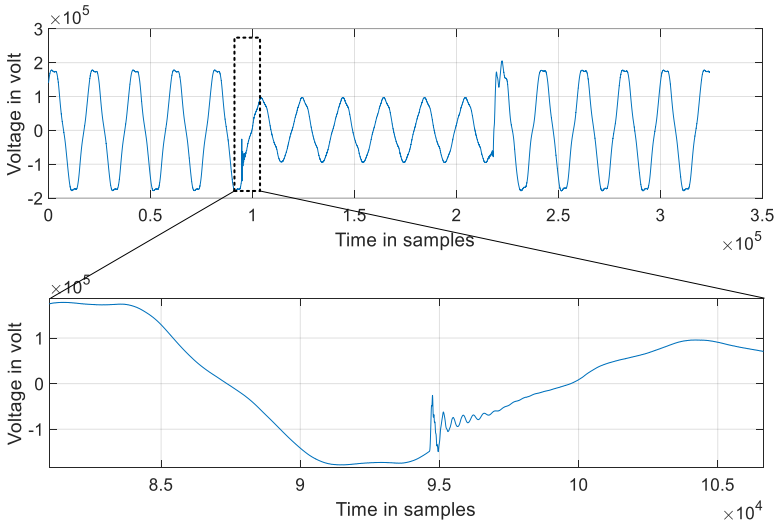
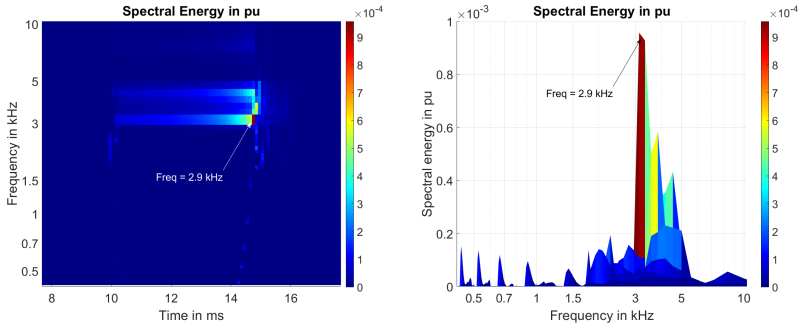


Figure 5.49: Fault at 40 km



(a) Frequency vs time

(b) SEI vs frequency

Figure 5.50: Time-frequency multiresolution: Fault at 40 km

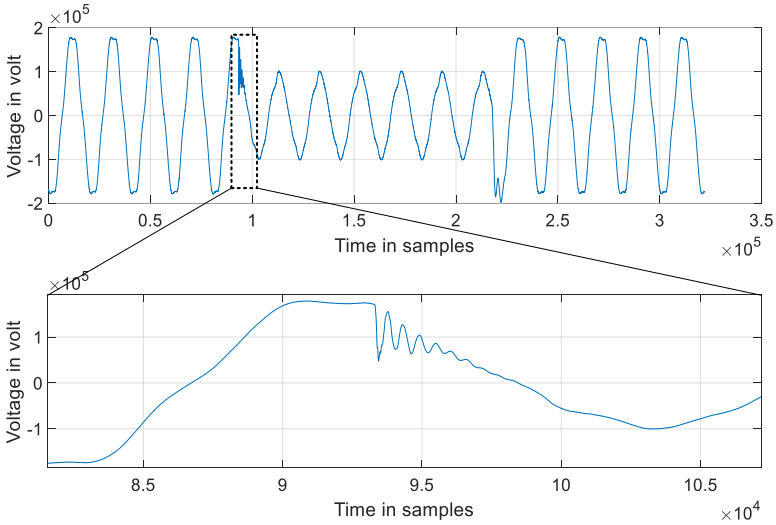
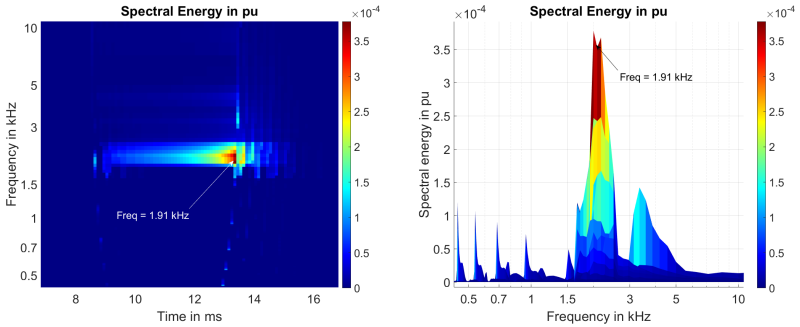


Figure 5.51: Fault at 60 km



(a) Frequency vs time

(b) SEI vs frequency

Figure 5.52: Time-frequency multiresolution: Fault at 60 km

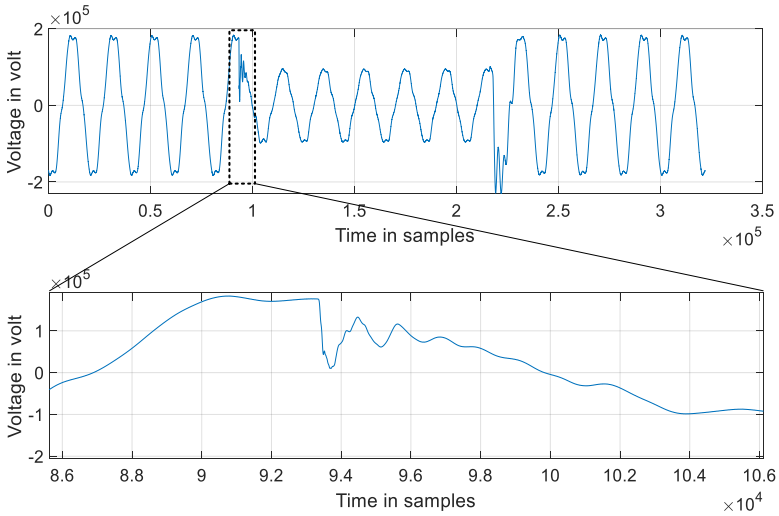
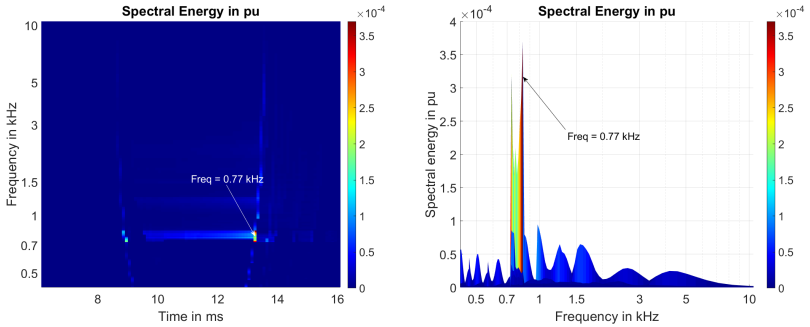


Figure 5.53: Fault at 90 km



(a) Frequency vs time (b) SEI vs frequency

Figure 5.54: Time-frequency multiresolution: Fault at 90 km

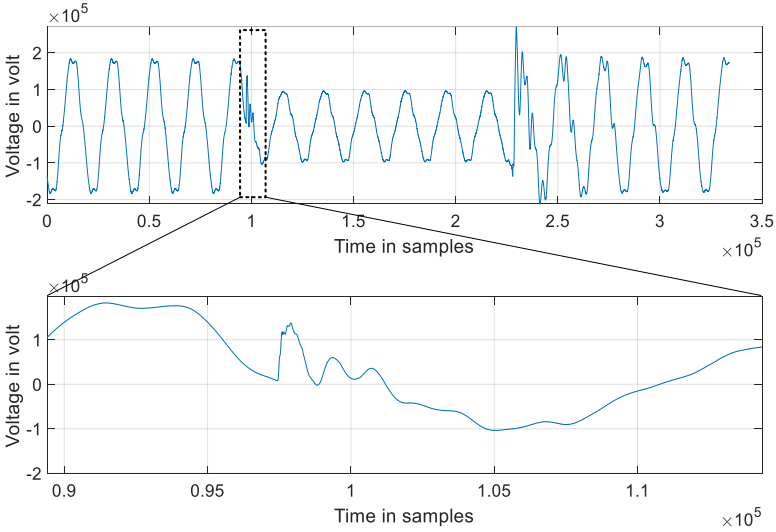
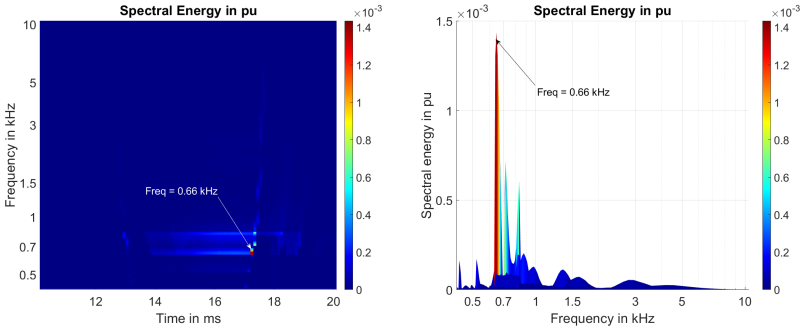


Figure 5.55: Fault at 100 km



(a) Frequency vs time

(b) SEI vs frequency

Figure 5.56: Time-frequency multiresolution: Fault at 100 km

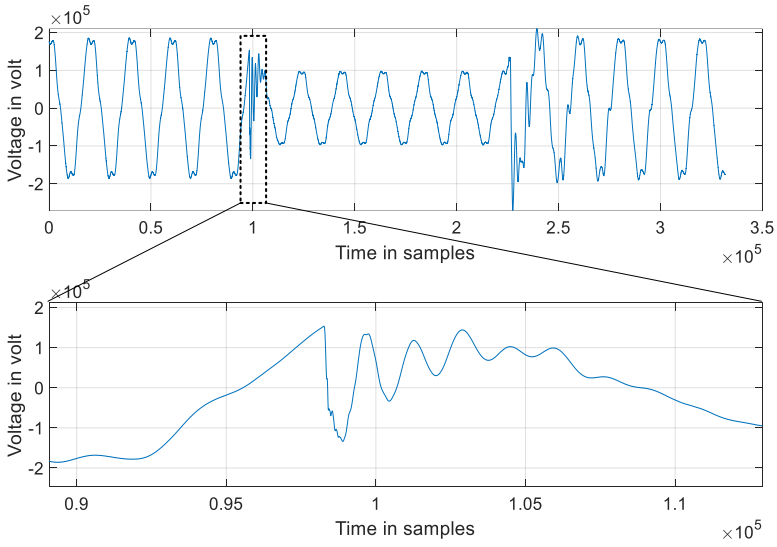
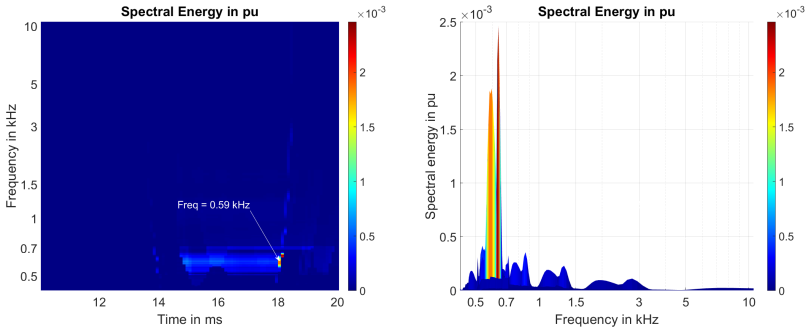


Figure 5.57: Fault at 120 km



(a) Frequency vs time

(b) SEI vs frequency

Figure 5.58: Time-frequency multiresolution: Fault at 120 km

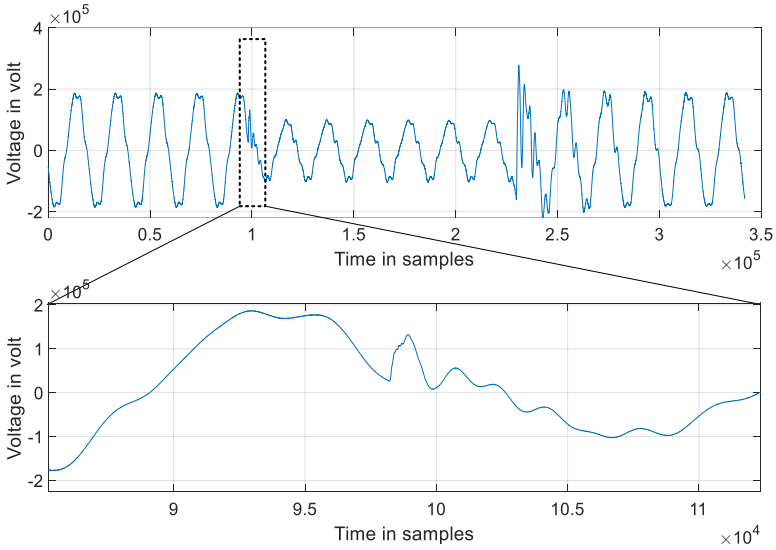
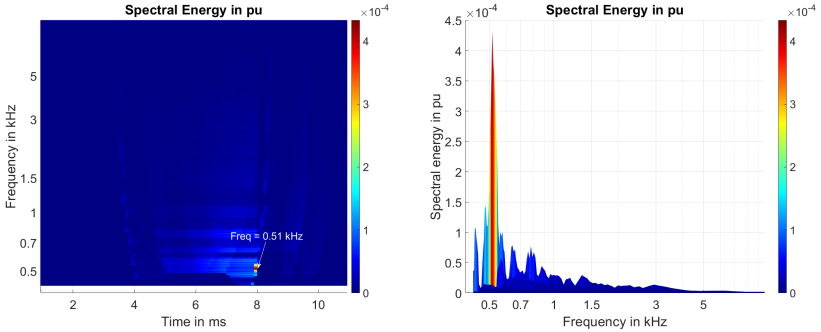


Figure 5.59: Fault at 140 km



(a) Frequency vs time

(b) SEI vs frequency

Figure 5.60: Time-frequency multiresolution: Fault at 140 km

Table 5.3: Traveling wave frequency

Fault location (km)	Frequency Theorical (kHz)	Frequency Simulated (kHz)	Error (%)
40	1.7638	2.90	39
60	1.1759	1.91	38
90	0.7839	0.77	1.7
100	0.7055	0.66	6.0
120	0.5879	0.59	0.3
140	0.5039	0.51	1.2

5.5.1 MRA using DWT

The MRA is determined by developing the wavelet packet transform. In order to compare with the same multiresolution level developed with the DMF, it is analyzed up to level 10. However, in order to avoid a broad spectrum of analysis, the signal from level $a3$ (0-125 kHz) is used. Based on this, $2^7 = 128$ multiresolution signals are obtained as shown in Fig. 5.61. In addition, the frequency resolution width is 0.9766 kHz.

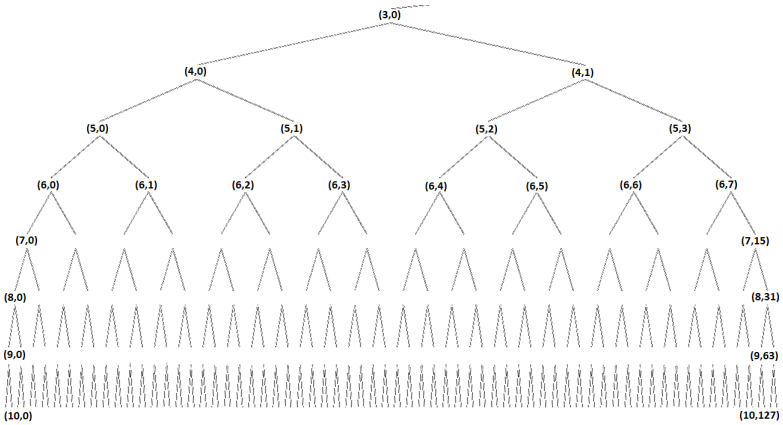


Figure 5.61: Decomposition tree using wavelet packet method.

The MRM is determined with the same 96 cases previously analyzed

with the DMF method. A characteristic is obtained as shown in Fig. 5.62 and Fig. 5.63. The magnitude of the SEI can be divided into the following zones:

- Cases 1-15: are in resolution range between 50-60 which represents [48.83-58.59] kHz.
- Cases 16-30: are in resolution range between 1-25 which represents [0.97-24.4] kHz.
- Cases from 31 - onwards: are in resolution range between 1-10 which represents [0.97-9.7] kHz.

As the fault distance increases, the frequency of the signal decreases, which verifies the theoretical section. The result is shown in Fig. 5.62, there is no good approximation, so it does not distinguish between internal and external faults by a frequency threshold.

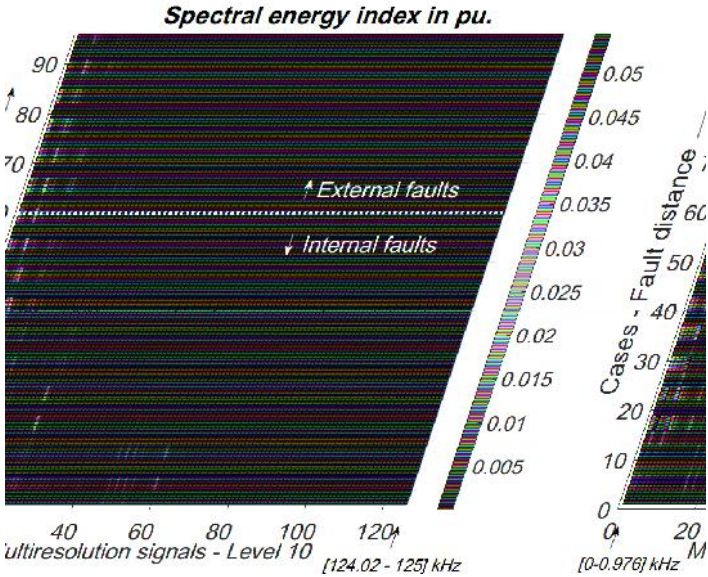


Figure 5.62: Spectral energy of multiresolution signals, 2D.

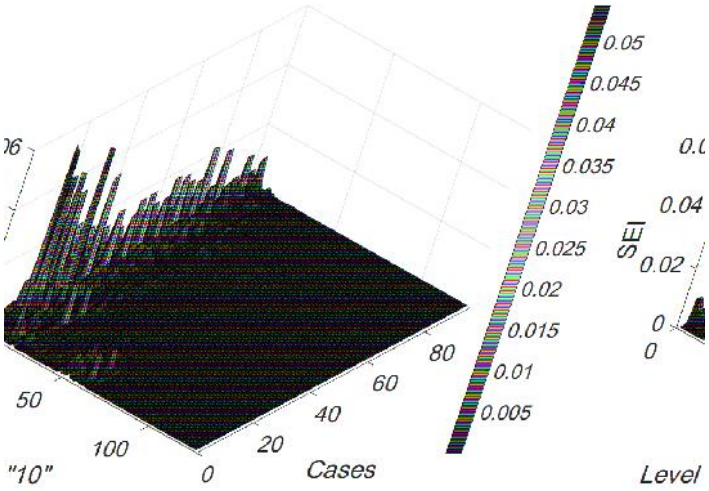


Figure 5.63: Spectral energy of multiresolution signals, 3D.

5.5.2 DWT vs DMF

- The values of the SEI determined using DWT are not well identified, while the values obtained using DMF have a defined behavior (Fig. 5.64), moreover, they have a direct relationship with the fault distance and present a linear behavior as a function of SE length (levels) both for internal or external faults, even for different fault resistances and inception angles.

- Internal faults present a higher magnitude of SEI compared to external faults, as high-frequency components are predominant in the main TL due to the propagation of waves from one medium to another. This can be observed in both methods.

- At level 10 of the DWT decomposition, the signals contain 15 samples, which means that there is very little information. This implies analyzing at lower levels, which results in a loss of accuracy, whereas the DMF method keeps all samples for each level.

- The DWT method analyzes for frequency ranges while the DMF method analyzes for exact frequency points.
- The basis of the mathematical operations of the DWT method are complex, while the DMF uses basic operations.

Finally, a comparative summary table with the main characteristics of both methods is presented (Table 5.4):

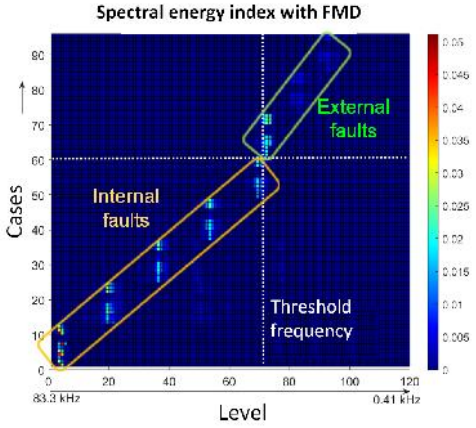
Table 5.4: Comparative table between two signal processing methods obtained for the analysis of this thesis

Characteristic	DWT	DMF
Transient analysis	Effective	Very effective
Transformation method	Little effective	Effective
MRA processing time	Little effective	Effective
Sampling window	Very effective	Very effective
Considers nonlinearity	Little effective	Effective
Mother function	Not effective	Little effective

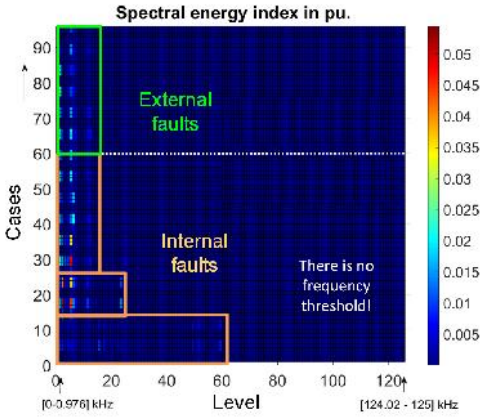
The DMF-based method shows better multiresolution analysis of the faulty signals compared to the DWT-based method. This was determined by the monitoring of 2 parameters, signal frequency and spectral energy index, both as a function of fault distance. It is important to note that this conclusion does not preclude the wavelet transform from being highly efficient for other applications.

5.6 Conclusions

This chapter shows the development of the distance protection algorithm using the high-frequency transient signals. The process of identifying protection zones is described by a logical scheme for determining the fault zone using a frequency threshold and an SEI threshold.. Then, the performance of the algorithm is verified through simulations for different fault conditions, such as: distance, resistance, inception angle, noise, sampling frequency, fault type and SE shape; where adequate results are finally achieved with low error rates. The analysis was also developed for two case studies considering the transient behavior of the IBR and the Type 3 wind generator, the results showed that the methodology was



(a) FMD



(b) DWT

Figure 5.64: Comparison of FMD and DWT methods

not affected by the type of generation, as it correctly identified the fault zone. In addition, it has been tested in a real electrical network in the

laboratory, where good results have been obtained for distant faults; the nearby faults do not provide adequate results due to the PI model of the TL in the laboratory. Finally, the MRA method was compared with the wavelet transform, where certain advantages were observed in favor of the FMD method, which motivates its use of its application.

CHAPTER 6

Conclusions and future works

The impact of IBRs on transmission line protection was analyzed in this thesis. Based on this, this research proposes a novel distance protection criterion using fault-generated high-frequency transient signals extracted from a digital filter based on mathematical morphology theory. As a result, a multi-resolution signal is obtained to evaluate the fault frequency characteristic, and then a comparison criterion based on spectral energy is used. Consequently, this method can identify fault zones of transmission lines.

Based on the thesis carried out, the following conclusions are presented:

- The protection functions most affected are the distance function. In this sense, the proposed scheme is not affected by the impedance of the source.
- A new starting element is presented based on the spectral energy index.
- This proposal does not require the use of communication between the line end relays.
- The protection logic for classification is based on the threshold criterion.

- The scheme is designed with a time window of 5 ms (faster than conventional relays). This makes it ultra-fast.
- The effects of the IBR power control system do not affect the study of the high-frequency transient signals due to the time scale of both phenomena.
- It has been verified that the theory of mathematical morphology as a digital filter of protection equipment proposes an interesting method of signal analysis. It has the ability to suppress noise and extract signals from different frequency components.
- The multiresolution analysis with MM of the faulted signals adequately verified the signal characteristic in the time-frequency domain. Therefore, under this criterion, it was possible to determine the location of a short-circuit in a transmission line.
- It is important to consider the use of new protection criteria using high-frequency transient signals, as future power grids present many challenges with the massive implementation of renewable energy sources.

In addition, the following contributions are presented:

- The proposed method uses a time window of a quarter cycle (5 ms) less than that used by traditional relays, thus achieving a high speed improving stability and avoiding the effect of the inverter power control system behavior.
- The decomposition of the three-phase signals is performed by modal transformation; therefore, it avoids the use of negative-sequence magnitudes since IBRs do not generate enough quantities.
- This method is robust against very high frequency noise, even at frequencies close to the order of the switching frequency of the converters.
- This method is verified for all factors influencing the fault behavior such as: resistance, inception angle, location, noise. In addition, it is verified for different equipment conditions such as: sampling frequency and shape of the structuring element. In all cases it has been possible to identify the fault location.

- The digital filter based on MM presents simplicity in its algorithm, since its theory is based on the use of basic mathematical operations. This can avoid the use of equipment with high computational costs. Furthermore, compared to the wavelet transform, MM can decompose the signals at a fixed frequency without losing the number of samples, while WT decomposes in frequency ranges and each decomposition loses samples.

- This method represents an attractive proposition for protection equipment or fault locators, as it can be implemented in a protection relay to identify protection zones through frequency thresholds or to determine the fault location through off-line analysis.

Finally, the following future works are presented:

- Based on this analysis, methodologies can be developed to determine the directionality of faults. Based on the feeder with the highest spectral energy index.

- Based on this analysis, methodologies can be developed to identify the type of faults. This can be developed by comparing the fault modal loops.

- It is possible to implement a real-time network diagnostic system by monitoring signals in the time-frequency domain, not only in high frequency but also in all desired frequency ranges.

- A method to differentiate events in the network that cause high frequency signals can be developed to complete this thesis.

CHAPTER 7

Resumen versión español

7.1 Resumen

Este trabajo desarrolla un nuevo algoritmo de protección de distancia para líneas de transmisión utilizando señales transitorias de alta frecuencia generadas por fallas mediante una nueva técnica de filtrado digital basada en la teoría de morfología matemática y energía espectral. Además, este método determina el comportamiento de las señales en el dominio tiempo frecuencia mediante un análisis multirresolución con una ventana de tiempo de 5 ms, lo que hace de este muy rápido y evite el efecto de las fuentes de energía renovables en comparación con los sistemas de protección tradicionales. Por lo tanto, el desarrollo de esta tesis proporciona las siguientes contribuciones: Un estudio detallado de las características de respuesta ante fallas de las fuentes de energía renovables y su influencia en las principales funciones de protección (distancia, diferencial, sobrecorriente y direccional) de las líneas de transmisión. Un estudio detallado del comportamiento de las señales transitorias de alta frecuencia causadas por las señales de onda viajera de cortocircuito en las líneas de transmisión. Por último, una metodología novedosa para la protección de distancia utilizando señales transitorias de alta frecuencia mediante el desarrollo de un nuevo filtro morfológico digital y su comparación con la transformada wavelet.

7.2 Introducción

Los estudios de protección eléctrica se realizan con el objetivo de determinar los ajustes de los relés de protección, que se establecen mediante algoritmos y lógicas implementadas por los fabricantes. Estos dispositivos están continuamente monitoreando las principales señales de una red eléctrica como tensión, corriente, frecuencia, entre otras; por lo tanto, a partir del comportamiento conocido de estas señales bajo fallas, los relés deben detectar, identificar y despejar la falla mediante los principios de rapidez, selectividad, fiabilidad y sensibilidad. Además, en los estudios de protección se suelen tener en cuenta las siguientes condiciones: tipo de falla, localización, resistencia y ángulo de inicio. Sin embargo, la inclusión de nuevas tecnologías de generación basadas en la electrónica de potencia experimenta cambios en el comportamiento habitual de las fallas, ya que éstas tienen diferentes características de contribución de la corriente. Existen dos tipos de tecnologías de generación:

- Generación basada en máquina síncrona: hidroeléctrica, térmica, nuclear, biomasa, entre otras.
- Generador basado en electrónica de potencia: fotovoltaica, generador eólico tipo-4, generador eólico tipo-3, entre otros.

Muchas de las fuentes de energía renovables son generadores basados en electrónica de potencia que cuentan con un inversor en su estructura. Por lo tanto, los dispositivos de protección de las líneas de transmisión que emanan de estas fuentes plantean desafíos. En consecuencia, en función de la topología del inversor y las configuraciones de tiempo de respuesta del sistema de control del inversor, los efectos más significativos sobre el sistema de protección se clasifican como sigue:

- Amplitud de corriente de falla limitada.
- Duración controlada de la corriente de falla.
- Depende de la configuración de FRT (códigos de red).
- Impedancia interna inestable.
- Ángulo de fase actual controlado.

- Baja cantidad de secuencia negativa.
- No hay cantidad de secuencia cero.

Estos efectos se manifiestan en diferentes problemas de funcionamiento de dispositivos de protección, en algunos casos en mayor medida que en otros, tales como como: problemas en alcances de zona, polarización, arranque, cantidades insuficientes de magnitudes de secuencia negativa, entre otros. Por lo tanto, es evidente la necesidad de desarrollar nuevos criterios para los algoritmos de protección que sean sencillos en su implementación, que consideren todos los escenarios posibles de falla y que además incluyen el comportamiento de las nuevas fuentes de generación o evitan ser afectadas. En este sentido, surge la siguiente pregunta: Cómo mejorar los esquemas de protección en el sistema de transmisión para evitar ser afectados por la alta penetración de fuentes de energía renovable?

7.2.1 Objetivo general

Desarrollar un nuevo algoritmo y esquema de protección para líneas de transmisión mediante el análisis de señales transitorias de alta frecuencia con una ventana de tiempo corta, convirtiéndolo en un método ultrarrápido que no se ve afectado por el comportamiento del sistema de control IBR.

7.2.2 Objetivos específicos

- Analizar el comportamiento de los algoritmos tradicionales debido a la inclusión de fuentes de energía renovable.
- Analizar el comportamiento de las señales transitorias de tensión y corriente de alta frecuencia mediante un método de morfología matemática.
- Desarrollo de simulaciones para diversos eventos en un sistema de transmisión.
- Desarrollo del algoritmo de protección para las líneas de transmisión.
- Verificación del nuevo algoritmo de protección comparándolo con otros métodos.

Finalmente, se espera que el desarrollo de esta tesis proporcione las siguientes aportaciones: Una metodología novedosa para esquemas de protección ya que considera el uso de señales transitorias de alta frecuencia mediante el desarrollo de un nuevo filtro digital. Además, un estudio detallado de las características de las fuentes de energía renovables que influyen en las principales funciones de protección de las líneas de transmisión.

7.3 Estado del arte

Actualmente, las protecciones de las líneas de transmisión están experimentando retos debido a la alta penetración de las fuentes de energía renovables, por lo que se estudió a profundidad de este tema y se consideró el análisis de las principales causas y soluciones de nuevos criterios metodológicos. En este capítulo se presenta una amplia revisión bibliográfica sobre la evaluación del rendimiento de las redes eléctricas y los efectos de las FER conectadas a la red eléctrica mediante inversores (IBR). Se obtienen datos bibliográficos de numerosas publicaciones representativas relacionadas para mostrar las líneas de investigación actuales y sus soluciones propuestas. Además, este trabajo identifica las principales funciones de protección afectadas y se describen los nuevos esquemas de protección que consideran FER. Por último, se presenta un análisis y discusión de la bibliografía seleccionada.

Se observó que el comportamiento de operación, gobernado por los ajustes de su sistema de control de potencia del inversor, y la estructura de estos IBRs provocan dichos efectos afectando principalmente a las funciones utilizadas por un relé de distancia y direccional. Además, los factores de influencia están relacionados con la misma escala temporal de funcionamiento, ya que los tiempos de respuesta del controlador de potencia de los inversores coinciden con los tiempos de actuación de los relés. Por lo tanto, la alta penetración de los IBR en los sistemas de transmisión requiere un estudio en profundidad del desarrollo de esquemas de protección nuevos y existentes, ya que la modificación o adaptación es inevitable en el futuro. Por otra parte, los esquemas de protección ultrarrápidos cuyas escalas de tiempo son inferiores al tiempo de respuesta del sistema de control de potencia no se ven teóricamente afectados, como es el caso de las protecciones basadas en ondas viajeras. Sin embargo, estos

métodos necesitan funciones complementarias y, en muchos casos, pueden depender del comportamiento de la fuente. Por lo tanto, para sistemas con alta penetración de IBRs, se requieren estudios pertinentes para confirmar la fiabilidad de estos esquemas.

7.4 Análisis de las señales transitorias

En esta sección se exponen los conceptos teóricos sobre el origen y las características de las señales transitorias causadas por fallas eléctricas en las líneas especialmente los cortocircuitos. Este análisis se centra en el cálculo de la frecuencia de la onda viajera. Por otra parte, los principales funcionamientos de los IBR y los equipos asociados en la gama de alta frecuencia. En conclusión, el estudio de las señales transitorias causadas por cortocircuitos implica el análisis del comportamiento de las ondas viajeras en las líneas de transmisión. Se ha demostrado que el efecto de las ondas viajeras produce una distorsión periódica y se superpone a las señales de tensión y corriente a frecuencias fundamentales. Además, este transitorio generado por la falla eléctrica tiene componentes de alta frecuencia lo que implica un estudio multirresolución. El fenómeno de atenuación en las líneas de transmisión debido al mayor efecto capacitivo de los componentes del sistema hace que la magnitud de las señales transitorias cambie mucho entre fallas internos y externos.

Por otro lado, se describe el comportamiento de los convertidores en el rango de alta frecuencia para comprobar los efectos en el sistema de transmisión desde el punto de vista del dominio de alta frecuencia, la frecuencia fundamental y los armónicos de baja frecuencia o las distorsiones generadas por el IBR. Además, el transitorio de alta frecuencia de una falla es aislado por el inversor porque los condensadores de enlace de DC actúan como un cortocircuito y el modelo IBR puede simplificarse. Por último, para un modelo de alta frecuencia no se tiene en cuenta el sistema de control de potencia porque el tiempo de respuesta se produce después de decenas o cientos de milisegundos, por lo que es mayor en comparación con el transitorio de falla inicial. Debido a este hecho, el modelo de frecuencia de un IBR no cambiará en caso de que se presenten diferentes ajustes del sistema de control de potencia.

7.5 Modelos teóricos

En este capítulo se describen las herramientas matemáticas utilizadas para el desarrollo de un nuevo filtro digital aplicado a los dispositivos de protección. Este filtro se basa en teoría de la morfología matemática. Además, el algoritmo de procesamiento basado en un índice de energía espectral y la señal MRA en el dominio tiempo frecuencia.

El valor de la frecuencia espectral indica la referencia de localización de las fallas, por lo que se propone un método de protección de líneas de transmisión basado en el cálculo de la frecuencia. La secuencia de cálculo de la señal en el dominio tiempo frecuencia es la siguiente:

- El proceso comienza con la detección de una falla eléctrica (cortocircuito) en las líneas de transmisión.
- Las señales trifásicas se leen del sistema a través de un IED. Estas señales se extraen a una determinada frecuencia de muestreo mediante un equipo analógico digital (conversión A/D). Sin embargo, este método puede adaptarse a dispositivos con diferente frecuencia de muestreo.
- Se propone una ventana temporal de análisis de 5 ms, esta ventana puede aumentar hasta 10 ms para una mayor precisión. Estos valores son inferiores que el tiempo utilizado por los relés tradicionales.
- Las señales trifásicas (ABC) se transforman en señales modales ($\alpha\beta 0$) mediante la transformación de Clarkes. Donde el subíndice 0 significa para las magnitudes de modo tierra, estando α y β relacionadas con las señales de modo aéreo.

En el bloque del filtro digital, el nivel máximo de resolución y la forma geométrica de la SE. El proceso comienza con el nivel "$n = 1$" en el que se determina la longitud de la SE. A continuación, se transforma la señal mediante el DMF y se determina "Hn". Por último, se calcula la energía espectral de esta última señal, esta información se almacena en un MRM.

- Se comprueba que el nivel n de análisis es inferior al máximo nivel establecido M.
- Si se cumple que $n < M$ se repite el proceso para el siguiente nivel.

- Por último, se extrae la señal multirresolución en el dominio tiempo-frecuencia.

El diagrama de flujo se muestra en la Fig. 4.9.

En conclusión, este capítulo desarrolla los modelos teóricos de este trabajo. Se basa en el desarrollo de un filtro digital morfológico para dispositivos de protección. Además, las características del elemento estructurante, el proceso de obtención de las señales multiresolución y la relación entre la longitud SE con la frecuencia de cada señal de resolución. Se presenta también para diferentes frecuencias de muestreo y el proceso de diferenciación para evitar un elevado coste computacional. Por otra parte, el algoritmo de procesamiento basado en el índice de energía espectral y la señal en el dominio tiempo-frecuencia con el fin de identificar las zonas de protección a través de los valores de frecuencia.

7.6 Desarrollo del algoritmo de protección

En este capítulo se describe un método de identificación de la zona de falla mediante la comparación de las energías espectrales máximas e incluye un diagrama de la secuencia lógica de protección. Además, se describen los resultados de las simulaciones de los eventos más graves (cortocircuitos) con el fin de verificar su adecuado funcionamiento.

A partir de las señales de tiempo-frecuencia previamente calculadas y descritas en el apartado anterior, se determinan los valores máximos y se comparan con dos umbrales. El umbral de frecuencia y el umbral de energía espectral, como se muestra en la Fig. 5.6. Para ello, es necesario establecer algunos parámetros como la energía espectral umbral y la frecuencia de señal umbral.

En conclusión, este capítulo muestra el desarrollo del algoritmo de protección de distancia utilizando las señales transitorias de alta frecuencia. El proceso de identificación de las zonas de protección y un esquema lógico para determinar la zona de fallo mediante un umbral de frecuencia y un umbral de la energía espectral. La Fig. 5.8 muestra las características de los casos en el dominio tiempo-frecuencia, donde puede identificarse claramente el espectro de frecuencias predominante en cada caso.

A continuación, se verifica el rendimiento del algoritmo mediante simulaciones para diferentes condiciones de falla: distancia, resistencia,

ángulo de incepción, ruido, frecuencia de muestreo, tipo de fallo, forma de SE, donde finalmente se obtienen resultados adecuados para identificar las zonas de falla. El análisis también se realiza para diversos casos de estudios donde se considera el comportamiento transitorio de un sistema convencional, IBRs y TW-III. Los resultados mostraron que la metodología no se ve afectada por el tipo de generación ya que identifica correctamente la zona de falla. Por último, el método MRA se comparó con la transformada wavelet, observándose ciertas ventajas a favor del método basado en morfología, lo que motiva su aplicación.

7.7 Conclusiones

Este trabajo realizó un análisis en profundidad de los efectos de los IBR en las protecciones de las líneas de transmisión. Basándose en ello, esta investigación propone un novedoso criterio de protección a distancia utilizando señales transitorias de alta frecuencia extraídas de un filtro digital basado en la teoría de morfología matemática. Como resultado, se obtiene una señal multiresolución que permite apreciar la característica de frecuencia de la falla y, también, un criterio de comparación basado en la energía espectral. En consecuencia, este método permite identificar las zonas de fallo de las líneas de transmisión. A partir del estudio realizado, se presentan las siguientes conclusiones:

- La funcion de protección más afectada es la función de distancia. En este sentido, el esquema propuesto no se ve afectado por la impedancia de la fuente.
- Se presenta un nuevo elemento que reconoce el cortocircuito basado en el índice de energía espectral.
- Esta propuesta no requiere el uso de comunicación entre los relés de los extremos de la línea.
- La lógica de protección para la clasificación se basa en el criterio del umbrales.
- El esquema está diseñado con una ventana de tiempo de 5 ms (más rápido que los relés convencionales). Esto lo hace ultrarrápido.

- Los efectos del sistema de control de potencia IBR no afectan el estudio de las señales transitorias de alta frecuencia debido a la escala temporal de ambos fenómenos.

- Se ha comprobado que la teoría de la morfología matemática como filtro digital de equipos de protección propone un interesante método de análisis de señales. Tiene la capacidad de suprimir el ruido y extraer señales de diferentes componentes de frecuencia.

- El análisis multiresolución con MM de las señales con fallas verificó adecuadamente la característica de la señal en el dominio tiempo-frecuencia. Por lo tanto, bajo este criterio, fue posible determinar la localización de un cortocircuito en una línea de transmisión.

- Es importante considerar el uso de nuevos criterios de protección que utilicen señales transitorias de alta frecuencia, ya que las futuras redes eléctricas presentan muchos desafíos con la implementación masiva de fuentes de energía renovables.

Además, se presentan las siguientes contribuciones:

- Este método utiliza una ventana de tiempo de un cuarto de ciclo (5 ms) menos que la utilizada por los relés tradicionales, logrando así una alta velocidad mejorando estabilidad y evitando el efecto del comportamiento del sistema de control de potencia del inversor.

- La descomposición de las señales trifásicas se realiza por transformación modal, por lo que se evita el uso de magnitudes de secuencia ya que los IBR no generan magnitudes suficientes.

- Este método es robusto frente a ruidos de muy alta frecuencia, incluso a frecuencias próximas al orden de la frecuencia de conmutación de los convertidores.

- Este método verifica los factores que influyen en el comportamiento del falla como: resistencia, ángulo de incepción, localización, ruido. Además, se verifica para diferentes condiciones del equipo como: frecuencia de muestreo y forma del elemento estructurante. En todos los casos ha sido posible identificar la localización de la falla.

- El filtro digital basado en MM presenta simplicidad en su algoritmo, ya que su teoría se basa en el uso de operaciones matemáticas básicas. Esto puede evitar el uso de equipos con elevados costes computacionales. Además, en comparación con la transformada wavelet, MM puede descomponer las señales en una frecuencia fija sin perder el número de muestras, mientras que WT descompone en rangos de frecuencia y cada descomposición pierde muestras.

- Este método representa una propuesta atractiva para los equipos de protección o los localizadores de fallas, ya que puede implementarse en un relé de protección para identificar las zonas de protección a través de umbrales de frecuencia o para determinar la localización de una falla mediante un análisis fuera de línea

Por último, se presentan los siguientes trabajos futuros:

Basándose en este análisis, se pueden desarrollar metodologías para determinar la direccionalidad de las fallas mediante la comparación de las energías espectrales de todos los alimentadores de un bus, es decir, el alimentador con el mayor índice de energía espectral indica la presencia de una falla.

A partir de este análisis, se pueden desarrollar metodologías para identificar el tipo de fallas. Esto puede desarrollarse comparando los bucles modales de falla.

Es posible implementar un sistema de diagnóstico de red en tiempo real mediante la monitorización de señales en el dominio tiempo-frecuencia, no sólo en alta frecuencia, sino también en todos los rangos de frecuencia deseados.

Finalmente, para completar esta tesis se puede desarrollar un método para diferenciar eventos en la red que causan señales de alta frecuencia.

APPENDIX A

Appendix A: Main protection schemes in TLs

This thesis focuses on the main protection schemes in TLs:

- Distance protection.
- Differential protection.
- Directional overcurrent protection.

In addition, the protection elements and logics that can be used as input to the above-mentioned schemes:

- Directional element protection.
- Negative-sequence protection.
- Fault-phase identification logic, fault identification selection (FIDS).

A.1 Distance protection (function 21)

Function 21 is a reliable and selective protection for TLs where their terminals are relatively far apart, i.e., for long lines [117]. It is a protective relay with responses to input quantities based mainly on a function of the electrical circuit distance between a relay location and the point of fault [137]. This protection scheme determines the fault impedance by

relating the phasor values of measured voltage and current. The calculated impedance is then compared with a zone settings by the TL's impedance in order to verify a condition where this impedance is within the protection zone, under that condition send a trip action to the breaker [138]. Eq.A.1 shows the fault impedance calculation for a TL. This fault is protected from both TL ends as shown in (Fig. A.1).

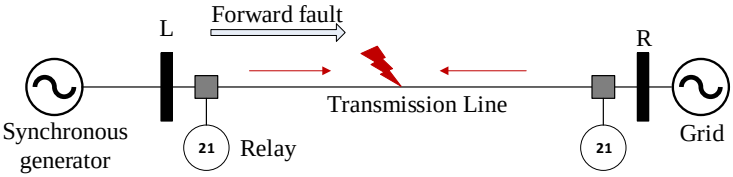


Figure A.1: Fault in TL with two power supplies

$$\mathbf{Z}_R = (m.\mathbf{Z}_{TL} + \mathbf{Z}_K) + \frac{\mathbf{I}_L}{\mathbf{I}_R}\mathbf{Z}_K \tag{A.1}$$

$$\Delta\mathbf{X} = \frac{I_L}{I_R}\mathbf{Z}_K sin(\angle(\mathbf{I}_L, \mathbf{I}_R)) \tag{A.2}$$

$$\Delta\mathbf{R} = \frac{I_L}{I_R}\mathbf{Z}_K cos(\angle(\mathbf{I}_L, \mathbf{I}_R)) \tag{A.3}$$

Where:

m: is the percentage of fault location.

$\mathbf{Z}_{TL}$: is the TL impedance.

$\mathbf{I}_L$ and $\mathbf{I}_R$: are the fault current contributions of the TL terminals.

$\mathbf{Z}_K$: is the fault impedance.

Eq. A.2 and Eq. A.3 represent the reactance and resistance impedance variations ($\triangle X$ and $\triangle R$) respectively and these are obtained from Eq. A.1. Therefore, the fault impedance calculated by relays depends on magnitude and phase angle relationships of the current signals from both ends and the fault impedance. In a three-phase system, distance relay algorithms determine three phase-phase loops (21AB, 21BC, and 21AC) and three phase-ground loops (21AG, 21BG, and 21CG). The operation logic consists of activating the following conditions using the AND logic:

- Impedance calculation: zone 1 setting is 80% of the TL impedance, zone 2 setting is 120% of the TL impedance with a time delay, and zone 3 covers almost all the TL adjacent with high time delay. When a fault impedance is inside the zone, this logic is activated.
- Fault detector threshold (starting): Overcurrent applied setting should be approximately $1.2 - 1.3$ maximum load current for phases (In) and $0.3 - 0.5$ of current transformer rating for ground fault currents. For under-impedance, voltage threshold is controlled by current, so that the pick-up sensitivity of voltage is increased as the current increases. Typical settings are: $I > 0.25I_n$, $I >> 2.5I_n$, as well as $U(I >) = 70\%Un$ and $U(I >>) = 90\%Un$. In addition, angle dependent under-impedance starting ($U/I/\phi$) and impedance staring are other methods [139].
- The directional element.
- Fault-phase identification logic.

The last two conditions will be detailed further below. It should be highlighted that directional elements and fault-phase identification logic use polarization of voltages, which includes phases not involved in the fault. Table 2 shows a summary of all operating and polarizing variables.

It is important to mention that some relay manufacturers use zero- and negative-sequences for polarization, as detailed further below.

A.2 Differential protection (function 87)

The operating principle of differential protection is represented as:

$$\mathbf{I}_{op} \geq \mathbf{I}_{op0}, \quad \mathbf{I}_{op} = \mathbf{I}_L + \mathbf{I}_R \tag{A.4}$$

$$\mathbf{I}_{op} \geq k.\mathbf{I}_{res}, \quad \mathbf{I}_{res} = \mathbf{I}_L - \mathbf{I}_R \tag{A.5}$$

where:

I_{op} is the differential current.

I_{res} is the restriction current.

An element generates a tripping signal if I_{op} is greater than a percentage of I_{res} and greater than a minimum pickup current. Therefore,

Table A.1: Polarization configuration

Polarization	Operating	Polarizing	Details
Self-polarization	$Z_R I_{XY} - V_{XY}$	V_{XY}	$XY = AB, BC, CA.$ Z_R: setting.
Cross-polarization without memory	$Z_R I_{XY} - V_{XY}$	$-jV_Z$	$XY = AB, BC, CA.$ $Z = C, A, B.$ Z_R: setting.
Cross-polarization with memory	$Z_R I_{XY} - V_{XY}$	$-jV_{Z-MEM}$	$XY = AB, BC, CA.$ $Z = C, A, B.$ Z_R: setting.
Positive-sequence memory polarized	$Z_R I_{XY} - V_{XY}$	$-jV_{Z1-MEM}$	$XY = AB, BC, CA.$ $Z = C, A, B.$ Z_R: setting.
Self-polarization	$Z_R(I_X + kI_R) - V_{XG}$	V_{XG}	$Z = A, B, C.$ $I_R = I_A + I_B + I_C.$ $k = (Z_0 - Z_1)/3Z_1.$
Cross-polarization without memory	$Z_R(I_X + kI_R) - V_{XG}$	jV_{YZ}	$X = A, B, C.$ $YZ = BC, CA, AB.$ $I_R = I_A + I_B + I_C.$ $k = (Z_0 - Z_1)/3Z_1.$
Positive-sequence memory polarized	$Z_R(I_X + kI_R) - V_{XG}$	V_{X1-MEM}	$X = A, B, C.$ $I_R = I_A + I_B + I_C.$ Z_R: setting.

I_{op0} is the threshold value that prevents relay malfunction when the restriction current is close to zero with k as the restriction coefficient.

The differential operation of the currents is conducted using phasor measurements for each phase. Furthermore, the operation logic of this protection function consists of the activation of the following conditions using an AND logic:

- Threshold current start.
- Fault-phase selection logic.
- Angular difference of currents.

For internal faults (Fig. A.2), the current angles for both sides of a TL are in phase under ideal conditions. In general, the angle difference depends on the source voltage angles (pre-fault power flow condition) and the angles of the system impedances at both sides of the fault point [138].

Many manufacturers also choose to use zero- and negative-sequence elements to provide sensitive protection in presence of unbalanced faults.

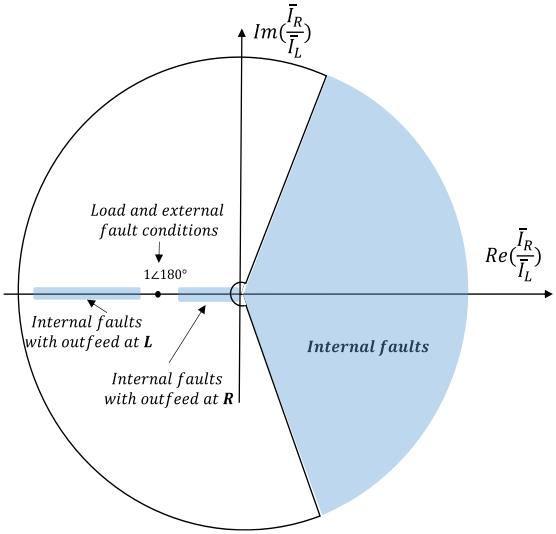


Figure A.2: Alpha plane characteristic

A.3 Directional element protection (function 32)

A.3.1 Directional elements for phase fault protection

The aim of directional elements is to determine fault direction (forward or backward) as shown in Fig. A.3. Therefore, they are part of the main protection schemes and these elements respond to the phase change between a polarized quantity and an operational quantity (Table A.1). An example in the Fig. A.4 shows that voltage (V) represents the polarized quantity and current (I) the operational quantity; also, the operating condition is shown in Eq. A.6.

Directional elements mainly determine the direction of faults (forward or backward). Therefore, they are part of the principal protection schemes

and these elements respond to a phase change between a polarized quantity and an operational quantity (Table. A.1). An example in Fig. A.4 shows that voltage (V_{an}) represents the polarized quantity and current (I_a) the operational quantity. The operating condition is given as:

$$\varphi_{sen} + 90^o > Arg(\frac{\mathbf{V}_{an}}{\mathbf{I}_a}) > \varphi_{sen} - 90^o \tag{A.6}$$

where φ_{sen}: represents the maximum sensitivity angle, which can be equal to the TL impedance angle from bus to fault point. This expression can be represented in an impedance plane ($R - X$) as shown in Fig.A.5.

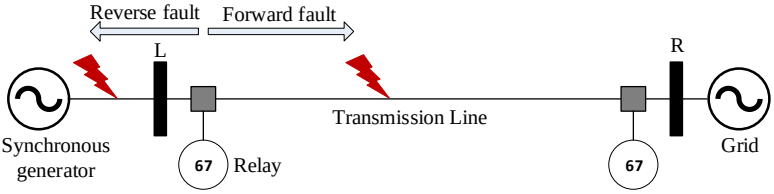


Figure A.3: General electrical system for directional element operation

TL impedance features are predominantly inductive. Thus, when the current lags with regard to the voltage, a forward fault occurs. In contrast, when the current signal changes its sign, it is considered as a backward fault.

A.3.2 Directional elements for ground fault protection

During a ground fault, the negative- and zero-sequence, voltage-polarized directional elements respond to impedance. Therefore, voltage-polarized directional elements are complemented by 32Q or 32G. The most common schemes that can be used to detect faults direction are show in Table. A.2.

The 32I element can determine the direction when the fault-type identification (FID) logic trips and indicates a balanced fault. In comparison, the 32Q or 32G elements are used when the FID logic

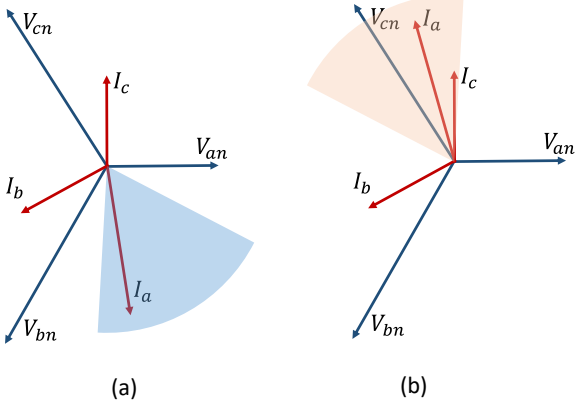


Figure A.4: (a) Blue zone means forward condition, and (b) Orange zone means reverse condition

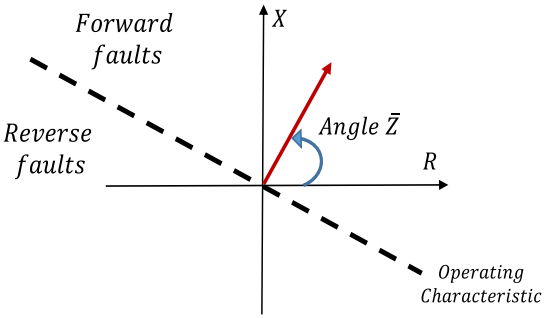


Figure A.5: $X - R$ plane of the forward and reverse fault characterization

asserts an unbalanced fault. In addition, some manufacturers also use combinations of these elements.

Table A.2: Polarization for zero- and negative-sequence

Polarization	Operating	Polarizing	Details
Zero-sequence current-polarization (32I)	$T = Re[3I_o I^*_{POL}]$	I_0, I_{POL}	I_{POL}: Current. polarization.
Negative-sequence voltage-polarization (32Q)	$z_2 = Re[V_2(I_2.1\angle Z1_{ANG})^*]/I_2^2$	$I_2, V_2, Z1_{ANG}$	$Z1_{ANG}$: setting $Z = C, A, B$.
Zero-sequence voltage-polarization (32V)	$z_0 = Re[3V_0(3I_0.1\angle Z0_{MTA})^*]/3I_0^2$	$3I_0, 3V_0, Z0_{MTA}$	$Z0_{MTA}$: maximun torque angle, setting.

In addition, some manufacturers can also use combinations of these elements.

A.4 Negative-sequence protection

This protection depends on negative-sequence current which has advantages over zero-sequence current. For instance, it is insensitive to zero-sequence mutual coupling and is not vulnerable to excessive tripping on external ground faults on TLs that share right of way. Moreover, it requires only a simple calculation. Its functions are as follows.

A.4.1 Negative-sequence overcurrent element (function 50Q/51Q)

This function operates from a starting threshold value known as a pickup setting and a time dial. With synchronous generators, it does not present any issue in starting because of high negative-sequence current. In practical applications, the thresholds are set at least higher than 1.5 times the nominal rated current.

A.4.2 Directional negative-sequence overcurrent element (function 67Q)

Unlike the previous function, this is characterized by determining the directionality of a fault based on the negative-sequence voltage (V_2) and current values, as shown in Fig. A.6.

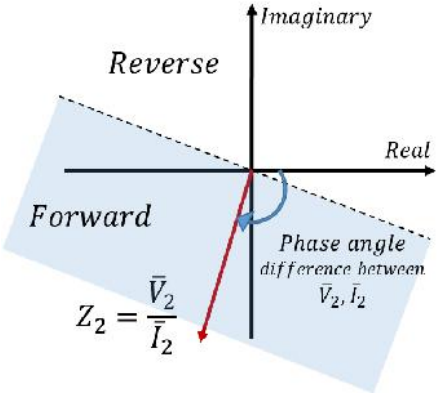


Figure A.6: Apparent negative-sequence fault impedance seen by 67Q

The criterion is based on that a forward/reverse fault causes a phase angle of approximately $-90^o/+90^o$ for the voltage phasor with regard to the current phasor [28; 140; 141]. This assumption stems from the highly inductive nature of the negative-sequence network in a network dominated by synchronous generators

A.5 Faulted-phase identification

Phase selection is important to prevent incorrect operation as it allows to identify faulty phases and is part of protection schemes. There are schemes that have changed and applied to phase fault selection loops, such as:

- A computationally efficient numerical method of characterizing distance elements onto a single point on a number line.
- Positive-sequence memory polarization for low- (or zero-) voltage faults for over 1 second.
- FIDS logic that uses measured negative- and zero-sequence currents.
- Decision trees (DTs) algorithm, including magnitude of currents, delta currents, magnitude of voltages, delta voltages, and

impedances. Due to the structure of the DT, not all criteria are evaluated to obtain a result.

Therefore, faults identification logic can also be used to differentiate balanced and unbalanced faults. This function serves as an input element for main functions.

A.5.1 FIDS Logic

This scheme involves the identification of a fault type based on a phase angle relationship between negative- and zero-sequence currents. The fault loop classification method was shown in Fig. A.4. A successful FIDS operation is based on the validity of the assumed mathematical relationships between the phase angles of zero- (I_{a0}) and negative-sequence (I_{a2}) quantities of phase A (Fig. A.7 and Table. A.3). In a network dominated by synchronous generators, this relationship is valid because of the inductive nature of the negative-sequence network and the impedance of the machines [142].

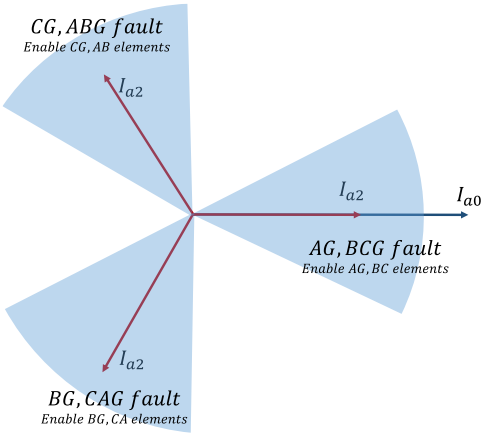


Figure A.7: Fault identification logic

where ptp is phase-to-phase, $Rag, Rbg, RcgareA, B, C$-phase-to-ground fault resistance respectively and Rf is the fault resistance.

Table A.3: FIDS logic

Angle between I_{a2} and I_{a0}	fault type permission
I_{a2} is $\pm 30^o$ of I_{a0}	Permit AG or BC
I_{a2} lags I_{a0} by $90^o - 150^o$	Permit BG or CA
I_{a2} leads I_{a0} by $90^o - 150^o$	Permit CG or AB
I_{a2} leads or lags I_{a0} by $30^o - 60^o$	Select the ptp mho element with the lowest calculated reach. Compare Rag with the Rf of that element
I_{a2} lags I_{a0} by $60^o - 90^o$ or $150^o - 180^o$	Select the ptp mho element with the lowest calculated reach. Compare Rbg with the Rf of that element
I_{a2} leads I_{a0} by $60^o - 90^o$ or $150^o - 180^o$	Select the ptp mho element with the lowest calculated reach. Compare Rcg with the Rf of that element.

A.6 Directional overcurrent protection (67)

Directional overcurrent protection uses directional elements to supervise the operation of overcurrent elements [138]. This element has been detailed in previous section. On the other hand, when three-phase and phase-to-phase SC faults occur at any point in a power system, the amplitude of the SC-current is usually bigger than the load current, and thus the overcurrent protection is distinguished from normal operating state by the amplitude of currents [143]. This criterion is simple and reliable, and easy to implement. The operating logic is based on (A.7), where I_{set} is the starting threshold current

$$I > I_{set} \tag{A.7}$$

APPENDIX B

Appendix B: Transmission line model

B.1 TL with distributed parameter model

A transmission line is modeled as a distributed parameter circuit to describe transient phenomena with greater accuracy. The circuit representation of the distributed parameter model is shown in Fig. B.1, which applies the $RLCG$ parameter of the line to an elementary section.

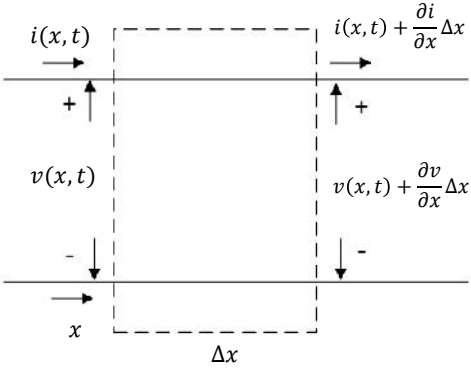


Figure B.1: Differential element of a transmission line

The voltage drop along the longitudinal element of the line depends on the differential element $\triangle x$. Therefore, the voltage and current relationships in the longitudinal element are expressed by Eq.B.1 and Eq.B.2.

$$\frac{\partial v(x,t)}{\partial x}\triangle x = -(Ri(x,t) + L\frac{\partial i(x,t)}{\partial t})\triangle x \tag{B.1}$$

$$\frac{\partial i(x,t)}{\partial x}\triangle x = -(Gv(x,t) + C\frac{\partial v(x,t)}{\partial t})\triangle x \tag{B.2}$$

where $R, G, L,$ and C represent the per unit length resistance, conductance, inductance, and capacitance of the path respectively.

Then, considering the lossless line. Equations (B.3) and (B.4) are obtained.

$$\frac{\partial v(x,t)}{\partial x} = -L\frac{\partial i(x,t)}{\partial t} \tag{B.3}$$

$$\frac{\partial i(x,t)}{\partial x} = -C\frac{\partial v(x,t)}{\partial t} \tag{B.4}$$

Moreover, it is partially derived with regard to x and t in both equations:

$$\frac{\partial^2 v(x,t)}{\partial x^2} - LC\frac{\partial^2 v(x,t)}{\partial t^2} = 0 \tag{B.5}$$

$$\frac{\partial^2 i(x,t)}{\partial x^2} - LC\frac{\partial^2 i(x,t)}{\partial t^2} = 0 \tag{B.6}$$

These expressions represent the equations of traveling waves.

Hyperbolic functions are solution to the traveling wave equation in the phasor domain. In this case, the value of the voltage (V_1) and the current (I_1) can be determined by using the following equations:

$$V_1 = V_2 cosh(\gamma\ell) + I_2 Z sinh(\gamma\ell) \tag{B.7}$$

$$I_1 = (V_2/Z) sinh(\gamma\ell) + I_2 cosh(\gamma\ell) \tag{B.8}$$

where:

$$Z = \sqrt{(R + jwL)/(G + jwC)} \tag{B.9}$$

$$\gamma = \sqrt{(R + jwL)(G + jwC)} \tag{B.10}$$

where ℓ is the total length of the line.

B.2 Transient wave propagation characteristics

A short circuit on the transmission line generates traveling wave signals that propagate from the fault to the line terminals with a propagation speed that depends on the inductance and capacitance of the line (close to the speed of light).

The time-domain solution of the traveling wave equations (B.5 and B.6) is given by the following equations:

$$v(x,t) = v_{forw}(x - ut) + v_{back}(x + ut) \tag{B.11}$$

$$i(x,t) = \frac{1}{Z_C} v_{forw}(x - ut) - \frac{1}{Z_C} v_{back}(x + ut) \tag{B.12}$$

where:

v_{forw} and v_{back} are the forward and backward voltage components, respectively.

Z_C is the characteristic impedance of the transmission line.

u is the propagation speed of the wave.

B.3 Reflections and refractions at the TL Terminals

A single-phase system representation is considered to explain Γ_v, ρ_v, Γ_i and ρ_i, which stand for voltage reflection and refraction, and current reflection and refraction coefficients at line terminals, respectively. These coefficients can be obtained as follows [144; 145]:

$$\Gamma_v = \frac{Z_t - Z_{line}}{Z_t + Z_{line}} \tag{B.13}$$

$$\rho_v = \frac{2Z_t}{Z_t + Z_{line}} \tag{B.14}$$

$$\Gamma_i = \frac{Z_{line} - Z_t}{Z_t + Z_{line}} \tag{B.15}$$

$$\rho_i = \frac{2Z_{line}}{Z_t + Z_{line}} \tag{B.16}$$

where Z_{line} is the transmission line surge impedance and Z_t is the terminal equivalent impedance.

APPENDIX C

Appendix C: Signal processing methods

C.1 Theory of Mathematical Morphology

Mathematical Morphology (MM) can be defined as a theory and technique for the analysis of spatial structures, based on set theory, integral geometry and lattice algebra. In contrast to the theory of linear signal processing, such as fourier transform or wavelet transform, MM is non-linear. The main function of morphological operators is to extract relevant structures of a set. The extraction is usually done by the interaction between the set and another set, which is called structuring element (SE). The shape of the SE is pre-defined according to some a priori knowledge about the shape of the signal [146].

C.1.1 Definitions for binary operations

Minkowski addition is a binary operation of two sets A and B in Euclidean space, named after Hermann Minkowski. It is denoted by $\frac{M}{\oplus}$ and is defined as the result of adding every element of A to every element of B:

$$A \frac{M}{\oplus} B = \{a + b \mid a \in A, b \in B\} = \cup_{b \in B}(A)_b \tag{C.1}$$

Minkowski subtraction, denoted by $\frac{M}{\ominus}$, and defined as:

$$A \overset{M}{\underset{\oplus}{}} B = \cap_{b \in B} (A)_b \tag{C.2}$$

C.1.2 Binary dilation and erosion

The definition of dilation is similar to Minkowski addition. Replacing the operator $\overset{M}{\underset{\oplus}{}}$ by $\oplus$ and use a reflected SE, $\overline{B}$.

$$A \oplus B = \cup_{b \in \overline{B}} (A)_b = \cup_{b \in B} (A)_{-b} = \cup_{b \in B} \{x \mid x = a - b, a \in A\} \tag{C.3}$$

Erosion derives from Minkowski subtraction, but this time b comes from the reflection set of B. The definition of erosion is:

$$A \ominus B = \cap_{b \in \overline{B}} (A)_b = \cap_{b \in B} (A)_{-b} = \cap_{b \in B} \{x \mid x = a - b, a \in A\} \tag{C.4}$$

C.1.3 Set representations of functions

Georges Matheron and Jean Serra [147] proposed the MM theory. This method was applied to signal processing of the one-dimensional non-linear type, which verified good robustness. Moreover, it is based on some basic operations that are defined as: dilation ($\oplus$), erosion ($\ominus$). Intuitively, dilation can be imagined as swelling or expanding, while erosion can be thought of as a shrinking procedure.

$$\begin{aligned}(f \oplus g)(x) = \max_m \{&f(x+m) + g(m) \\ &|(x+m) \in D_f, m \in D_g\}\end{aligned} \tag{C.5}$$

$$\begin{aligned}(f \ominus g)(x) = \min_m \{&f(x+m) - g(m) \\ &|(x+m) \in D_f, m \in D_g\}\end{aligned} \tag{C.6}$$

where:
$f(x)$ is the original one-dimensional discrete signal.
$g(x)$ is defined as the structuring element (SE) function.

D_f and D_g are defined as the domains of f and g, respectively.

x is the signal sample.

The dilation operation usually uses a structuring element for probing and expanding the shapes contained in the input signal as shown in Fig. C.1.

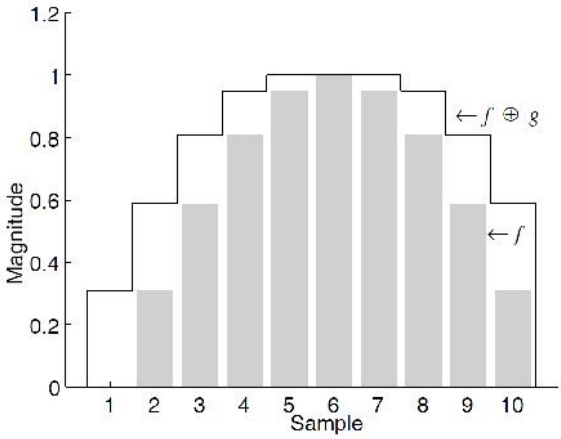


Figure C.1: Dilation of a one-dimensional signal

The erosion operation usually uses a structuring element for probing and reducing the shapes contained in the input signal as shown in Fig. C.2.

C.2 Morphological filters

Morphological filters are non-linear signal transforms that locally modify the geometrical features of signals or image objects The idempotence and increasing properties are necessary and sufficient conditions for a transform, to be a morphological filter [146].

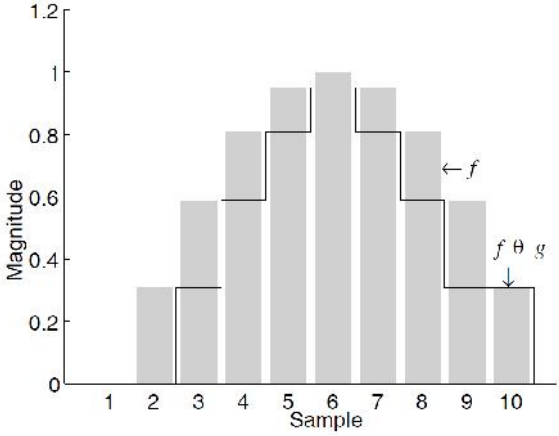


Figure C.2: Erosion of a one-dimensional signal

C.2.1 Opening and Closing

The opening ($\bullet$) and closing ($\circ$) are constructed operations based on the combination of dilation and erosion, as shown below:

$$(f \bullet g)(x) = \{(f \oplus g) \ominus g\}(x) \tag{C.7}$$

$$(f \circ g)(x) = \{(f \ominus g) \oplus g\}(x) \tag{C.8}$$

The opening operation erodes a signal and then dilates the eroded signal, using the same structuring element for both operations as shown in Fig. C.3.

The closing operation dilates an image and then erodes the dilated image, using the same structuring element for both operations as shown in Fig. C.4.

C.2.2 Morphological Gradient Algorithm

The morphological gradient is defined as the arithmetic difference between the dilation and erosion of a signal by an SE. When using a flat SE, the morphological gradient is a powerful tool for edge detection. The

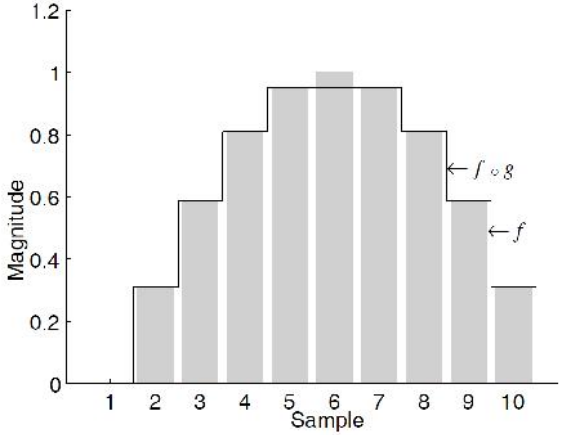


Figure C.3: Opening of a one-dimensional signal

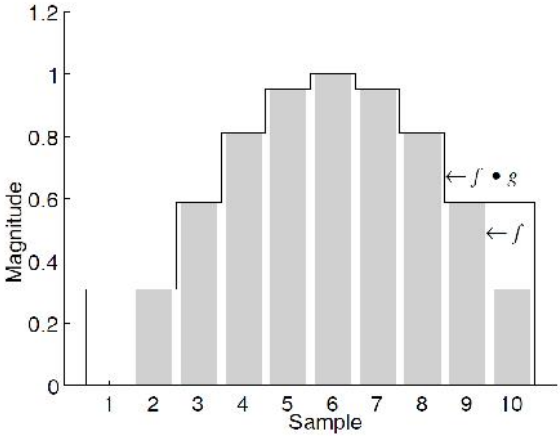


Figure C.4: Closing of a one-dimensional signal

morphological gradient is frequently used for edge detection in image and signal processing. Before giving its definition, two residual operators should be defined first. Denote the input signal and the SE by f and g,

respectively. The dilation residual, G_d, is defined as the difference between the dilation of f by g and f, which is:

$$G_d(f) = (f \oplus g) - f \tag{C.9}$$

The erosion residual G_e is the difference between f and the erosion of f by g, as follows:

$$G_e(f) = f - (f \ominus g) \tag{C.10}$$

Then, the morphological gradient is usually defined as:

$$G(f) = (f \oplus g) - (f \ominus g) = G_d(f) + G_e(f) \tag{C.11}$$

The multi-resolution morphological gradient is an improved morphological gradient, which aims at depressing the steady state components and enhancing the transients ones.

C.3 Discrete Wavelet Transform (DWT)

The DWT is an extended version of the wavelet transform. Samples represented by the function $\phi_j(x)$ are passed through a low-pass filter with impulse response or wavelet mother function $\psi_j(x)$, which results in a convolution according to the equation (C.12):

$$y(x) = [\phi * \psi](x) = \sum_{k=-\infty}^{\infty} \phi(k)\psi(x-k) \tag{C.12}$$

Then, the function is associated with a high-pass filter with coefficients $H = h(x)$ and a low-pass filter with coefficients $G = g(x)$[148], as shown in equation (C.13) and equation (C.14).

$$y_{low}(x) = \sum_{k=-\infty}^{\infty} \phi(k)g(2x-k) \tag{C.13}$$

$$y_{high}(x) = \sum_{k=-\infty}^{\infty} \phi(k)h(2x-k) \tag{C.14}$$

The DWT can be considered as a filter bank where the signal is decomposed into the detailed coefficient d_1 and an approximation coefficient a_1. To continue the decomposition procedure, the approximation coefficient is sent to the second stage to produce new coefficients. The process is repeated up to the desired level n (Fig.C.5).

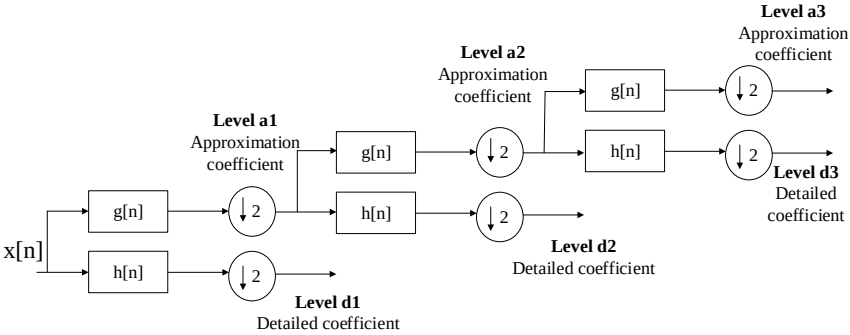


Figure C.5: Decomposition of signals by DWT.

The MRA is a useful implementation of the DWT. In this case, both the detailed d and approximation a coefficients are decomposed at each level as shown in Fig. C.6 where the exponential increase in the number of the signals is observed, this method is also known as Wavelet Packets.

The frequency ranges at each level are presented in Table C.1, where N is considered as the initial total number of samples and F_s is the sampling frequency. It should be noted that the decomposition in each level corresponds to a range of frequencies and not to a specific frequency.

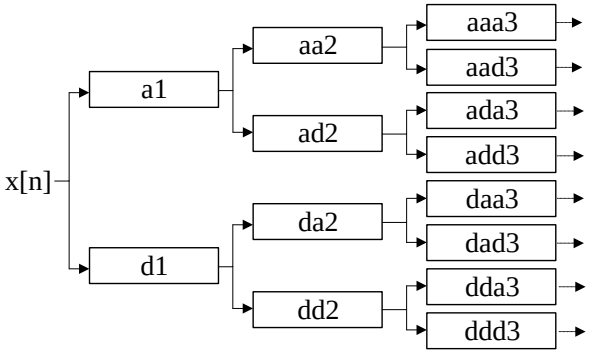


Figure C.6: Decomposition based on Wavelet packtes.

Table C.1: Wavelet decomposition

Level (n)	**Coef.**	**Frequency range**	**Samples**
1	$d1$	$f_s/2 - f_s$	$N/2^1$
1	$a1$	$0 - f_s/2$	$N/2^1$
2	$dd2$	$3 * f_s/4 - f_s$	$N/2^2$
2	$da2$	$f_s/2 - 3 * f_s/4$	$N/2^2$
2	$ad2$	$f_s/4 - f_s/2$	$N/2^2$
2	$aa2$	$0 - f_s/4$	$N/2^2$
:	:	:	:

APPENDIX D

Appendix D: Equipment characteristics of test models

D.1 Generic model of a power system

The Table D.1 shows the characteristics of the equivalent of the electrical network.

Table D.1: Grid parameters

	Parameter	Value
Main grid	Voltage	220 kV
	Frequence	50 Hz
	Impedance $R0$	0.08 Ω
	Impedance $L0$	1.77 Ω
	Impedance $R+$	0.24 Ω
	Impedance $L+$	3.82 Ω
Busbar	Parasitic capacitance Cs	0.05 uF

The Fig. D.1 shows the configuration of the tower structures of the two transmission lines.

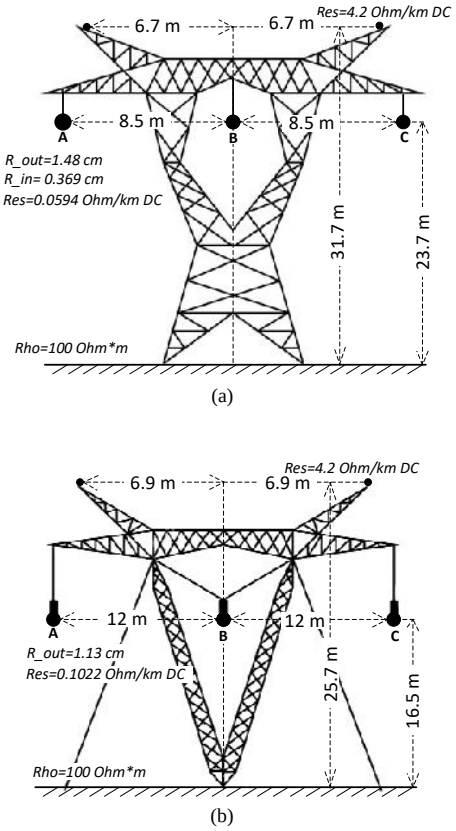


Figure D.1: TL configuration (a)Line L-R (b) Line R-T

D.2 Current-source type generator

The Table D.2 shows the characteristics of the transformer of the Current-source generator.

The Table D.3 shows the characteristics of the Current-source generator.

Table D.2: Step-up power transformer

	Parameter	Value
Transformer (TR)	Voltage	220/33 kV
	Power	90 MVA
	Connections	YD11
	SC Impedance	11.72%
	Loss	223.56 kW

Table D.3: Current-source characteristics

	Parameter	Value
Inverter	Rated power	1.5 MW
	Rated Voltage	2.2 kV
LCL filter	Inductance $L1$	1 mH
	Resistance $R1$	0.01 Ω
	Inductance $L2$	0.3 mH
	Resistance $R2$	0.01 Ω
	Capacitor C	20 uF
	Resistance $R3$	0.2 Ω
DC-link	Rated volatge	1.2 kV
	Capacitor Cd	4500 uF

D.3 Type 3 wind generator

The Table D.4 shows the characteristics of the type 3 wind generator. The characteristics of the power control system are described in detail in [134].

Table D.4: DFIG characteristics

	Parameter	Value
Grid-side inverter	Rated power	1.5 MW
	Rated Voltage	2.2 kV
	Switching frequency	10kHz
Step-up transformer	Rated capacity	1.6 MW
	Voltage	33/2.2 kV
	SC impedance	6.7%

D.4 IEEH TU-Dresden laboratory

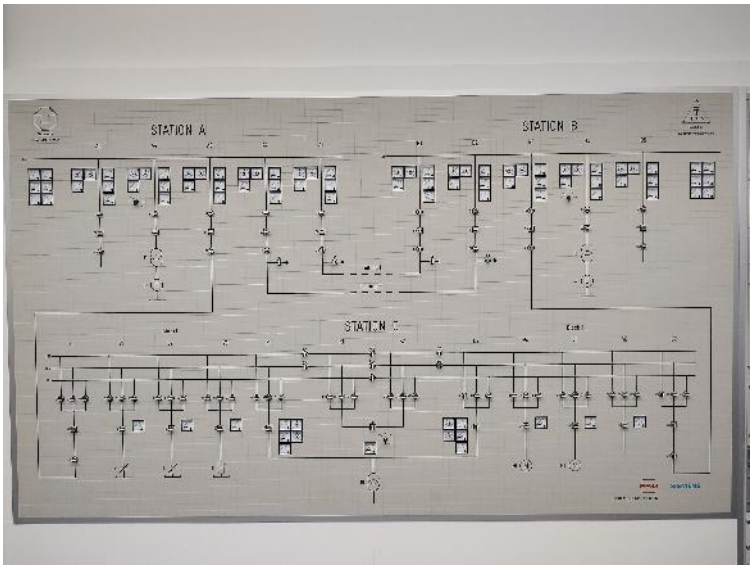


Figure D.2: Power system model



Figure D.3: Transmission line model



Figure D.4: PI model of a line section

Z/mΩ	a	b	c	A	B	C
a	20,85+117,41i	0,66+71,51i	0,38+49,66i	0,18+45,23i	0,23+43,73i	0,09+30,83i
b	0,66+71,51i	21,77+112,71i	1,02+81,27i	0,40+48,01i	0,81+66,78i	0,45+47,20i
c	0,38+49,66i	1,02+81,27i	22,17+114,60i	0,23+36,93i	0,88+66,67i	0,80+60,54i
A	0,18+45,23i	0,40+48,01i	0,23+36,93i	20,70+116,30i	0,82+77,91i	0,45+53,03i
B	0,23+43,73i	0,81+66,78i	0,88+66,67i	0,82+77,91i	22,36+117,82i	1,07+82,77i
C	0,09+30,83i	0,45+47,20i	0,80+60,54i	0,45+53,03i	1,07+82,77i	21,37+110,61i

Figure D.5: Mean values of self- and coupling impedances per component

C/nF	a	b	c	A	B	C	E	$R_{n\bar{E}}$/kΩ
a		299,7	93,2	31,5	0,0	0,0	838,6	14,95
b	299,7		299,4	44,7	31,5	0,0	650,7	15,05
c	93,2	299,4		140,3	44,6	31,5	762,4	14,89
A	31,5	44,7	140,3		298,8	93,3	765,8	14,51
B	0,0	31,5	44,6	298,8		299,1	651,2	14,45
C	0,0	0,0	31,5	93,3	299,1		836,4	14,56
E	838,6	650,7	762,4	765,8	651,2	836,4		

Figure D.6: Mean values of coupling capacitances and leakage resistances

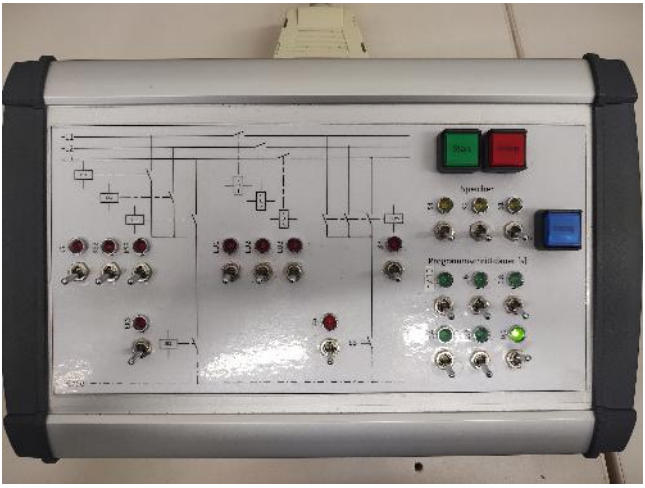


Figure D.7: Fault simulation control equipment

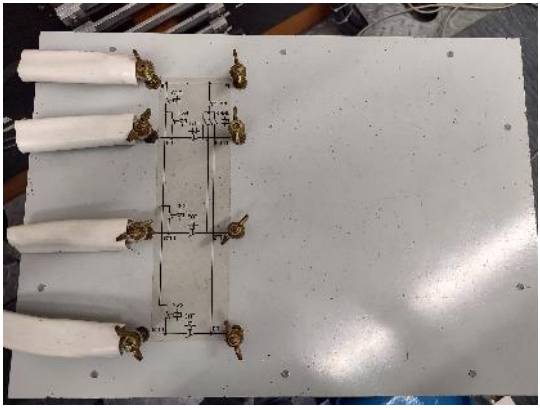


Figure D.8: Short-circuit device

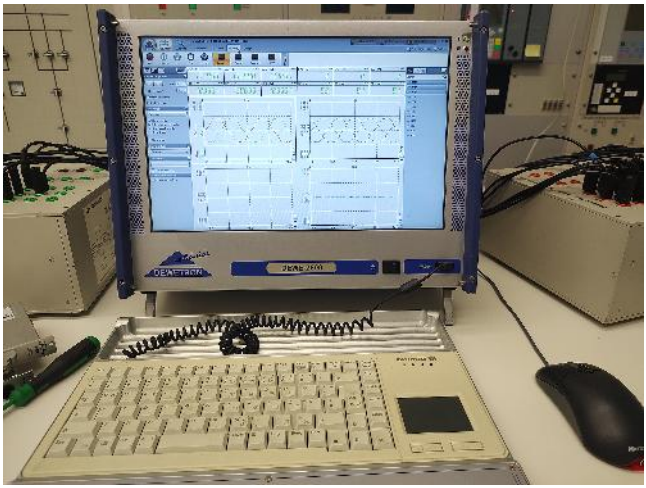


Figure D.9: High-frequency signal extraction device



Figure D.10: Substation control equipment

Bibliography

[1] R. Chowdhury and N. Fischer, "Transmission line protection for systems with inverter-based resources - part i: Problems," *IEEE Transactions on Power Delivery*, vol. 36, no. 4, pp. 2416–2425, 2021.

[2] A. Haddadi, M. Zhao, I. Kocar, U. Karaagac, K. W. Chan, and E. Farantatos, "Impact of inverter-based resources on negative sequence quantities-based protection elements," *IEEE Transactions on Power Delivery*, vol. 36, no. 1, pp. 289–298, 2021.

[3] A. Haddadi, I. Kocar, J. Mahseredjian, U. Karaagac, and E. Farantatos, "Performance of phase comparison line protection under inverter-based resources and impact of the german grid code," in *2020 IEEE Power and Energy Society General Meeting (PESGM)*, pp. 1–5, 2020.

[4] R. Belhomme, E. Corsetti, C. Gutschi, K. Kessels, A. Virag, M. Qadrdan, X. Xu, H. Li, and J. Jurasz, "Bottom-up flexibility in multi-energy systems: Real-world experiences from europe," *IEEE Power and Energy Magazine*, vol. 19, no. 4, pp. 74–85, 2021.

[5] F. Blaabjerg, Z. Chen, and S. Kjaer, "Power electronics as efficient interface in dispersed power generation systems," *IEEE Transactions on Power Electronics*, vol. 19, no. 5, pp. 1184–1194, 2004.

[6] J. Carrasco, L. Franquelo, J. Bialasiewicz, E. Galvan, R. PortilloGuisado, M. Prats, J. Leon, and N. Moreno-Alfonso, "Power-electronic systems for the grid integration of renewable energy sources: A survey," *IEEE Transactions on Industrial Electronics*, vol. 53, no. 4, pp. 1002–1016, 2006.

[7] E. Muljadi, N. Samaan, V. Gevorgian, J. Li, and S. Pasupulati, "Different factors affecting short circuit behavior of a wind power plant," *IEEE Transactions on Industry Applications*, vol. 49, no. 1, pp. 284–292, 2013.

[8] G. Custer, "Inverter protection and ride-through: Today's photovoltaic and energy storage inverters," *IEEE Electrification Magazine*, vol. 9, no. 2, pp. 43–49, 2021.

[9] S. A. Saleh, A. S. Aljankawey, M. S. Abu-Khaizaran, and B. Alsayid, "Influences of power electronic converters on voltage-current behaviors during faults in dgus-part i: Wind energy conversion systems," *IEEE Transactions on Industry Applications*, vol. 51, no. 4, pp. 2819–2831, 2015.

[10] S. A. Saleh, A. S. Aljankawey, B. Alsayid, and M. S. Abu-Khaizaran, "Influences of power electronic converters on voltage-current behaviors during faults in dgus-part ii: Photovoltaic systems," *IEEE Transactions on Industry Applications*, vol. 51, no. 4, pp. 2832–2845, 2015.

[11] R. Henriquez-Auba, J. D. Lara, D. S. Callaway, and C. Barrows, "Transient simulations with a large penetration of converter-interfaced generation: Scientific computing challenges and opportunities," *IEEE Electrification Magazine*, vol. 9, no. 2, pp. 72–82, 2021.

[12] A. Bose, "Renewable energy integration and the control and protection paradigms of the future," in *2012 IEEE Power and Energy Society General Meeting*, pp. 1–3, 2012.

[13] P. Chirapongsananurak and S. Santoso, "Multi-time-scale simulation tool for renewable energy integration analysis in distribution circuits," *Inventions*, vol. 2, no. 2, p. 7, 2017.

[14] "Ieee draft standard for interconnection and interoperability of inverter-based resources (ibr) interconnecting with associated transmission electric power systems," *IEEE P2800/D6.0, March 2021*, pp. 1–170, 2021.

[15] M. Curzi, R. Sharma, and F. Martin, "In fault ride through reactive current rise time requirements of various european grid codes analysis based on a full converter wind turbine," *Wind Energy*, vol. 19, no. 6, p. 1121 â 1133, 2016.

[16] Z. G. Molina, B. S. Lopez, I. Del Castillo, and M. Del Pino, "Impact on the power system protection of high penetration of wind farms technology," 2010.

[17] R. A. Walling, E. Gursoy, and B. English, "Current contributions from type 3 and type 4 wind turbine generators during faults," in *PES T and D 2012*, pp. 1–6, 2012.

[18] T. Neumann, T. Wijnhoven, G. Deconinck, and I. Erlich, "Enhanced dynamic voltage control of type 4 wind turbines during unbalanced grid faults," *IEEE Transactions on Energy Conversion*, vol. 30, no. 4, pp. 1650–1659, 2015.

[19] M. Tsili and S. Papathanassiou, "A review of grid code technical requirements for wind farms," *IET Renewable power generation*, vol. 3, no. 3, pp. 308–332, 2009.

[20] "Ieee draft application guide for ieee std 1547(tm), ieee standard for interconnecting distributed resources with electric power systems," *IEEE P1547.2/D6.2, March 2022*, pp. 1–316, 2022.

[21] Z. Yong and L. Zaiwen, "Review of frt requirements for integration of wind energy in china and europe," in *The 2nd International Symposium on Power Electronics for Distributed Generation Systems*, pp. 589–592, IEEE, 2010.

[22] B. Nhlapo and K. Awodele, "Review and comparison of the south african grid code requirements for wind generation with the european countries grid codes," in *2020 International SAUPEC/RobMech/PRASA Conference*, pp. 1–6, IEEE, 2020.

[23] D. Popovic and I. Wallace, "International review of fault ride through for conventional generators," *London*, 2010.

[24] H. A. Villarroel-Gutierrez and M. Molina, "Analysis of dynamic voltage support schemes for pv generators implemented in latin america," *IEEE Latin America Transactions*, vol. 18, no. 04, pp. 641–651, 2020.

[25] A. Bapary, J. Barsch, M. Bloder, S. Brahma, D. Buchanan, R. Chowdhury, J. Deaton, R. Cunico, A. Deronja, R. Fan, E. Farantatos, K. Garg, Y. Gong, F. Gotte, J.-F. Hache, A. Hooshyar, A. Kifle, H. Ladner, B. Magruder, J. Martinez, D. Morrissey, K. Narendra, A. Nguyen, M. Patel, N. Perera, J. Perez, D. Reckerd, J. Seuss, J. Van de Ligt, and A. Zamani, "Protection challenges and practices for interconnecting inverter based resources to utility transmission systems," *IEEE Power Energy Society Resource Center*, 2020.

[26] R. Chowdhury, M. Alla, N. Fischer, and S. Samineni, "Restricted earth fault protection in low-impedance grounded systems with inverter-based resources," *IEEE Transactions on Power Delivery*, vol. 38, no. 1, pp. 505–512, 2023.

[27] M. M. Mobashsher, A. A. Abdoos, S. M. Hosseini, S. M. Hashemi, and M. Sanaye-Pasand, "An accelerated distance protection scheme for the lines connected to inverter-based resources," *IEEE Systems Journal*, vol. 17, no. 4, pp. 6272–6281, 2023.

[28] Y. Ohura, T. Matsuda, M. Suzuki, F. Andow, Y. Kurosawa, and A. Takeuchi, "A digital distance relay using negative sequence current," *IEEE Transactions on Power Delivery*, vol. 5, no. 1, pp. 79–84, 1990.

[29] M. R. Behnke, G. Custer, E. Farantatos, N. Fischer, R. Guttromson, A. Isaacs, R. Majumder, S. Pant, M. Patel, V. Reddy-Konala, *et al.*, "Impact of inverter based resource negative sequence current injection on transmission system protection," tech. rep., 2020.

[30] I. Erlich, T. Neumann, F. Shewarega, P. Schegner, and J. Meyer, "Wind turbine negative sequence current control and its effect on power system protection," in *2013 IEEE Power and Energy Society General Meeting*, pp. 1–5, 2013.

[31] A. Haddadi, I. Kocar, and E. Farantatos, "Impact of inverter-based resources on protection schemes based on negative sequence components," *EPRI: Palo Alto, CA, USA*, 2019.

[32] G. Kou, J. Jordan, B. Cockerham, R. Patterson, and P. VanSant, "Negative-sequence current injection of transmission solar farms," *IEEE Transactions on Power Delivery*, vol. 35, no. 6, pp. 2740–2743, 2020.

[33] A. Hooshyar, M. A. Azzouz, and E. F. El-Saadany, "Distance protection of lines emanating from full-scale converter-interfaced renewable energy power plants-part i: Problem statement," *IEEE Transactions on Power Delivery*, vol. 30, no. 4, pp. 1770–1780, 2015.

[34] Y. Fang, K. Jia, Z. Yang, Y. Li, and T. Bi, "Impact of inverter-interfaced renewable energy generators on distance protection and an improved scheme," *IEEE Transactions on Industrial Electronics*, vol. 66, no. 9, pp. 7078–7088, 2019.

[35] M. Sarkar, J. Jia, and G. Yang, "Distance relay performance in future converter dominated power systems," in *2017 IEEE Manchester PowerTech*, pp. 1–6, 2017.

[36] N. Nimpitiwan, G. T. Heydt, R. Ayyanar, and S. Suryanarayanan, "Fault current contribution from synchronous machine and inverter based distributed generators," *IEEE Transactions on Power Delivery*, vol. 22, no. 1, pp. 634–641, 2007.

[37] J. C. Quispe H, H. Villarroel-Gutierrez, and E. Orduna, "Analyzing short-circuit current behavior caused by inverter-interfaced renewable energy sources. effects on distance protection," in *2020 IEEE PES Transmission and Distribution Conference and Exhibition - Latin America (T and D LA)*, pp. 1–6, 2020.

[38] L. Qin-hao, Z. Yong-jun, Y. Wei-peng, and L. Feng, "A study on influence of wind power on positive sequence voltage polarized impedance relay," in *2012 Power Engineering and Automation Conference*, pp. 1–4, 2012.

[39] A. Hooshyar, M. A. Azzouz, and E. F. El-Saadany, "Distance protection of lines connected to induction generator-based wind farms during balanced faults," *IEEE Transactions on Sustainable Energy*, vol. 5, no. 4, pp. 1193–1203, 2014.

[40] J. Alshehri, M. Khalid, and F. Alismail, "Distance protection performance in ac power system with back-to-back converter interface," in *2019 IEEE Industry Applications Society Annual Meeting*, pp. 1–6, 2019.

[41] J. Jia, G. Yang, A. H. Nielsen, and P. RÃ¸nne-Hansen, "Impact of vsc control strategies and incorporation of synchronous condensers on distance protection under unbalanced faults," *IEEE Transactions on Industrial Electronics*, vol. 66, no. 2, pp. 1108–1118, 2019.

[42] L. He, C.-C. Liu, A. Pitto, and D. Cirio, "Distance protection of ac grid with hvdc-connected offshore wind generators," *IEEE Transactions on Power Delivery*, vol. 29, no. 2, pp. 493–501, 2014.

[43] K. Jia, R. Chen, Z. Xuan, Z. Yang, Y. Fang, and T. Bi, "Fault characteristics and protection adaptability analysis in vsc-hvdc-connected offshore wind farm integration system," *IET Renewable Power Generation*, vol. 12, no. 13, pp. 1547–1554, 2018.

[44] Y. Liu, G. Li, H. Wang, Z. Wang, and M. Yu, "Research on ac line distance relay in the presence of modular multilevel converter based hvdc," in *2016 IEEE PES Asia-Pacific Power and Energy Engineering Conference (APPEEC)*, pp. 1622–1626, 2016.

[45] V. Chakeri, H. Seyedi, and M. Tarafdar Hagh, "A new approach to transmission line pilot protection in the presence of inverter-interfaced distributed generators," *IEEE Systems Journal*, vol. 15, no. 4, pp. 5383–5392, 2021.

[46] M. Khoddam and H. K. Karegar, "Effect of wind turbines equipped with doubly-fed induction generators on distance protection," in *2011 International Conference on Advanced Power System Automation and Protection*, vol. 2, pp. 1349–1353, 2011.

[47] S. De Rijcke, P. S. Perez, and J. Driesen, "Impact of wind turbines equipped with doubly-fed induction generators on distance relaying," in *IEEE PES General Meeting*, pp. 1–6, 2010.

[48] H. Sadeghi, "A novel method for adaptive distance protection of transmission line connected to wind farms," *International Journal of Electrical Power and Energy Systems*, vol. 43, no. 1, pp. 1376–1382, 2012.

[49] M. Nagpal and C. Henville, "Bc hydro protection interconnection practices for sources with inverter or converter interface," in *Proc. 45th Annu. Western Protective Relay Conf.*, pp. 17–18, 2018.

[50] M. Nagpal and C. Henville, "Impact of power-electronic sources on transmission line ground fault protection," *IEEE Transactions on Power Delivery*, vol. 33, no. 1, pp. 62–70, 2018.

[51] S. Shen and P. Zhang, "Characteristics of sequence impedances of dfig wind farm and the impacts on the phase selection elements," in *2014 IEEE PES General Meeting Conference and Exposition*, pp. 1–5, 2014.

[52] G. Yang, M. Dong, Z. Zhou, C. Zhou, D. Du, Z. Zhan, and D. Yang, "The influences and countermeasures of wind farm access to transmission line differential protection," in *2012 IEEE Power Electronics and Machines in Wind Applications*, pp. 1–4, 2012.

[53] Y. Li, K. Jia, T. Bi, R. Yan, W. Li, and B. Liu, "Analysis of line current differential protection considering inverter-interfaced renewable energy power plants," in *2017 IEEE PES Innovative Smart Grid Technologies Conference Europe (ISGT-Europe)*, pp. 1–6, 2017.

[54] B. Chen, A. Shrestha, F. A. Ituzaro, and N. Fischer, "Addressing protection challenges associated with type 3 and type 4 wind turbine generators," in *2015 68th Annual Conference for Protective Relay Engineers*, pp. 335–344, 2015.

[55] H. Herrmann, H. Kuhn, H. Fohring, A. Ludwig, F. Oechsle, and P. Schegner, "Impact of renewable generation on protection and disconnecting solutions-german practice and experiences," *43rd Conseil International des Grands Reseaux Electriques (CIGRE)[43rd International Council of Large Electric Resources], Paris, France*, pp. B5–208, 2010.

[56] A. Hooshyar, M. A. Azzouz, and E. F. El-Saadany, "Distance protection of lines emanating from full-scale converter-interfaced renewable energy power plants-part ii: Solution description and evaluation," *IEEE Transactions on Power Delivery*, vol. 30, no. 4, pp. 1781–1791, 2015.

[57] S. Chen, N. Tai, C. Fan, J. Liu, and S. Hong, "Adaptive distance protection for grounded fault of lines connected with doubly-fed induction generators," *IET Generation, Transmission and Distribution*, vol. 11, no. 6, pp. 1513–1520, 2017.

[58] A. K. Pradhan and G. Joos, "Adaptive distance relay setting for lines connecting wind farms," *IEEE Transactions on Energy Conversion*, vol. 22, no. 1, pp. 206–213, 2007.

[59] S. Manson, F. Calero, and A. Guzman, "Advancements in line protection for the future grid," *IEEE Power and Energy Magazine*, vol. 20, no. 2, pp. 125–131, 2022.

[60] J. Blumschein, C. Dzienis, and Y. Yelgin, "New design of distance protection for smart grid applications," in *13th International Conference on Development in Power System Protection 2016 (DPSP)*, pp. 1–8, 2016.

[61] B. Li and M. Lin, "Analysis of directional pilot protection on transmission line with wind farm integration," in *2011 International Conference on Advanced Power System Automation and Protection*, vol. 1, pp. 303–308, 2011.

[62] O. Janke, "The directional reactive power undervoltage protection - a protection concept for connecting decentralized renewable energy sources," in *2011 2nd IEEE PES International Conference and Exhibition on Innovative Smart Grid Technologies*, pp. 1–5, 2011.

[63] K. Jia, Y. Li, Y. Fang, L. Zheng, T. Bi, and Q. Yang, "Transient current similarity based protection for wind farm transmission lines," *Applied energy*, vol. 225, pp. 42–51, 2018.

[64] Z. Chen, Z. Bo, and X. Dong, "A transient signal based protective relay in power systems with power electronic converters," in *2005 IEEE/PES Transmission and Distribution Conference and Exposition: Asia and Pacific*, pp. 1–6, 2005.

[65] M. A. Aftab, S. S. Hussain, I. Ali, and T. S. Ustun, "Dynamic protection of power systems with high penetration of renewables: A review of the traveling wave based fault location techniques," *International Journal of Electrical Power and Energy Systems*, vol. 114, p. 105410, 2020.

[66] M. S. Abdelrahman, I. Kharchouf, and O. A. Mohammed, "Ann-tw analysis based transmission line fault identification and location with high penetration of inverter-based resources," in *2023 IEEE Green Technologies Conference (GreenTech)*, pp. 134–138, 2023.

[67] N. Tong, L. Chen, W. Wang, X. Lin, and Z. Li, "Local-measurement-based high-speed protection for half-wavelength uhv lines," *IEEE Transactions on Power Delivery*, vol. 35, no. 5, pp. 2481–2494, 2020.

[68] F. Wilches-Bernal, A. Bidram, M. J. Reno, J. Hernandez-Alvidrez, P. Barba, B. Reimer, R. Montoya, C. Carr, and O. Lavrova, "A survey of traveling wave protection schemes in electric power systems," *IEEE Access*, vol. 9, pp. 72949–72969, 2021.

[69] Z. Yang, K. Jia, Y. Fang, Z. Zhu, B. Yang, and T. Bi, "High-frequency fault component-based distance protection for large renewable power plants," *IEEE Transactions on Power Electronics*, vol. 35, no. 10, pp. 10352–10362, 2020.

[70] S. Kanwal and S. Jiriwibhakorn, "Artificial intelligence based faults identification, classification, and localization techniques in transmission lines-a review," *IEEE Latin America Transactions*, vol. 21, no. 12, pp. 1291–1305, 2023.

[71] P. Jafarian and M. Sanaye-Pasand, "A traveling-wave-based protection technique using wavelet/pca analysis," *IEEE Transactions on Power Delivery*, vol. 25, no. 2, pp. 588–599, 2010.

[72] E. Vazquez, J. Castruita, O. L. Chacon, and A. Conde, "A new approach traveling-wave distance protectionâpart i: Algorithm," *IEEE Transactions on Power Delivery*, vol. 22, no. 2, pp. 795–800, 2007.

[73] Y. Wu, Z. Li, X. Lin, Z. Feng, S. Cao, and F. Wei, "A novel single-ended transient-based boundary protection based on the instantaneous energy of traveling waves," *IEEE Transactions on Power Delivery*, pp. 1–15, 2024.

[74] Z. Guo, J. Huang, Q. Huang, Y. Deng, Y. Luo, and Z. Huang, "A weak fault adaptive traveling wave protection method for bus and transmission line," in *2023 IEEE International Conference on Advanced Power System Automation and Protection (APAP)*, pp. 30–34, 2023.

[75] F. Namdari and M. Salehi, "High-speed protection scheme based on initial current traveling wave for transmission lines employing mathematical morphology," *IEEE Transactions on Power Delivery*, vol. 32, no. 1, pp. 246–253, 2017.

[76] R. Godse and S. Bhat, "Mathematical morphology-based feature-extraction technique for detection and classification of faults on power transmission line," *IEEE Access*, vol. 8, pp. 38459–38471, 2020.

[77] M. Khodadadi and S. M. Shahrtash, "A new noncommunication-based protection scheme for three-terminal transmission lines employing mathematical morphology-based filters," *IEEE Transactions on Power Delivery*, vol. 28, no. 1, pp. 347–356, 2013.

[78] O. Noureldeen and I. Hamdan, "Design of robust intelligent protection technique for large-scale grid-connected wind farm," *Protection and Control of Modern Power Systems*, vol. 3, no. 1, pp. 1–13, 2018.

[79] M. Tasdighi and M. Kezunovic, "Preventing transmission distance relays maloperation under unintended bulk dg tripping using svm-based approach," *Electric Power Systems Research*, vol. 142, pp. 258–267, 2017.

[80] J. Morales, E. Orduna, H. Villarroel, and J. Quispe, "High-speed directional protection without voltage sensors for distribution feeders with distributed generation integration based on the correlation of signals and machine learning," *Electric Power Systems Research*, vol. 184, p. 106295, 2020.

[81] O. D. Naidu, N. George, S. Zubic, and M. Krakowski, "Time-domain-based distance protection for transmission networks: Secure and reliable solution for complex networks," *IEEE Access*, vol. 11, pp. 104656–104675, 2023.

[82] L. Zou, Q. Zhao, X. Lin, and P. Liu, "Applications of multi-resolution morphological analysis in ultra high speed protection of transmission line," in *IEEE Power Engineering Society General Meeting, 2005*, pp. 707–713 Vol. 1, 2005.

[83] M. Chamia and S. Liberman, "Ultra high speed relay for ehv/uhv transmission lines – development, design and application," *IEEE Transactions on Power Apparatus and Systems*, vol. PAS-97, no. 6, pp. 2104–2116, 1978.

[84] K. Hicks and W. Butt, "Feasibility and economics of ultra-high-speed fault clearing," *IEEE Transactions on Power Apparatus and Systems*, vol. PAS-99, no. 6, pp. 2138–2145, 1980.

[85] W. E. Vargas and J. C. Quispe H., "Economic benefit and improve of stability in the power system through the ultra-high speed fault clearing in transmission lines," in *2018 IEEE XXV International Conference on Electronics, Electrical Engineering and Computing (INTERCON)*, pp. 1–4, 2018.

[86] G. W. Swift, "The spectra of fault-induced transients," *IEEE Transactions on Power Apparatus and Systems*, vol. PAS-98, no. 3, pp. 940–947, 1979.

[87] A. A. Girgis and R. G. Brown, "Modelling of fault-induced noise signals for computer relaying applications," *IEEE Transactions on Power Apparatus and Systems*, vol. PAS-102, no. 9, pp. 2834–2841, 1983.

[88] J. Pinto de Sa, "The stochastic modeling of fault-induced transients," *IEEE Transactions on Power Delivery*, vol. 7, no. 3, pp. 1156–1166, 1992.

[89] X. G. Wang, S. F. Huang, and Q. K. Liu, "Study of transient spectrum in transmission lines," in *2008 IEEE Power and Energy Society General Meeting - Conversion and Delivery of Electrical Energy in the 21st Century*, pp. 1–6, 2008.

[90] S.-y. He, A. Cozza, and Y.-z. Xie, "On the spatial resolution of fault-location techniques based on full-fault transients," *IEEE Transactions on Power Delivery*, vol. 35, no. 3, pp. 1527–1540, 2020.

[91] S. F. Huang and X. G. Wang, "A protection scheme for phase-to-phase faults based on spectrum characteristic of fault-generated high-frequency transient signals," in *2009 IEEE Power and Energy Society General Meeting*, pp. 1–5, 2009.

[92] Y. Nie, Y. Liu, D. Lu, and B. Wang, "An improved natural frequency based transmission line fault location method with full utilization of frequency spectrum information," *IET Generation, Transmission and Distribution*, vol. 15, no. 19, pp. 2787–2803, 2021.

[93] S. F. Huang and X. G. Wang, "A fault location scheme based on spectrum characteristic of fault-generated high-frequency transient signals," in *2009 IEEE Power and Energy Society General Meeting*, pp. 1–5, 2009.

[94] D. E. Hedman, "Attenuation of traveling waves on three-phase lines," *IEEE Transactions on Power Apparatus and Systems*, vol. PAS-90, no. 3, pp. 1312–1320, 1971.

[95] G. Gemelli, F. Palone, M. Rebolini, and F. Falorni, "Factors affecting the single-ended travelling wave-based fault location in hv lines," in *2018 IEEE International Conference on Environment and Electrical Engineering and 2018 IEEE Industrial and Commercial Power Systems Europe (EEEIC / ICPS Europe)*, pp. 1–6, 2018.

[96] Z. Zhao, L. Yuan, H. Bai, and T. Lu, *Electromagnetic transients of power electronics systems*. Springer, 2019.

[97] J. Behkesh Noshahr, "Emission phenomenon of supra-harmonics caused by switching of full-power frequency converter of wind turbines generator (pmsg) in smart grid," in *2016 IEEE 16th International Conference on Environment and Electrical Engineering (EEEIC)*, pp. 1–6, 2016.

[98] T. Yalcin, M. Ozdemir, P. Kostyla, and Z. Leonowicz, "Analysis of supra-harmonics in smart grids," in *2017 IEEE International Conference on Environment and Electrical Engineering and 2017 IEEE Industrial and Commercial Power Systems Europe*, pp. 1–4, 2017.

[99] T. Yalcin, M. Ozdemir, P. Kostyla, and Z. Leonowicz, "Discrete wavelet analysis of supra-harmonic emissions in smart grid (pv inverter implementation)," in *2018 IEEE International Conference on Environment and Electrical Engineering and 2018 IEEE Industrial and Commercial Power Systems Europe*, pp. 1–5, 2018.

[100] H. Rathnayake, D. Solatialkaran, F. Zare, and R. Sharma, "Grid-tied inverters in renewable energy systems: Harmonic emission in 2 to 9 khz frequency range," in *2019 21st European Conference on Power Electronics and Applications (EPE '19 ECCE Europe)*, pp. P.1–P.10, 2019.

[101] D. Yang, X. Ruan, and H. Wu, "Impedance shaping of the grid-connected inverter with lcl filter to improve its adaptability to the weak grid condition," *IEEE Transactions on Power Electronics*, vol. 29, no. 11, pp. 5795–5805, 2014.

[102] Y. Han, M. Yang, H. Li, P. Yang, L. Xu, E. A. A. Coelho, and J. M. Guerrero, "Modeling and stability analysis of *lcl* -type grid-connected inverters: A comprehensive overview," *IEEE Access*, vol. 7, pp. 114975–115001, 2019.

[103] K. Jia, Z. Ren, L. Li, Z. Xuan, and D. Thomas, "High-frequency transient comparison based fault location in distribution systems with dgs," *IET Generation, Transmission & Distribution*, vol. 11, no. 16, pp. 4068–4077, 2017.

[104] K. Jia, Z. Yang, Y. Fang, T. Bi, and M. Sumner, "Influence of inverter-interfaced renewable energy generators on directional relay and an improved scheme," *IEEE Transactions on Power Electronics*, vol. 34, no. 12, pp. 11843–11855, 2019.

[105] N. O. Mogaru, "The basics of transmission line protection," in *2020 IEEE PES/IAS PowerAfrica*, pp. 1–5, 2020.

[106] M. M. Islam, P. Sanjeevikumar, J. K. Pedersen, and C. W. Brice, "Advanced digital signal processing based transmission line fault detection and classification," in *IECON 2019 - 45th Annual Conference of the IEEE Industrial Electronics Society*, vol. 1, pp. 4991–4996, 2019.

[107] L. U. Iurinic, R. G. Ferraz, and A. S. Bretas, "Characteristic frequency of travelling waves applied for transmission lines fault location estimation," in *2013 IEEE Grenoble Conference*, pp. 1–5, 2013.

[108] M. Okamura, F. Andow, I. Mitani, Y. Okita, and M. Masui, "Development of new relays with significantly improved performance against badly distorted transient waveforms," *IEEE Transactions on Power Apparatus and Systems*, vol. PAS-99, no. 4, pp. 1426–1436, 1980.

[109] P. Jafarian and M. Sanaye-Pasand, "High-frequency transients-based protection of multiterminal transmission lines using the svm technique," *IEEE Transactions on Power Delivery*, vol. 28, no. 1, pp. 188–196, 2013.

[110] S. G. Mallat, "A theory for multiresolution signal decomposition: the wavelet representation," 1987.

[111] B. L. Sturm, "Stephane mallat: A wavelet tour of signal processing, 2nd edition," *Computer Music Journal*, vol. 31, no. 3, pp. 83–85, 2007.

[112] J. Zhang, Z. Zeng, L. Zhang, Q. Lu, and K. Wang, "Application of mathematical morphological filtering to improve the resolution of chang'e-3 lunar penetrating radar data," *Remote Sensing*, vol. 11, no. 5, 2019.

[113] T. Jing-Tian, L. Jin, X. Xiao, Z. Lin-Cheng, and L. Qing-Tian, "Mathematical morphology filtering and noise suppression of magnetotelluric sounding data," 2012.

[114] P. Vaidyanathan, "Generalizations of the sampling theorem: Seven decades after nyquist," *IEEE Transactions on Circuits and Systems I: Fundamental Theory and Applications*, vol. 48, no. 9, pp. 1094–1109, 2001.

[115] W. C. Duesterhoeft, M. W. Schulz, and E. Clarke, "Determination of instantaneous currents and voltages by means of alpha, beta, and zero components," *Transactions of the American Institute of Electrical Engineers*, vol. 70, no. 2, pp. 1248–1255, 1951.

[116] M. H. J. Bollen and I. Y.-H. Gu, "On the analysis of voltage and current transients in three-phase power systems," *IEEE Transactions on Power Delivery*, vol. 22, no. 2, pp. 1194–1201, 2007.

[117] P. M. Anderson, C. Henville, R. Rifaat, B. Johnson, and S. Meliopoulos, "Analysis of distance protection," 2022.

[118] X. Wang, Q. Qian, and W. Chen, "Analyzing fault-induced transients with wavelets," in *IEEE Power Engineering Society Summer Meeting,*, vol. 3, pp. 1090–1093 vol.3, 2002.

[119] T. Hisakado, K. Tanaka, and K. Okumura, "A transmission line fault-location system using the wavelet transform," *Electrical Engineering in Japan*, vol. 140, no. 4, pp. 27–37, 2002.

[120] T. Hisakado and K. Okumura, "An application of wavelet transform to fault location and its implementation on fpga," in *Proceedings of the 44th IEEE 2001 Midwest Symposium on Circuits and Systems*, vol. 2, pp. 528–531, IEEE, 2001.

[121] P. Crossley and P. McLaren, "Distance protection based on travelling waves," *IEEE transactions on power apparatus and systems*, no. 9, pp. 2971–2983, 1983.

[122] R. Liang, Z. Wang, N. Peng, F. Zare, X. Liu, and C. Liu, "Traveling wave protection based on asynchronously sampled time difference of arrival of modulus traveling waves in per unit line length," *Electric Power Systems Research*, vol. 165, pp. 250–258, 2018.

[123] Z. Bo, M. Redfern, and G. Weller, "Positional protection of transmission line using fault generated high frequency transient signals," *IEEE Transactions on Power Delivery*, vol. 15, no. 3, pp. 888–894, 2000.

[124] M. Islam, H. A. Mohammadpour, A. Ghaderi, C. W. Brice, and Y.-J. Shin, "Time-frequency-based instantaneous power components for transient disturbances according to ieee standard 1459," *IEEE Transactions on Power Delivery*, vol. 30, no. 3, pp. 1288–1297, 2015.

[125] H. Panahi, R. Zamani, M. Sanaye-Pasand, and H. Mehrjerdi, "Advances in transmission network fault location in modern power systems: Review, outlook and future works," *IEEE Access*, vol. 9, pp. 158599–158615, 2021.

[126] L. L. Zhang, M. S. Li, T. Y. Ji, Q. H. Wu, L. Jiang, and J. P. Zhan, "Morphology singular entropy-based phase selector using short data window for transmission lines," *IEEE Transactions on Power Delivery*, vol. 29, no. 5, pp. 2162–2171, 2014.

[127] X. Luo, L. Zhang, H. Shan, and T. Ji, "Traveling wave velocity independent fault location scheme with adaptive mathematical filters for distribution network," *Electric Power Systems Research*, vol. 209, p. 108040, 2022.

[128] A. Saad, M. El-Naggar, and E. Shehab-Eldin, "Modeling and testing of multi-resolution morphological gradient distance relay algorithm," *Energy Procedia*, vol. 14, pp. 271–279, 2012.

[129] S. Gautam and S. M. Brahma, "Overview of mathematical morphology in power systems a tutorial approach," in *2009 IEEE Power and Energy Society General Meeting*, pp. 1–7, IEEE, 2009.

[130] J. Martinez, J. Mahseredjian, and R. Walling, "Parameter determination: procedures for modeling system transients," *IEEE Power and Energy Magazine*, vol. 3, no. 5, pp. 16–28, 2005.

[131] F. M. d. M. Junior and F. V. Lopes, "Mathematical study on traveling waves phenomena on three phase transmission lines - part i: Fault-launched waves," *IEEE Transactions on Power Delivery*, vol. 37, no. 2, pp. 1151–1160, 2022.

[132] R. L. de Andrade Reis, W. L. A. Neves, F. V. Lopes, and D. Fernandes, "Coupling capacitor voltage transformers models and impacts on electric power systems: A review," *IEEE Transactions on Power Delivery*, vol. 34, no. 5, pp. 1874–1884, 2019.

[133] K. Nayak, S. Jena, and A. K. Pradhan, "Travelling wave based directional relaying without using voltage transients," *IEEE Transactions on Power Delivery*, vol. 36, no. 5, pp. 3274–3277, 2021.

[134] P. L. Seta, "Modeling and control of wind turbines based on doubly-fed induction generators (dfig)," in *EEUG Training Course 2009, Part 1, EEUG Meeting 2009, TU Delft, The Netherlands*, 2009.

[135] S. Hacker, "Messung der modellparameter des dynamischen netzmodells und implementierung in ein simulationsprogramm," in *Studienarbeit, Institut fur Elektrische Energieversorgung und Hochspannungstechnik, TU-Dresden*, 2011.

[136] Y. Tang, H. Chen, H. Wang, F. Dai, and S. Jiang, "Transmission line models used in travelling wave studies," in *1999 IEEE Transmission and Distribution Conference (Cat. No. 99CH36333)*, vol. 2, pp. 797–803 vol.2, 1999.

[137] "Ieee guide for protective relay applications to transmission lines," *IEEE Std C37.113-2015 (Revision of IEEE Std C37.113-1999)*, pp. 1–141, 2016.

[138] H. J. A. Ferrer and E. O. Schweitzer, *Modern solutions for protection, control, and monitoring of electric power systems*. Schweitzer Engineering Laboratories Pullman, WA, USA, 2010.

[139] G. Ziegler, *Numerical distance protection: principles and applications*. John Wiley & Sons, 2011.

[140] K. Zimmerman and D. Costello, "Fundamentals and improvements for directional relays," in *2010 63rd Annual Conference for Protective Relay Engineers*, pp. 1–12, 2010.

[141] J. Horak, "Directional overcurrent relaying (67) concepts," in *59th Annual Conference for Protective Relay Engineers, 2006.*, pp. 13 pp.–, 2006.

[142] D. Costello and K. Zimmerman, "Determining the faulted phase," in *2010 63rd Annual Conference for Protective Relay Engineers*, pp. 1–20, 2010.

[143] J. Ma and Z. Wang, "Basic theories of power system relay protection," 2017.

[144] A. Greenwood, "Electrical transients in power systems," 1991.

[145] F. M. de Magalhaes Junior and F. V. Lopes, "Mathematical study on traveling waves phenomena on three phase transmission lines - part ii: Reflection and refraction matrices," *IEEE Transactions on Power Delivery*, vol. 37, no. 2, pp. 1161–1170, 2022.

[146] Q.-H. Wu, Z. Lu, and T. Ji, *Protective relaying of power systems using mathematical morphology*. Springer Science & Business Media, 2009.

[147] G. Matheron and J. Serra, "The birth of mathematical morphology," in *Proc. 6th Intl. Symp. Mathematical Morphology*, pp. 1–16, Sydney, Australia, 2002.

[148] B. Chen, Y. Li, and N. Zeng, "Centralized wavelet multiresolution for exact translation invariant processing of ecg signals," *IEEE Access*, vol. 7, pp. 42322–42330, 2019.



Nombres y apellidos:	**Juan Carlos Quispe Huarcaya.**
Estado civil:	Soltero
Posición:	Ing, MSc.
IEEE & PES:	(Member N° # 95044308)
CIP:	(Member N° # 260159)
ORCID:	0000-0002-6104-2007
SCOPUS:	57204944017
E-mail:	jcquispeh@gmail.com, jcquispeh@uni.pe
Número celular:	+51 941400391

Educación:

2007 – 2012 **Ingeniero Eléctrico**
Universidad Nacional de Ingeniería (UNI), Lima, Perú.

2013 Apr – Nov **Diplomado en proyectos de energías renovables**
UNI, Lima, Perú.
Proyecto subvenciones: Ministerio de Energía y Minas – CARELEC.

2016 – 2018 **Maestría en Ingeniería Eléctrica**
Universidad Nacional de San Juan (UNSJ), Argentina.
German Academic Exchange Service (DAAD).

2018 – 2023 **Doctorado en Ingeniería Eléctrica**
Universidad Nacional de San Juan (UNSJ), Argentina.
German Academic Exchange Service (DAAD).
Consejo Nacional de Investigaciones Científicas y Técnicas (CONICET).

Experiencia laboral y de investigación:

2023– Presente Comité de Operación Económica del Sistema Interconectado Nacional (COES SINAC), Lima, Perú.
Cargo: Ingeniero especialista en el área de nuevos proyectos

2021–2023	Institute of Electrical Power Systems and High Voltage Engineering, TU Dresden, Alemania Cargo: Investigador doctoral en ingeniería eléctrica
2016 – 2021	Instituto de Energía Eléctrica, UNSJ – CONICET, San Juan, Argentina. Cargo: Investigador en ingeniería eléctrica
2012 – 2016	Comité de Operación Económica del Sistema Interconectado Nacional (COES SINAC), Lima, Perú. Cargo: Ingeniero analista en el área de nuevos proyectos
2012 July – October	Red de Energía del Perú (ISA REP), Lima, Peru. Cargo: Joven profesional
2012 March – July	PLM Energy and Automation, Lima, Peru. Cargo: Ingeniero analista en protección de sistemas eléctricos
2010 – 2011	Instituto de Investigación de la Facultad de Ingeniería Eléctrica y Electrónica – UNI, Lima, Perú. Cargo: Investigador

Publicaciones:

[1] J. C. Quispe H., J. Morales, and E. Orduna, "MRA of Fault-generated High-frequency Transient Signals using Mathematical Morphology. Comparison with Wavelet Transform," pp. 1–8, Nov. 2022, doi: 10.1109/ARGENCON55245.2022.9939830.

[2] H. Juan Carlos Quispe, "Analysis of Directional Protections in Distributed Generation System with Synchronous Generators and Inverter-Based Resources," 2022 IEEE XXIX Int. Conf. Electron. Electr. Eng. Comput., pp. 1–4, Aug. 2022, doi: 10.1109/INTERCON55795.2022.9870165.

[3] J. C. Quispe and E. Orduña, "Transmission line protection challenges influenced by inverter-based resources: a review," Prot. Control Mod. Power Syst. 2022 71, vol. 7, no. 1, pp. 1–17, Jul. 2022, doi: 10.1186/S41601-022-00249-8.

[4] J. C. Quispe H, H. Villarroel-Gutierrez, and E. Orduna, "Analyzing Short-Circuit Current Behavior Caused by Inverter-Interfaced Renewable Energy Sources. Effects on Distance Protection," Jan. 2021, pp. 1–6, doi: 10.1109/tdla47668.2020.9326226.

[5] J. C. Quispe H., "Time–frequency multiresolution of fault-generated transient signals in transmission lines using a morphological filter", 2023, "Protection and Control of Modern Power Systems", doi: 10.1186/s41601-023-00294-x



ISBN: **978-631-00-4934-2**